kiran chholak

THESIS F1.docx

Delhi Technological University

Document Details

Submission ID
trn:oid:::27535:124127336

Submission Date
Dec 10, 2025, 2:58 AM GMT+5:30

Download Date
Dec 10, 2025, 3:07 AM GMT+5:30

File Name
THESIS F1.docx

File Size
10.8 MB

189 Pages

40,282 Words

241,930 Characters

7% Overall Similarity

The combined total of all matches, including overlapping sources, for each database.

Filtered from the Report

- Bibliography
- Quoted Text
- Cited Text
- Small Matches (less than 10 words)

Exclusions

- 2 Excluded Sources

Match Groups

199 Not Cited or Quoted 7%
Matches with neither in-text citation nor quotation marks

0 Missing Quotations 0%
Matches that are still very similar to source material

0 Missing Citation 0%
Matches that have quotation marks, but no in-text citation

0 Cited and Quoted 0%
Matches with in-text citation present, but no quotation marks

Top Sources

4% Internet sources
5% Publications
2% Submitted works (Student Papers)

Integrity Flags

0 Integrity Flags for Review

No suspicious text manipulations found.

Our system's algorithms look deeply at a document for any inconsistencies that would set it apart from a normal submission. If we notice something strange, we flag it for you to review.

A Flag is not necessarily an indicator of a problem. However, we'd recommend you focus your attention there for further review.

Match Groups

- **199** Not Cited or Quoted 7%
  Matches with neither in-text citation nor quotation marks
- **0** Missing Quotations 0%
  Matches that are still very similar to source material
- **0** Missing Citation 0%
  Matches that have quotation marks, but no in-text citation
- **0** Cited and Quoted 0%
  Matches with in-text citation present, but no quotation marks

Top Sources

- 4% Internet sources
- 5% Publications
- 2% Submitted works (Student Papers)

Top Sources

The sources with the highest number of matches within the submission. Overlapping sources will not be displayed.

1	Internet	
www.researchgate.net		<1%
2	Internet	
ntnuopen.ntnu.no		<1%
3	Internet	
link.springer.com		<1%
4	Internet	
www.hindawi.com		<1%
5	Internet	
journals.sagepub.com		<1%
6	Internet	
archive.org		<1%
7	Submitted works	
Taylor's Education Group on 2016-11-23		<1%
8	Publication	
Emil Aggestam, Jens C. O. Nielsen, Rikard Bolmsvik. "Simulation of vertical dynam...		<1%
9	Publication	
D.P. Connolly, P. Alves Costa. "Geodynamics of very high speed transport systems...		<1%
10	Publication	
Xiaoyan Lei. "High Speed Railway Track Dynamics", Springer Science and Busines...		<1%

11 Submitted works
Nottingham Trent University on 2025-09-26 <1%

12 Internet
www.scribd.com <1%

13 Internet
www.tandfonline.com <1%

14 Publication
Kaiwen Liu, Qian Su, Fei Yue, Bao Liu, Ruizhe Qiu, Ting Liu. "Effects of suffosion-in... <1%

15 Internet
scholarbank.nus.edu.sg <1%

16 Internet
idus.us.es <1%

17 Publication
Priti Rani, Kiran Chholak, Yamika Patel. "Chapter 45 Design and Simulation Study ... <1%

18 Internet
www.mdpi.com <1%

19 Publication
Baoguo Han, Liqing Zhang, Jinping Ou. "Smart and Multifunctional Concrete Tow... <1%

20 Publication
Yamika Patel, Vikas Rastogi, Wolfgang Borutzky. "Simulation study on the influen... <1%

21 Internet
old.jozsefvaros.hu <1%

22 Internet
research.birmingham.ac.uk <1%

23 Publication
Shi, Hongmei, and Zujun Yu. "Estimation of Track Irregularity Based on Genetic Al... <1%

24 Publication
Tuo Lei, Jian Dai, Kok Keng Ang, Kun Li, Yi Liu. "Moving Element Analysis of High-S... <1%

25 Publication
"Dynamic Soil Properties and Liquefaction", Springer Science and Business Media... <1%

26 Publication
Wen-Bin Li, Hua-Peng Chen, Yu Jiang. "Lifetime damage evolution of concrete join... <1%

27 Internet
bilselkongreleri.com <1%

28 Internet
pure-oai.bham.ac.uk <1%

29 Publication
"Noise and Vibration Mitigation for Rail Transportation Systems", Springer Natur... <1%

30 Publication
M. Attar, A. Karrech, K. Regenauer-Lieb. "Non-linear modal analysis of structural c... <1%

31 Publication
Martin Rosenberger, Manfred Pl�chl, Klaus Six, Johannes Edelmann. "The Dynam... <1%

32 Publication
Mehmet Ali Toprak, Ahmet Güllü, Bayezid Özden, Beyazıt Ölçer, Yavuz Durgun, Fa... <1%

33 Publication
Minh Thi Tran, Kok Keng Ang, Van Hai Luong. "Vertical dynamic response of non-... <1%

34 Publication
Wanming Zhai, Kaiyun Wang, Chengbiao Cai. "Fundamentals of vehicle–track cou... <1%

35 Internet
spectrum.library.concordia.ca <1%

36 Publication
"Computational and Experimental Simulations in Engineering", Springer Science ... <1%

37 Submitted works
Universiti Tenaga Nasional on 2025-06-16 <1%

38 Internet
metrorailtoday.com <1%

39 Submitted works
Nottingham Trent University on 2025-02-13 <1%

40 Publication
Shi, Hong Mei, and Jia Liang Zhou. "Vibration Analysis of High-Speed Vehicles und... <1%

41 Publication
Ting Li, Qian Su, Sakdirat Kaewunruen. "Influences of dynamic material propertie... <1%

42 Publication
Keith D. Hjelmstad. "Fundamentals of Structural Dynamics", Springer Science and... <1%

43 Submitted works
University of Birmingham on 2018-04-03 <1%

44 Publication
"Advances in Dynamics of Vehicles on Roads and Tracks", Springer Science and B... <1%

45 Publication
Niels Olhoff, John Rasmussen, Erik Lund. "A Method of “Exact” Numerical Differen... <1%

46 Publication
Springer Proceedings in Physics, 2011. <1%

47 Submitted works
University of Leeds on 2025-05-08 <1%

48 Internet
diva-portal.org <1%

49 Internet
www.lajss.org <1%

50 Publication
Mingze Wang, Chengbiao Cai, Shengyang Zhu, Wanming Zhai. "Experimental stud... <1%

51 Internet
www.ros.hw.ac.uk <1%

52 Publication
Ashish Juneja, Anil Joseph, Dasaka S. Murty. "GeoVadis - The Future of Geotechnic... <1%

53 Submitted works
University of Basrah on 2015-06-02 <1%

54 Publication
Xinwen Yang, Shaojie Gu, Shunhua Zhou, Jianjin Yang, Yu Zhou, Songliang Lian. "E... <1%

55 Publication
Xinwen Yang, Yao Shu, Shunhua Zhou. "An explicit periodic nonlinear model for e... <1%

56 Publication
Zheng Li, Weidong Wang, Lei Xu, Jingmang Xu. "Study on the long-distance settle... <1%

57 Internet
espace.etsmtl.ca <1%

58 Internet
theses.lib.polyu.edu.hk <1%

59 Submitted works
Heriot-Watt University on 2025-04-07 <1%

60 Publication
Khatib, J.M.. "Properties of concrete incorporating fine recycled aggregate", Cem... <1%

61 Submitted works
Nottingham Trent University on 2022-03-10 <1%

62 Publication
Qingyuan Xu, Xi Wang. "Experimental study on high-cycle flexural fatigue behavi... <1%

63 Submitted works
Thomas Edison State College on 2018-04-26 <1%

64 Submitted works
University of Hong Kong on 2023-07-28 <1%

65 Submitted works
University of Pretoria on 2014-07-17 <1%

66 Internet
ebin.pub <1%

67 Internet
eprints.qut.edu.au <1%

68 Internet
vdoc.pub <1%

69 Internet
www.theseus.fi <1%

70 Submitted works
Addis Ababa University on 2023-07-14 <1%

71 Submitted works
City University of Hong Kong on 2025-04-18 <1%

72 Publication
Deepak Kumar, P. Sriram Karthick Raja, Subhadeep Metya. "Chapter 16 Performa... <1%

73 Publication
Gibson, Arthur C.. "Synthesis and Electrochemical Analysis of Metallopolymers Co... <1%

74 Publication
He Xia, Nan Zhang, Weiwei Guo. "Dynamic Interaction of Train-Bridge Systems in ... <1%

75 Publication
Jian Zhang, Yan Zhao, Ya-hui Zhang, Xue-song Jin, Wan-xie Zhong, Frederic W Willi... <1%

76 Publication
Judith Cowan. "Reproductive patterns and thalassaemia major", Journal of Biosoc... <1%

77 Publication
Lei, X., and J. Wang. "Dynamic analysis of the train and slab track coupling system... <1%

78 Publication
X Lei. "Track vibration analysis for railways with mixed passenger and freight traf... <1%

79 Publication
Yu Guo, Qiang Sun, Yu Sun. "Dynamic evaluation of vehicle-slab track system und... <1%

80 Publication
Zhang, J., Q. Gao, S.J. Tan, and W.X. Zhong. "A precise integration method for solvi... <1%

81 Internet
backend.orbit.dtu.dk <1%

82 Internet
digitalcommons.aaru.edu.jo <1%

83 Internet
repositorium.sdum.uminho.pt <1%

84 Internet
www.researchwithnj.com <1%

85 Internet
www.rose-hulman.edu <1%

86 Submitted works
Anadolu University on 2021-09-07 <1%

87 Submitted works
CEPT University on 2025-05-05 <1%

88 Submitted works
Heriot-Watt University on 2021-12-06 <1%

89 Submitted works
Heriot-Watt University on 2022-04-14 <1%

90 Submitted works
Heriot-Watt University on 2025-04-10 <1%

91 Publication
Hua-Peng Chen, Wen-Bin Li, Yu Jiang, Lin-Fa Xiao. "Fatigue life prediction for CA m... <1%

92 Publication
Inge Hoff, Helge Mork, Rabbira Garba Saba. "Eleventh International Conference o... <1%

93 Publication
Jianjin Yang, Shengyang Zhu, Wanming Zhai. "A novel dynamics model for railway... <1%

94 Publication
Juyeop Park, Donghoon Kang, Hak-Sung Kim. "Optimization and field evaluation ... <1%

95 Publication
Kiran Chholak, Nirendra Dev. "Modelling and numerical simulation of high-speed ... <1%

96 Publication
Lin Liang, XiaoZhen Li, Jing Zheng, KangNing Lei, Hongye Gou. "Structure-borne n... <1%

97 Publication
Lu Sun, Liliang Chen, Habtamu H. Zelelew. "Stress and Deflection Parametric Stud... <1%

98 Publication
Miao Su, Wenxiao Zhang, Qizhi Zhu, Jun Wang, Hui Peng. "Static and fatigue expe... <1%

99 Publication
Mohamed Abubakar Ali, Nadja Oneschkow, Ludger Lohaus, Michael Haist. "Influe... <1%

100 Publication
Mustafa Eroğlu, Mehmet Akif Koç, İsmail Esen, Recep Kozan. "Realistic Modelling ... <1%

101 Submitted works
NEBOSH on 2025-10-14 <1%

102 Submitted works
North Harris Montgomery Community College District on 2016-07-12 <1%

103 Publication
Ping Wang, Hao Xu, Rong Chen. "Effect of Cement Asphalt Mortar Debonding on ... <1%

104 Publication
Ren Juanjuan, Yang Rongshan, Wang Ping, Dai Feng, Yan Xiaobo. "Influence of co... <1%

105 Publication
Rocha, Joao Miguel dos Santos Pereira da. "Probabilistic methodologies for the sa... <1%

106 Publication
Shiraz D. Tayabji, David Bilow. "Concrete Slab Track State of the Practice", Transp... <1%

107 Publication
Springer Tracts on Transportation and Traffic, 2013. <1%

108 Publication
Sufen Dong, Yanlei Wang, Ashraf Ashour, Baoguo Han, Jinping Ou. "Uniaxial com... <1%

109 Submitted works
University of Birmingham on 2024-03-20 <1%

110 Publication
Virajan Verma, K. Nallasivam. "Dynamic interaction analysis of a high-speed train... <1%

111 Publication
Xi Wang, Qingyuan Xu, Shengwei Sun, Bin Li, Qi Wei, Hao Sun. "Evaluation of dyna... <1%

112 Publication
Xiaoyan Lei, Bin Zhang. "Analysis of Dynamic Behavior for Slab Track of High-Spe... <1%

113 Publication
Xuyou Long, Jin Shi, Yingjie Wang, Xingyu Liu. "Dynamic Modeling and Applicatio... <1%

114 Publication
Zhenxing He, Xu Zhang, Shuzhen Wang, Yanbo Bai, Quanbao Feng. "Research on ... <1%

115 Internet
dokumen.pub <1%

116 Internet
epdf.tips <1%

117 Internet
eprints.lib.hokudai.ac.jp <1%

118 Internet
jozsefvaros.hu <1%

119 Internet
oaresource.library.carleton.ca <1%

120 Internet
revistaalconpat.org <1%

121 Publication
Álvaro Mena-Alonso, Ángel Aragón-Torre, Miguel A. Vicente, Dorys C. González, Je... <1%

CHAPTER 1: INTRODUCTION

1.1 General

India's rapid economic growth, expanding cities, and rising mobility demands have accelerated the need for safe, efficient, and high-capacity transportation systems. Within this context, high-speed rail (HSR) has emerged as a transformative solution capable of providing fast, reliable, and environmentally sustainable transport. As India moves toward large-scale adoption of high-speed railway corridors, the structural systems that support these networks require careful evaluation to ensure long-term safety, stability, and performance.

Among the various track forms available globally, the slab track system (STS) has increasingly gained prominence due to its superior durability, reduced maintenance requirements, and ability to withstand demanding load cycles associated with high-speed operations. Despite its widespread adoption in countries such as Japan, China, and several European nations, the introduction of slab-track systems in India poses distinctive obstacles. India's diverse climatic conditions, subgrade variability, temperature fluctuations, and distinctive operational demands necessitate a more profound understanding of how different slab-track configurations perform under high-frequency dynamic loading.

A critical component within many slab-track systems, particularly Shinkansen-type structures, is Cement Asphalt Mortar (CAM) layer, which plays a vital role in load transfer, vibration attenuation, and overall structural integration. However, insights from international experience indicate that CAM is sensitive to fatigue degradation, temperature variations, and long-term stiffness decay. Furthermore, existing fatigue laws and material models have largely been developed for foreign CAM compositions and do not necessarily reflect the material properties or performance expectations of CAM used in Indian projects. This knowledge gap becomes especially significant as India embarks on its first HSR networks, where track reliability and service life prediction are paramount. In light of these challenges, advancing our understanding of slab-track behavior

particularly the static, dynamic, and fatigue performances of key components such as the rail, rail pad, CAM layer, hydraulically bonded layer (HBL), and subgrade is essential for developing context-specific design guidelines for Indian HSR systems. This kind of understanding not only helps make railway infrastructure safer and more durable, but it also fits with the national goals of long-term and sustainable transportation development.

This chapter introduces the fundamental aspects of railway track structures, with emphasis on international slab-track systems, their components, and their suitability for high-speed operations. It also outlines the scope of high-speed rail development in India, motivation behind present study, and the specific research objectives addressed in this thesis. The chapter concludes with structured overview of thesis organization, explaining how subsequent chapters systematically explore static behavior, vibration characteristics, vehicle–track interaction, and fatigue performance of slab-track systems to fulfil the stated research goals.

1.2 Historical Background: Railway Track Structure

The evolution of railway infrastructure has played an important part in creating modern transportation systems worldwide. Traditional railway systems initially relied on ballasted track configurations, which consist of rails supported by sleepers and a bed of crushed stone ballast. While this system served effectively for conventional train speeds, increasing demand for faster, more efficient, and more stable transportation led to development of advanced track structures.

The concept of high-speed rail originated in Japan with 1964 inauguration of Shinkansen, or "bullet train." This system revolutionized rail travel by enabling operating speeds exceeding 200 km/h, setting new benchmarks for speed, safety, and passenger comfort. The Shinkansen success demonstrated the need for more stable and maintenance-efficient track systems, particularly under high-speed dynamic loads. Consequently, Japan pioneered use of slab track systems, which eliminate need for ballast and provide a continuous, rigid support for rails.

Europe soon followed suit, with France launching its high-speed TGV in the 1980s. Other countries, including Germany, China, South Korea, and India, later adopted and advanced high-speed rail technologies, each contributing to innovations in track design, materials, and construction methods. These developments highlighted the limitations of ballasted tracks in high-speed scenarios, especially regarding settlement, maintenance, and dynamic stability.

As high-speed railways continue to expand globally, adoption of slab track systems has become increasingly prevalent. These systems offer numerous advantages, such as higher geometric precision, lower life-cycle costs, reduced maintenance, and improved dynamic performance, making them a critical focus in contemporary railway engineering research and infrastructure development. With rapid expansion of high-speed rail networks and increasing freight loads, it is crucial to understand stress distribution and structural behavior of railway track components. Accurate assessment of these stresses enables the prediction of the service life of individual components and facilitates timely maintenance. Consequently, detailed analytical approach is essential to guide design methodology of modern railway track structures.

In response to increasing traffic demands, the Indian Railways has launched the National Rail Plan 2030, which envisions development of seven new high-speed rail corridors across the country. These projects aim to improve passenger connectivity and reduce travel time. In parallel, the implementation of Dedicated Freight Corridors (DFC) notably between Delhi–Mumbai and Delhi–Kolkata is designed to separate freight operations from passenger traffic, thereby alleviating congestion and improving the overall efficiency of the railway network. The rising volume of passengers and freight has placed considerable pressure on existing infrastructure, resulting in reduced operating speeds and service reliability. The proposed segregation of traffic types is expected to enhance operational performance significantly.

With the advancement of HSR, the adoption of slab track systems also known as ballast less tracks have become widespread globally. Slab track technology represents a modern alternative to traditional ballasted tracks and offers several advantages. These

include a lower structural height, reduced maintenance requirements, longer service life, and greater lateral and vertical stability. Additionally, the absence of ballast eliminates the problem of ballast fouling or churning under repetitive loads. These characteristics make slab track an ideal solution for high-speed and heavy-haul railways.

A railway track system performs the essential function of providing a stable and continuous surface for train movement while guiding the vehicle safely along its intended path. The system consists of various structural elements, broadly classified into superstructure and substructure. The superstructure includes visible and load-carrying components such as rails (typically steel I-section profiles), rail pads (for damping and load transfer), fastening systems, and sleepers (made of concrete, steel, or composite materials) as shown in Figure 1.1. The substructure refers to the geotechnical foundation beneath the superstructure, which consists of ballast (in conventional tracks), concrete slab (in ballast less tracks), sub-ballast, and subgrade.

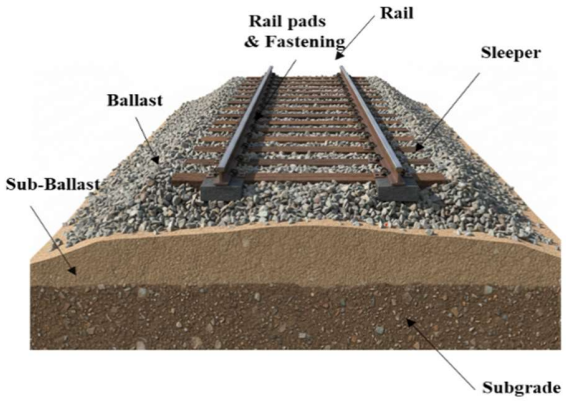

Figure 0.1 Conventional railway track structure

The integration of these components ensures that dynamic loads from trains are effectively distributed, vibrations are mitigated, and long-term track stability is maintained. As India moves towards adopting advanced slab track systems in its high-speed rail corridors, a detailed understanding of the behavior and interaction of these components under varying operational and environmental conditions becomes indispensable.

89

1.3 Slab Track System

Slab track systems are specific form of railway track system. Ballasted track systems use a layer of ballast material as a substructure. The requirement for ballast is eliminated with non-ballasted track systems, where a solid concrete slab or other support structures instead support the track components. These systems have gained attention due to their potential benefits in track stability, reduced maintenance, and increased longevity.

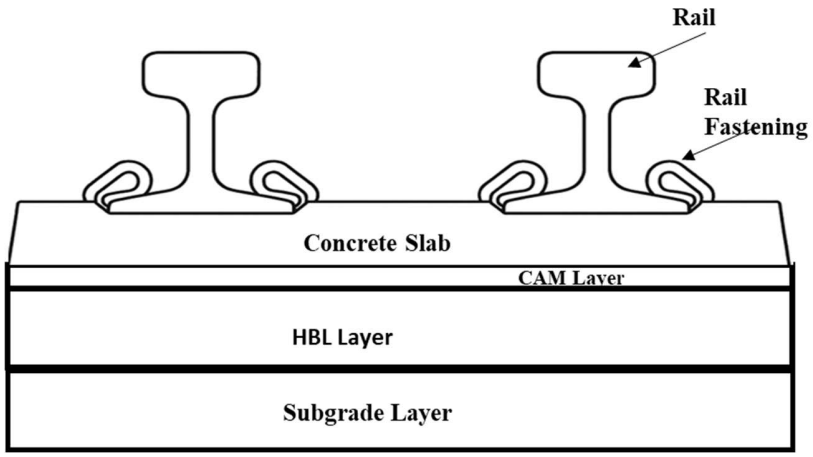

Figure 0.2 Slab track structure

72

Non-ballasted railway track systems offer several advantages over ballasted track systems. One key benefit is increased track stability. In traditional ballasted track systems, the ballast may degrade over time, leading to track settlement and misalignment. This situation requires frequent maintenance and tamping to ensure proper track geometry. In contrast, non-ballasted track systems provide a stable and uniform support structure, reducing likelihood of track settlement and associated maintenance requirements. This stability improves ride quality and reduces track maintenance costs (Rungskunroch et al., 2019). Figure 1.2 below illustrates the different slab track components that comprise the substructure and superstructure of slab track, both of which are made of concrete or asphalt. Various types of ballast-less tracks created across the globe may be further divided into two main groups: discretely rail-supported and continuously rail-supported, as illustrated in Figures 1.3 and 1.4.

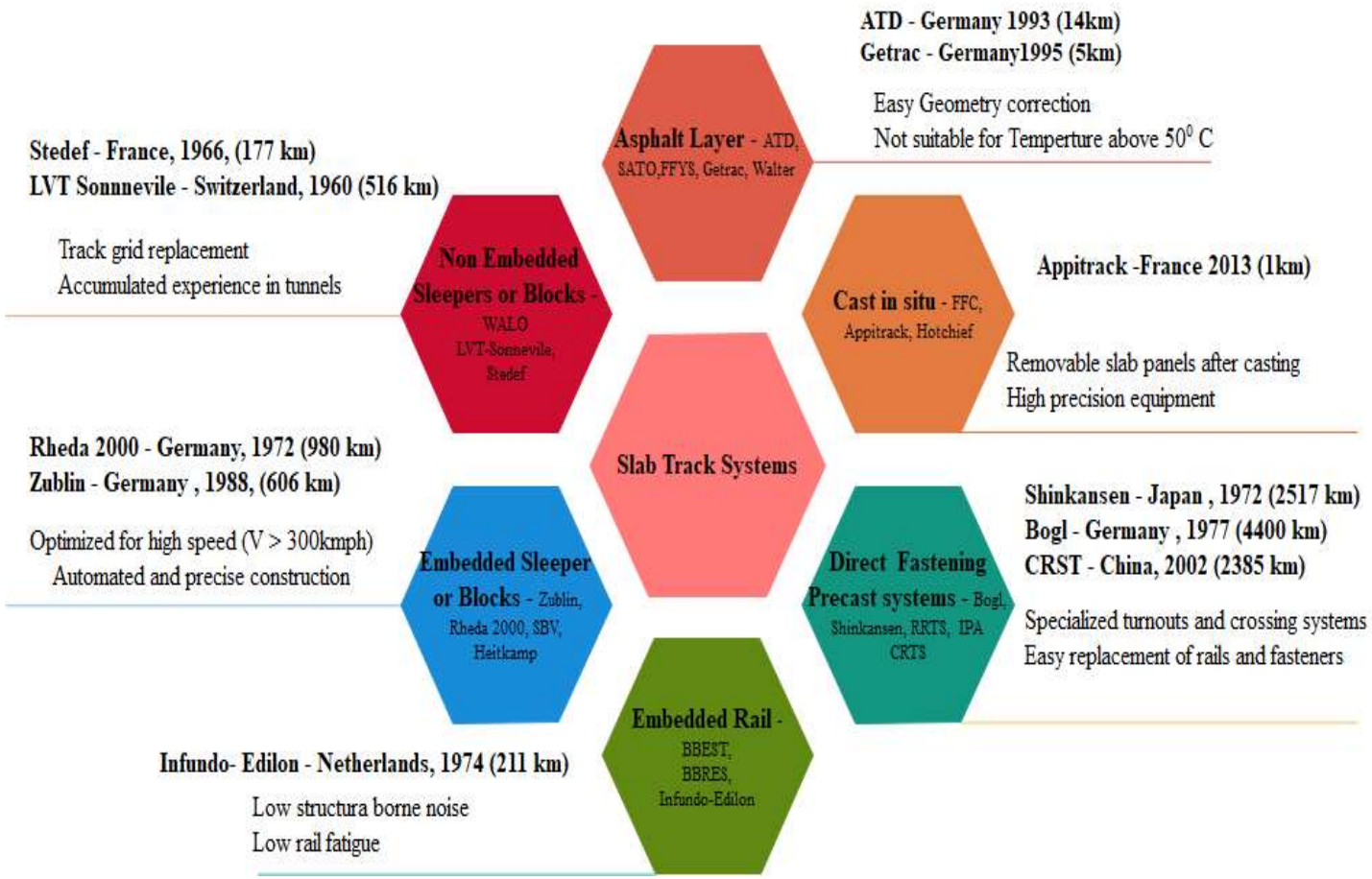

Figure 0.3 Most widely used slab track systems

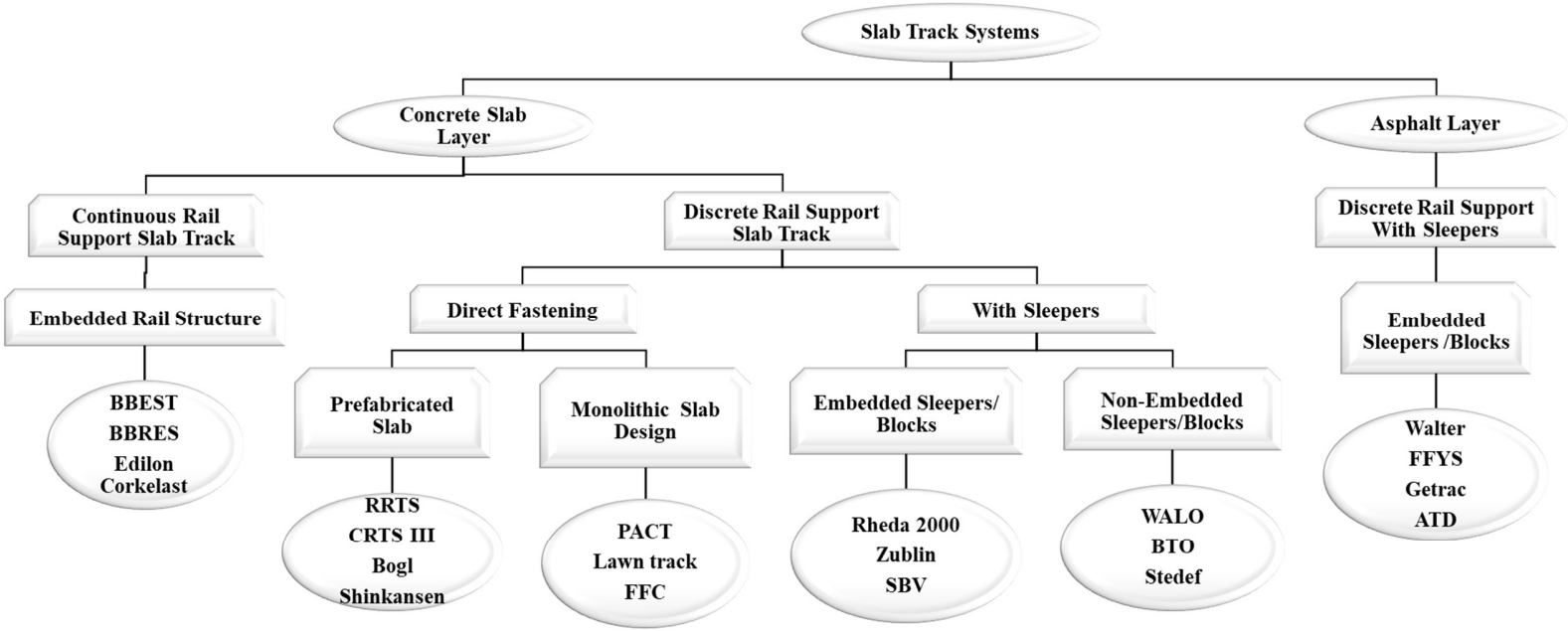

Figure 0.4: Various slab track systems

1.3.1 Prefabricated concrete slab track system

Prefabricated concrete slab track systems have gained popularity in railway networks worldwide due to their numerous advantages in design, implementation, and maintenance. These systems utilize direct rail fastening on precast concrete plates, eliminating the need for wet concrete during the construction process. They are widely used in urban rail systems and interregional high-speed rail systems, particularly in areas where noise and vibration control are essential.

The Shinkansen, Japan's bullet train system, features a slab track design constructed using precast concrete. First built in 1964, the Shinkansen high-speed railway connected Tokyo and Osaka. Welded rails and precast concrete slabs create the Shinkansen slab track system. tracks are preassembled at depots as 200-meter-long components and then transferred on trolleys along the temporarily installed tracks, which have a gauge of 1435 mm. The gaps between slabs are filled with cement-emulsified mortar made from asphalt (CA mortar) while the workers move on temporary rails. The slabs, with a gauge of 3000 mm, are transported to the construction site and connected with standard fasteners. This system provides a reparable and innovation-friendly solution for high-speed rail tracks (Prabhakaran et al., 2022).

Another example of a prefabricated concrete STS is Bögl slab track. This track system was first installed in Karslfeld, Germany, in 1977, to provide long-endurance, maintenance-free operation for high-speed lines. Similar to Shinkansen system, the Bögl slab track may be employed in various settings, including cuttings, hills, bridges, viaducts, and tunnels. The Bögl slab track technology was used to construct 12 km of China's Beijing-Tianjin high-speed railway line. The Bögl method uses concrete slabs that are 20 cm thick, 6.45 m in length, and either 2.55 or 2.80 m wide. They are manufactured from B55 steel fiber-reinforced concrete. The slabs are prestressed in lateral direction and reinforced longitudinally. The incorporation of spindles in the slabs allows for adjustments in the slab system (S. Zhou et al., 2020)(Edwards et al., 2020).

Prefabricated concrete slab track systems offer several advantages, including increased track quality, reduced labor requirements, and decreased risk of failure. These systems provide reparable and innovation-friendly solutions for high-speed rail projects. By utilizing prefabricated components and advanced construction techniques, these systems contribute to the efficient and cost-effective implementation of high-speed rail networks.

1.3.2 Slab track structure with asphalt concrete roadbed

Using asphalt layers in railway construction, similar to those commonly used in highway construction, has significantly improved the structures for slab tracks that require rigid foundation. This advancement has enabled the construction of track and support structures of superior quality with a longer lifespan. These structures can handle the significant increase in rail traffic volumes, revenue ton-miles, axle loadings, and tonnages seen globally(AASHTO, 1993). Sleepers are placed over an asphalt-concrete roadbed layer using ordinary paving equipment in ballast-less constructions. This method allows for achieving a remarkable level of accuracy, with a precision of 2 mm and the capacity to compensate for a cant deficit of up to 180 mm. The asphalt layer serves as a solid and smooth base for the sleepers, providing stability and optimal performance (Michas, 2012). A different method is directly placing concrete plates onto an asphalt-concrete layer. Asphalt does not need hardening; therefore, the concrete plates may be loaded and unloaded immediately after cooling (Edwards et al., 2020).

High-speed rail systems are an example of slab track design with an asphalt-concrete roadbed. Using asphalt-concrete layers has become common in these projects, enabling the construction of rigid and durable track systems. The asphalt layer is first applied to the prepared subgrade, providing a solid and resilient foundation. The sleepers, typically made of concrete or other materials, are placed on the asphalt layer at predetermined intervals. The sleepers support the rail tracks, ensuring stability and even load distribution. One advantage of using an concrete roadbed in slab track structures is ease of installation. The asphalt layer can be quickly and efficiently placed using ordinary

paving equipment, minimizing construction time and labor requirements. Additionally, the precise level of accuracy achieved through this method ensures a smooth and consistent track surface, reducing vibrations and enhancing passenger comfort. Moreover, the durability of asphalt-concrete roadbed contributes to longevity of track system. The asphalt layer protects against moisture, preventing subgrade erosion and preserving the structural integrity of track. This results in reduced maintenance needs and increased overall lifespan.

1.3.3 Monolithic slab track designs

Since the 1970s, monolithic slab track systems have been created, and the direct rail attachment methods distinguish them from bolted-to steel or concrete slabs. This slab track system is particularly suitable for bridges or viaducts, where continuous monolithic slabs can be installed without sleepers (Freudenstein, 2010). The direct fixation system used in this method allows for vertical adjustment of approximately 50 mm and lateral adjustment of 46 mm (Freudenstein, 2010). Regarding benefits, monolithic slab track designs are applied in areas with weak and soft soil layers. By using this system, the minimum requirements for the substructure can be reduced, leading to cost savings in ground improvements in certain situations (Hoff et al., n.d.). The continuous, stiff, and rigid slab, supported by elastic beams, provides stable and durable track structure.

An example of monolithic slab track design application can be found in high-speed rail projects. These projects often involve bridge and viaduct construction to accommodate the high-speed trains. Using monolithic slabs without sleepers allows for a streamlined and efficient track system on these elevated structures. The direct rail fastening system ensures connection between rails and slabs, maintaining track stability and integrity. Monolithic slab track designs also offer advantages in areas with challenging soil conditions. When the subgrade is prone to local settlement, the continuous slab structure can help distribute the load and minimize the impact of settlement on the track. As a result, there is a lower chance of track damage, and less maintenance is required.

1.3.4 Embedded rail slab track system

Slab track systems with embedded rails, also known as Embedded Rail Structure (ERS), are designed to provide continuous support for rail by embedding it underneath concrete. The rail is encased in elastic materials, such as cork and polyurethane, except for its head. As a result, no additional materials are required for maintaining track gauge during regular use. In the construction phase, the rail is secured within a U-steel frame and fine-tuned using top and bottom adjustment methods. Meanwhile, the continuous concrete slab permits unrestricted settlement on the underlying soil.(Edwards et al., 2020). ERS slab track systems offer several advantages. Firstly, they absorb dynamic forces, resulting in improved track stability and reduced wear on the rail. Secondly, they contribute to noise reduction, making them suitable for use in areas where noise pollution is a concern. Additionally, the life span of the rails is increased, leading to reduced maintenance requirements.

The ERS system also allows for free settlement, minimizing the potential for track deformations. Furthermore, ERS can provide a smooth surface for rail crossings, decreasing the construction height required for level crossings (Edwards et al., 2020). A pilot track utilizing the ERS system in the Netherlands was constructed in 1976 for trains traveling at speeds of up to 160 km/h. The initial test results were promising, and subsequent pilots were carried out in October 1999, demonstrating a 5 dB reduction in noise levels. The ERS system also resulted in a 60% reduction in the required UIC54 elastic design to secure the rails (Edwards et al., 2020). Deck track is another ballast-less track system that addresses settlement issues and reduces life-cycle costs. This track system is designed for use on relatively soft soils and can employ embedded rails or direct fastening. The concrete deck of the track acts as a hollow tube with a weight equal to that of the removed soil, resulting in reduced vibration and settlement due to the structure's weight (Vossloh, 2019). After a five-year testing period, the concrete structure and embedded track system of the deck track showed no signs of deterioration. The most

expansive cracks observed were at casting joints and measured less than 0.1 millimeters in width, which is considered acceptable (Edwards et al., 2020).

1.3.5 Sleeper or block embedded in concrete

The Rheda 2000 slab track system is a type of sleeper or block embedded in concrete, widely used in railway construction since its initial installation in 1970. Over the years, the system has undergone continuous development and improvements. In the original design, reinforced concrete was put into the mono-block sleepers. However, the German Rheda system was improved in the Rheda 2000 system, created for use in commuter traffic applications under Rheda City. Settlement is a significant factor in these slab track systems; however, track structure of Rheda 2000 system allows for correction in both lateral and longitudinal directions. The Rheda system was created with the optimization of design and consistency in track construction as its key goals. The rails are held firmly in place by deliberately placed geometrical supports. These high-quality concrete supporting points provide a strain-resistant bond between the rail fastening system and the concrete track layer (CEBECI, 2020). The Rheda systems have seen various versions over time, but the Rheda 2000 system stands out as a significant improvement. In addition to rail and sleeper construction, cast concrete track layer is a distinctive feature. The rail fastening method allows for fine-tuning to account for long-term differential settlement of substructure, and track components can still perform their intended functions.

The cost-effectiveness of Rheda system lies in its ability to accommodate a range of track situations, including earthworks, bridges, and tunnels (Edwards et al., 2020). Another notable system is the Zublin system (J. Matias, 2019), which dates back to 1974 and offers an affordable construction method. The concrete sleepers are twin blocks, also known as monoblocs, on a solid concrete base plate. The concrete sleepers, known as "twin blocks," are two pieces joined together at the top. Reinforcing bars improve the sleepers' grip on the concrete and ensure precise geometry during installation. The geometry of sleepers is designed to accommodate Vossloh AG's rail fastenings (Giunta & Praticò, 2017). The twin-block sleepers already have the rail fasteners attached.

Mechanization reduced labor costs, and optimized track manufacturing are all goals of the Zublin system.

The construction process of the Zublin system (J. Matias, 2019) involves preparing and constructing the sub-base and base course. Subsequently, the concrete bearing slab is reinforced, concreted, and compacted without interference from the sleepers. The sleepers are then fixed and placed by compacting them with pre-mounted fasteners. Rails are subsequently installed, and the slab's surface is implemented manually. The concrete is left to harden, and finally, the frames are disconnected from the sleepers(Esveld and Markine, 2003). The use of sleepers or blocks embedded in concrete systems, such as Rheda 2000 and Zublin systems, provides reliable and cost-effective solutions for railway construction. These systems offer improved track quality, long-term durability, adjustable frameworks, and reduced maintenance.

1.3.6 Clamped and continuously supported rail

Clamped and constantly supported rail installations provide stable track support and reliable fastening. This method involves attaching rail to a support structure at regular intervals along its length, ensuring stability and reducing the risk of lateral movement. The continuous support system helps distribute the load evenly, improving track performance and reducing maintenance requirements.

One example of a clamped and continuously supported rail system is the Pandrol FASTCLIP. This system utilizes elastic clips to attach the rail to a concrete or steel baseplate, which is supported by sleepers or a concrete slab. The clips provide lateral resistance, preventing the rail from shifting under dynamic loads while allowing vertical movement to accommodate thermal expansion and contraction(Esveld & Markine, 2003). There are numerous advantages to clamped and continuously supported rail systems. Firstly, the clamping mechanism enhances track stability, reducing need for frequent adjustments and maintenance. The continuous support also improves load distribution, minimizing stress concentrations and extending lifespan of track components. In addition to boosting passenger comfort and lowering environmental impact, this method also helps

lower noise and vibration levels. The continuous support of the rail in clamped systems allows for efficient installation and alignment. The rail is securely fastened to the baseplate, ensuring precise gauge control and alignment accuracy. This eliminates the need for additional materials or procedures to maintain track geometry, streamlining the construction process and reducing costs. Clamped and continuously supported rail systems find applications in various railway environments, including high-speed lines, heavy freight routes, and urban transit networks. These systems offer reliable performance and long-term durability, making them suitable for high-demand and demanding operating conditions. Table 1.1 explains the distinctive characteristics of different slab tracks used worldwide.

In summary, the global adoption of slab track systems reflects their proven advantages in terms of stability, durability, and reduced maintenance compared to conventional ballasted tracks. Various structural configurations such as prefabricated slabs (Shinkansen system in Japan), sleeper-embedded concrete slabs (Rheda 2000 in Germany), monolithic slabs, embedded rail structures, and asphalt-supported systems have been successfully implemented in countries including Japan, Germany, China, and Switzerland, each tailored to specific operational and geotechnical conditions. These innovations have demonstrated the capability of slab track systems to support high train speeds, heavy axle loads, and long service lives with minimal intervention. However, despite extensive international experience, India is only beginning to integrate slab track technology through projects such asm Mumbai–Ahmedabad High-Speed Rail (MAHSR) corridor and Regional Rapid Transit System (RRTS), which remain under development. This transition highlights the importance of evaluating the mechanical behavior, component interaction, and long-term performance of slab track systems under Indian climatic and operational conditions. The subsequent chapters, therefore, focus on critically examining the static, dynamic, and fatigue behaviours of slab track structures to establish a framework suited to the Indian railway context.

Table 0.1 Distinctive characteristics of slab tracks used worldwide (Bastin, 2006); (Esveld et. al 2003); (Lichtberger, 2011)

System of Slab-Based Tracks	Country	Year, first operation	Total Track Span (km)	Speed (km/h)	Principal Characteristics
Shinkansen	Japan	1972	2517	300	The prefabricated concrete slab, supported on HBL, is 4.95 m x 2.34 m x 0.19 m in size. In tunnels, the slab thickness is 0.16 m. It has a 4 cm-thick CAM layer under the concrete slab.
Rheda	Germany	1960	2205	300	The grade of the concrete slab is C30/37. The length of sleeper is 2600 mm. The system is very flexible, supported by 30 cm thick HBL and a 50 cm thick FPL.
Rheda 2000	Germany, China, Spain, Netherlands	1972	980	350	The author uses B 355 W60M SBS twin-block modified sleepers in this case. The Vossloh 300 elastic rail fastening system is used.
RRTS	India	2015	82.12	180	The concrete slab is prefabricated. High-quality concrete provides these track slabs strength and a professional design.
Shinkansen:Bullet Train	India	2015	508 (In Progress)	320	Slab track technology made of precast concrete is 4.90 m x 2.2 m x 0.19 m in size. In tunnels, slab thickness is 0.16 m. A 4cm thick CAM layer beneath the slab creates a 2.86 m x 0.8 m void.

82

CRTS III	China	2002	2385	350-400	The track's asphalt surface measures 5.6 m x 2.5 x m 0.2 m. Self-compacting concrete is utilized. The base has a 30 cm thick HBL and a 50 cm thick FPL.
Sonnevile-LVT	Swiss	1960	1031	250	The rubber boot protects the sleeper's robust cushion, providing excellent flexibility and vibration absorption. It is easy to construct. However, water may cause the rubber boot to erode. The Vossloh is the fastener W14, and the Pandrol e-clip is employed.
Stedef	France	1966	177	250	Like Sonnevile-LVT, the critical feature is a polyurethane membrane that blocks water and protects the rubber boot from deterioration.
Infundo-Edilon	Netherland	1974	211	160	Essential characteristics include quick assembly, minimal noise output, and a rail held in place by elastic material in the groove. The Concrete Slab Layer (CSL) is 40 cm in depth and 2.4 m in width.
OBB-Porr	Austria	2012	130	250	All slab surfaces in contact with sealing concrete are coated with a 2.5–3 mm thick layer of resilient polyurethane cement mixed with rubber granules. With a one-tonne mass per linear metre, the BB-Porr design system effectively mitigates vibrations.

109

Sato	Germany	1996	36	250-300	The Y-shaped steel sleeper is welded to the asphalt subgrade.
WALTER	Germany	1993	9.4	200	An asphalt layer supports the mono block sleeper. A clamp fastening is employed; every second sleeper has a clip glove at the halfway point.
Bogl	Germany	1977	4400	200	The slab is 6.45 m x 2.55 m (2.80 m) x 20 cm. It is a steel fibre concrete slab, reinforced longitudinally by GEWI bars and laterally prestressed.
Zublin	Germany	1988	606	300	The CBL measures 2.25 m x 2.8 m x 0.28 m and contains longitudinal and lateral steel reinforcement at the bottom. It is supported by 30 cm thick HBL and 50 cm thick FPL.

1.4 Components of Slab Track System

1.4.1 Rail

The rail is the primary load-bearing and guiding element in a slab track system, typically made of high-strength steel with profiles such as UIC 60 to ensure stiffness and fatigue resistance. It transmits vertical, lateral, and longitudinal forces to the underlying structure, maintains wheel guidance, and accommodates thermal expansion. In dynamic modeling, it is represented as an Euler-Bernoulli or Timoshenko beam to capture bending and shear effects (Esveld, 2001) .

1.4.2 Rail Pad and Fastening Systems

In railway track dynamics, rail pad is a fundamental component due to their substantial influence on the overall track stiffness and dynamic behavior. Softer rail pad allows for greater rail deflection under train-induced loads, enabling an increased distribution of axle load across a larger number of sleepers, which helps reduce localized stresses. Additionally, soft rail pads are effective in attenuating transmission of high-frequency vibrations to sleepers and ballast, thereby improving vibration isolation within the track structure. Rail pads are typically modeled using a spring–damper formulation, in which spring is commonly treated as linear and damping is considered proportional to deformation rate. Both stiffness and damping characteristics are critical to dynamic performance, particularly within the ranges of sleeper resonance frequencies(Padhi et al., 2022).

Numerical and experimental investigations confirm that the inclusion of rail pad behavior is essential for realistic track modeling and accurate reproduction of dynamic responses. For instance, analyses of pad stiffness and wheel polygonization effects have underscored how pad stiffness significantly influences vehicle–track interaction dynamics(Restrepo-Barrientos et al., 2025) . Empirical studies have demonstrated that reducing rail pad stiffness can effectively decrease wheel–rail contact forces, albeit at the cost of increased rail displacement a trade-off that must be carefully considered when optimizing pad stiffness for dynamic performance (Song et al., 2020). Similarly,

sensitivity analyses of rail pad parameters emphasize that stiffness variations have a marked effect on vertical dynamic behavior, influencing rail displacement and load distribution across sleepers (Maider et al., 2017).

1.4.3 Concrete Slab

The concrete slab is primary load-bearing components of slab track system, serving as a rigid structural layer that directly supports rails and distributes train-induced loads to underlying base. Unlike conventional ballasted tracks, where the ballast serves as a load distributor and damper, the slab itself provides structural stability, dimensional accuracy, and durability. Its rigid nature ensures consistent track geometry, which is essential for maintaining the stringent alignment tolerances required in high-speed railway operations (Michas, 2012)and (Gautier, 2015). Concrete slabs are typically reinforced to resist flexural stresses and fatigue damage caused by repeated train loading. Their geometry, thickness, and reinforcement design significantly influence the stiffness and service life of the track structure. A well-designed slab ensures that axle loads are transferred efficiently to the supporting layers, thereby minimizing stress concentrations and settlement issues in the substructure(Tayabji & Bilow, 2001; Yu et al., 2012). However, the high stiffness of the slab also reduces the system's ability to absorb vibrations, necessitating the inclusion of intermediate elastic layers such as cement asphalt mortar (CAM) to improve vibration isolation and reduce dynamic forces transmitted to the subgrade (Q.-Y. Xu & Zeng, 2009; Zeng et al., 2015).Although initial construction cost of concrete slabs is higher compared to ballasted systems, their superior fatigue resistance, minimal maintenance requirements, and longer service life make them more sustainable for modern high-speed and heavy-haul railway networks. Therefore, the concrete slab not only serves as a structural support element but also as a key determinant of the long-term performance and cost-effectiveness of slab track systems (Ferreira et al., 2024; Ren et al., 2021; Y. Xiao et al., 2020).

1.4.4 Cement Asphalt Mortar (CAM) Layer

The CAM layer functions as elastic interlayer between concrete slab and hydraulically bonded base, primarily to attenuate vibrations and redistribute stresses induced by repeated wheel–rail interactions. Its viscoelastic nature enhances energy dissipation and contributes significantly to fatigue resistance, thereby preventing crack initiation in the overlying slab. Recent studies have confirmed that the mechanical properties of CAM, particularly its dynamic modulus and temperature sensitivity, play a vital role in improving the service life of high-speed slab tracks (B. Liu & Liang, 2017; Q. Wang et al., 2011) and (Rutherford et al., 2014).Furthermore, numerical modeling has demonstrated that incorporating CAM reduces vertical accelerations and stress concentrations, which directly improve ride comfort and track durability (C. Liu et al., 2019); (Park et al., 2024; Zhang et al., 2025)

1.4.5 Hydraulically Bonded Layer (HBL)

The Hydraulically Bonded Layer (HBL), typically constructed from cement-treated base or lean concrete, provides a stiff and bonded platform for supporting the concrete slab and transferring axle loads into the subgrade. The HBL must balance stiffness and flexibility: insufficient stiffness can result in excessive settlement, while excessive rigidity may induce reflective cracking in the slab above (Esveld, 2001) . Experimental and finite element studies have emphasized that the thickness, material composition, and curing quality of the HBL significantly influence long-term structural stability in high-speed slab track systems (Jiang et al., 2014; L. Wang et al., 2022). Recent research also highlights the role of HBL in minimizing frost-induced degradation and enhancing durability under varying climatic conditions (X. Liu et al., 2010; Z. P. Zeng et al., 2022).

1.4.6 Subgrade

The subgrade serves as natural foundation for slab track systems, and its performance critically determines the long-term stability and alignment of these systems. Variability in subgrade stiffness or differential settlement can lead to track irregularities, increased dynamic stresses, and potential structural damage to the slab and HBL layers. Field

investigations and numerical simulations have demonstrated that weak subgrades often necessitate soil stabilization techniques, such as cement treatment, geogrid reinforcement, or deep soil mixing, to meet the demands of high-speed rail (X. Sheng et al., 2004; Zhao et al., 2021). Recent research has further indicated that the subgrade track interaction is particularly sensitive under repeated loading and high-speed conditions, making resilient subgrade design a prerequisite for sustainable slab track systems (Cai et al., 2022; M. Chen et al., 2021; Cui & Ling, 2021).

1.5 Scope of High-Speed Rail in India

India is on the verge of a transformative leap in railway transportation through the implementation of its first dedicated high-speed rail corridor: the Mumbai–Ahmedabad High-Speed Rail (MAHSR) project. This project marks the country's entry into the realm of advanced rail infrastructure, aiming to offer faster, safer, and more energy-efficient mobility for millions of passengers.

The MAHSR spans approximately 508 km connecting Mumbai (Maharashtra) and Ahmedabad (Gujarat), with planned operational speeds of up to 320 km/h. The project is being developed by National High-Speed Rail Corporation Limited (NHSRCL) with technical and financial support from Government of Japan, adopting the proven Shinkansen (E5 Series) technology. The alignment includes multiple elevated viaducts, bridges, tunnels, and dedicated stations designed for high-speed rail operations. A notable feature of this project is use of precast slabs for track, which is being implemented for the first time on such a scale in India. This technology involves the use of precast reinforced concrete slabs supported by CAM layer placed on a base concrete bed. The track system also incorporates UIC 60 rails, resilient rail pads, and continuous welded rail (CWR) for enhanced ride quality and minimal maintenance.

From an engineering perspective, the MAHSR corridor provides a unique and relevant case for evaluating the static, dynamic, and fatigue behaviors of slab track systems under Indian environmental and geotechnical conditions. The project passes through diverse terrains, including coastal zones, river crossings, and seismic regions,

making it ideal for investigating the influence of subgrade stiffness, temperature variation, and vibration control measures on long-term track performance.

As this corridor is India's pilot high-speed railway line, its success will serve as a benchmark for upcoming corridors planned under the National Rail Plan. The design standards, materials, and construction practices developed through MAHSR will play a key role in shaping future high-speed rail infrastructure across the country.

In this study, the MAHSR slab track configuration and material specifications have been considered the reference model for finite element modelling, dynamic simulations, fatigue analysis, and parametric studies. The findings are expected to contribute meaningfully to optimization and standardization of high-speed railway track design in India.

1.6 Objectives of the Study

This study aims to evaluate structural performance of precast slab track systems for high-speed rail applications. The key objectives are:

1. The study aims to evaluate the static response of the precast railway slab-track system through a detailed finite-element-based parametric study, with a focus on stress distribution, deflection profiles, and load transfer efficiency under standard wheel loading conditions.
2. The study aims to mitigate vibrations in the high-speed railway slab-track system by introducing a resilient slab-mat layer and evaluating its effects on vibration amplitude, damping behavior, and resonance frequency characteristics.
3. The study also aims to investigate the dynamic vehicle-track interaction of the precast slab-track system, evaluating the influence of key structural and operational parameters such as train speed, axle load, and rail-pad stiffness.
4. The aim is to analyze the fatigue behavior of the Cement-Asphalt Mortar (CAM) layer of the precast slab-track structure through cyclic laboratory testing, and to develop an empirical relationship between stress level and fatigue life under repetitive load conditions.

1.7 Significance of the Research

This research addresses several critical challenges in design and performance optimization of precast track systems for high-speed rail applications, particularly under Indian environmental, operational, and geotechnical conditions. As India embarks on an ambitious transformation of its railway infrastructure through projects like the Mumbai–Ahmedabad High-Speed Rail (MAHSR) and National Rail Plan 2030, the need for scientifically validated, efficient, and sustainable track systems becomes increasingly urgent.

One of the core challenges in high-speed slab track design is ensuring **dynamic stability and passenger comfort**, which is heavily influenced by rail–track interaction, vibration levels, and noise transmission. This study contributes to mitigating these issues by incorporating nonlinear rail pad behaviors and assessing the damping performance of slab mat layers under dynamic loading.

A second critical aspect addressed by this research is the **fatigue resistance** of vital structural components such as CAM and concrete slabs. Through laboratory testing and finite element simulations, this study aims to understand degradation mechanisms and improve long-term durability of these materials under repeated loading thus reducing life-cycle costs and minimizing maintenance interruptions.

Beyond technical benefits, the research is closely aligned with the **United Nations Sustainable Development Goals (SDGs)**, reinforcing its societal and environmental relevance. As illustrated in Figure 1.5 (United Nation Development Programme, 2024) the study contributes to **eight core SDGs**, supporting sustainable development in the following ways:

SDG 3 (Good Health and Well-Being): By reducing noise and air pollution through high-speed electric rail systems, the project contributes to improved public health and commuter well-being.

SDG 7 (Affordable and Clean Energy): Integration of renewable energy in station design and traction systems supports reduced fossil fuel dependency and enhances energy efficiency.

SDG 8 (Decent Work and Economic Growth): Large-scale infrastructure development promotes industrial innovation, job creation, and skilled employment in the rail sector.

SDG 9 (Industry, Innovation, and Infrastructure): The adoption of slab track systems fosters resilient infrastructure with long-term performance and reduced maintenance needs.

SDG 11 (Sustainable Cities and Communities): Enhanced mobility through high-speed rail reduces urban congestion, improves regional connectivity, and promotes low-emission travel alternatives.

SDG 12 (Responsible Consumption and Production): The use of optimized CAM mix designs and predictive maintenance strategies minimizes material wastage and extends the infrastructure's lifespan.

SDG 13 (Climate Action): Transitioning freight and passenger movement from high-emission modes to electrified rail significantly lowers carbon emissions.

SDG 17 (Partnerships for the Goals): International collaboration in high-speed rail technology, funding, and policy-making accelerates India’s integration into global sustainable transport initiatives.

In India, several transformative railway projects such as high-speed rail corridors, dedicated freight corridors, electrification upgrades, and track modernization reflect the country’s commitment to the SDGs. By adopting innovative slab track solutions and enhancing computational design capabilities, this study contributes to engineering knowledge and supports India’s broader vision of a resilient, environmentally responsible, and globally aligned railway network. In conclusion, this research is of strategic national importance. It bridges theoretical modelling, experimental validation,

and sustainable design, thereby offering a comprehensive solution for implementation of next-generation high-speed rail infrastructure in India and beyond.

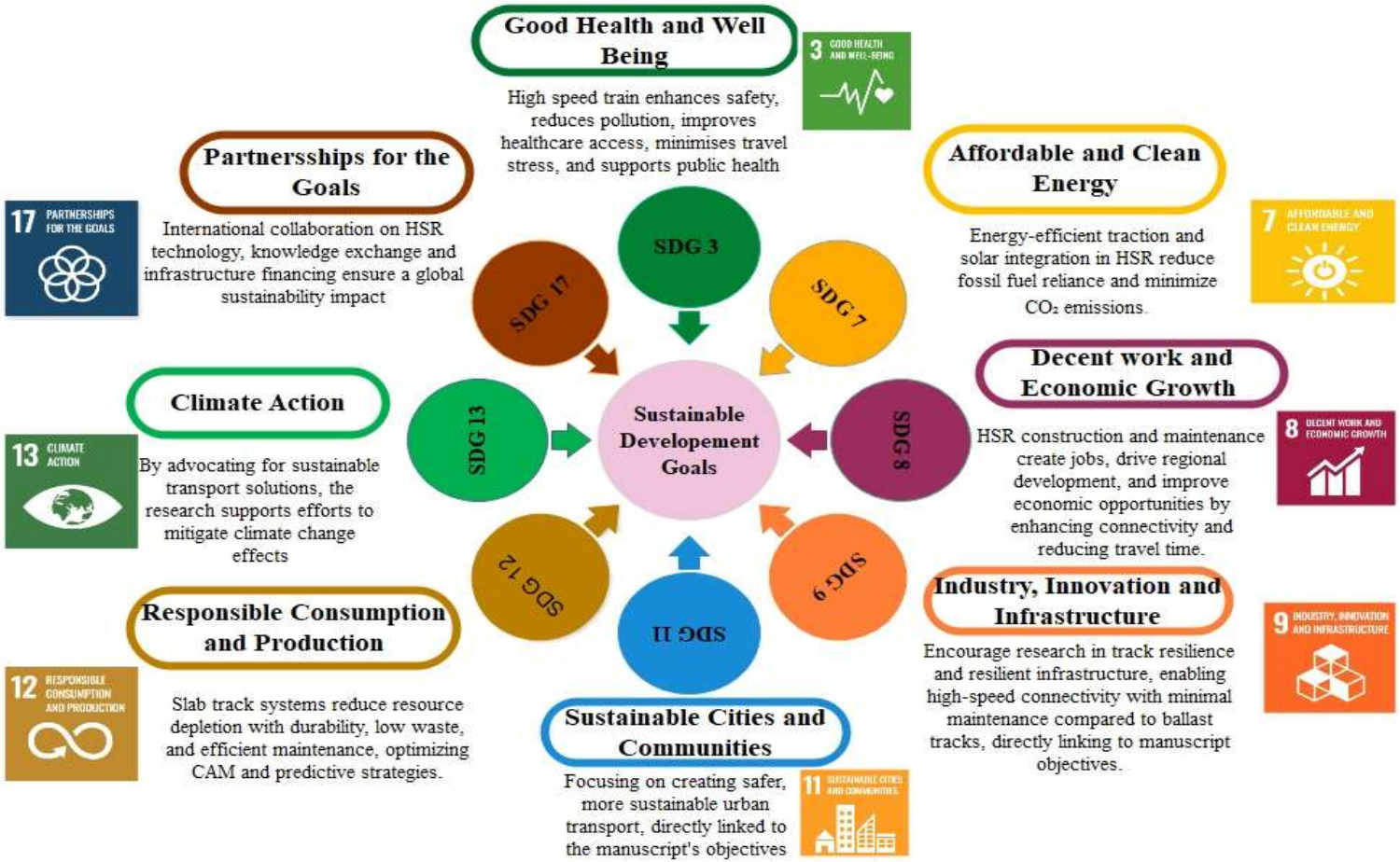

Figure 0.5 Coordination of research with sustainable development goals

1.8 Outline of the Thesis

This thesis is organized into eight chapters, each addressing specific component of research from background studies to numerical modelling, detailed analysis, and concluding insights.

Chapter 1: Introduction provides an overview of railway track systems, with emphasis on slab-track configurations and their components. It presents the motivation for the study, the scope of high-speed rail development in India, research objectives, and significance of the work.

Chapter 2: Literature Review summarizes previous research on modelling track components, static and dynamic behavior of rail systems, fatigue performance of cement asphalt mortar (CAM), and identifies research gaps relevant to high-speed slab-track applications. This chapter establishes the theoretical foundation and justifies the need for the present study.

Chapter 3: Numerical Simulation and Methodology. defines the modelling framework, simulation techniques, and analytical procedures used in the study. It details the modelling of the slab-track system, meshing, and boundary conditions, as well as the methodologies developed for evaluating the static response, vibration characteristics, vehicle-track interaction, and fatigue behavior of CAM.

Chapter 4: Static Response Results and Discussion present the numerical results for Objective 1, including static deformation patterns, stress distributions, and comparative analysis between ballast and slab-track systems. It also includes parameter studies related to rail pad stiffness, CAM stiffness, subgrade stiffness, slab thickness, CAM thickness, and HBL thickness.

Chapter 5: Vibration Response Results and Discussion address the analyzing the modal characteristics and vibration behavior of the slab-track system. Both time-domain and frequency-domain analyses are presented, along with parametric investigations on slab-mat stiffness, damping, thickness, and vehicle-speed effects.

Chapter 6: Dynamic vehicle–track interaction Results and Discussion correspond to Objective 3. This chapter includes model validation, influence of track irregularities and train speed, and effect of key parameters such as rail pad stiffness, CAM stiffness, and subgrade stiffness on dynamic interaction forces and system response.

Chapter 7: Fatigue Response Results and Discussion present Objective 4 and focusing on the static flexural strength, fatigue life analysis, strain evolution, and modulus degradation of CAM under cyclic loading. The chapter also discusses fatigue damage mechanisms relevant to slab-track applications.

Chapter 8: Conclusions, Future Scope and Social Impact summarize the major findings of the study across all objectives, outlines the future research directions, and highlights the societal impact of developing reliable and durable slab-track systems for India's high-speed rail corridors.

57 **Publications** resulting from this research work are listed at the end of the thesis.

CHAPTER 2: LITERATURE REVIEW

2.1 General

The preceding chapter discussed the fundamental concepts of High-Speed Railway slab track systems, including their development, structural components, and relevance in the Indian HSR context. Building upon this foundation, the present chapter offers a detailed review of existing literature pertaining to mathematical modelling and performance evaluation of HSR track structures. The review encompasses studies related to static and dynamic responses of slab track systems, vibration mitigation strategies, and fatigue behavior of CAM under different operational conditions. By identifying limitations and research gaps, this review establishes the foundation for the present study, which aims to develop a more representative framework for analyzing slab track systems within the broader context of high-speed railway engineering.

2.2 Mathematical Modeling of Track Components

2.2.1 Rail beam model

The classical Euler–Bernoulli theory considers bending deformation and translational inertia while neglecting both shear deformation and rotary inertia. This theory is suitable for low-frequency analyses and slender beams, where these effects are minimal.

For transverse vibrations, a rail beam characterized by a distributed mass per unit length $m = A\,\rho$ flexural rigidity (EI), and subjected to an external load q (x, t), is governed by the following partial differential equation(Dahlberg, 2003):

$$EI\frac{\partial^4 w(x,t)}{\partial x^4} + \rho A\frac{\partial^2 w(x,t)}{\partial t^2} = \mathrm{q(x,t)} \qquad (2.1)$$

where:

w (x, t) is transverse deflection, ρ is material density, A is cross-sectional area, EI is bending stiffness, q (x, t) is externally applied load. This formulation assumes no damping. For free vibrations (no external force), the solution typically takes the form:

$$w(x,t) = X(x)T(t) = X(x)sin\omega t \qquad (2.2)$$

where X(x) represents spatial mode shape and ω is angular frequency.

The Timoshenko beam theory extends the E-B model by incorporating both rotational inertia and shear deformation, making it more accurate for modeling higher-frequency vibrations or shorter, thicker beams, such as rails (Blanco et al., 2019). The theory treats transverse deflection w (x, t) and rotation angle ψ(x, t) as independent variables. The governing equation for deflection is:

$$EI\frac{\partial^4 w(x,t)}{\partial x^4} + \rho A\frac{\partial^2 w(x,t)}{\partial t^2} + \rho I\left(1 + \frac{E}{kG}\right)\frac{\partial^4 w(x,t)}{\partial x^2 \partial t^2} + \frac{\rho^2 I}{kG}\frac{\partial^4 w(x,t)}{\partial x^4} = q(x,t) \qquad (2.3)$$

where: G is the shear modulus, k is the shear correction factor, I is the second moment of area, and other symbols are as previously defined. This theory highlights the contribution of shear flexibility and rotary inertia, particularly significant at higher vibration modes. When shear deformation is suppressed by letting k approach infinity and rotary inertia is neglected by letting $I\rho$ approach zero, the Timoshenko beam equation simplifies to the classical Euler–Bernoulli form, as discussed in studies such as (Dahlberg, 2003) have shown that for a UIC60 rail, shear deformation becomes significant above 500 Hz, where the E-B theory overestimates the natural frequency by approximately 10–15%.

2.1.2 Rail beam on elastic foundation model (BOEF)

Winkler first introduced Beam on Elastic Foundation (BOEF), also known as Winkler model, which represents the earliest and most classical formulation of rail–foundation interaction. In this concept, rail is modelled as an infinitely long Euler–Bernoulli beam supported by a continuous distribution of vertical springs as shown in Figure 2.1. The foundation reaction is proportional to local beam deflection, leading to the governing relationship:

$$EI\frac{d^4w(x)}{dx^4} + kw(x) = q(x) \tag{2.4}$$

In this equation, w(x) represents the rail deflection, q(x) indicates the applied distributed load, EI refers to the flexural rigidity of the rail, and k signifies the foundation modulus.

(Kerr, 2000) and (Esen, 2011) highlighted that although mathematically elegant and simple to apply, the BOEF model has several drawbacks. It assumes a linear, continuous, and time-independent support, neglects shear deformation, and allows the development of tensile stresses in the supporting springs, which is unrealistic for granular soils. This limitation often leads to unphysical predictions, such as track uplift near wheel loads. (Kouroussis et al., 2011) emphasise that more advanced nonlinear models have been developed to address these deficiencies.

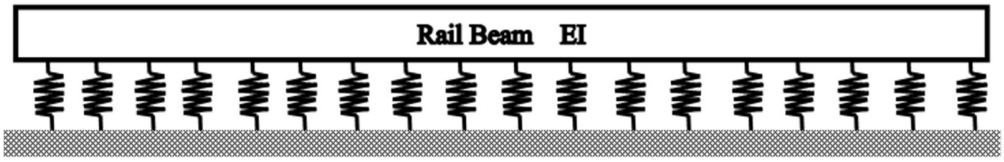

Figure 0.1 A schematic showing a continuous beam on Winkler springs

2.1.3 Rail beam on Discrete Supports

(Esveld, 2001) and (Dahlberg, 2004) proposed discrete support models to overcome Winkler's limitations, where the track is represented by localized supporting elements. In this configuration, the rail rests on a spring–damper system representing the rail pad, beneath which a sleeper beam is introduced as shown in Figure 2.2. The sleeper itself is supported by ballast and subgrade, typically modelled as another spring–damper layer. (Zhai & Sun, 1994)and (Connolly et al., 2020) demonstrated that this representation is closer to real track mechanics, as it accounts for rail pad compliance, sleeper flexibility, and ballast damping. It is particularly effective for studying the dynamic responses of tracks under moving loads and serves as the basis for finite element and lumped-parameter simulations of railway systems.

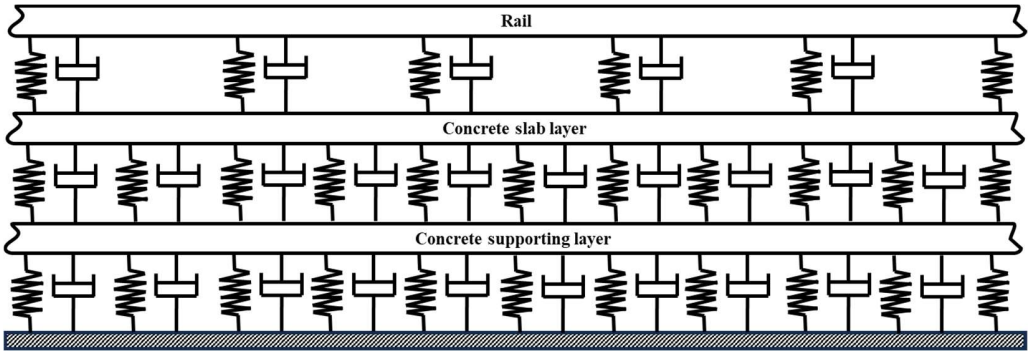

Figure 0.2 A layered schematic showing rail → rail pad (spring–damper) discrete → concrete slab layer→ concrete supporting layer- subgrade

2.1.4 Pasternak Foundation Model

(Colajanni et al., 2009)proposed an improved formulation over Winkler's concept by incorporating shear interaction between springs. In this model, a shear layer links the ends of adjacent springs, resisting transverse deformation as illustrated in Figure 2.3. This modification introduces a shear stiffness term that is dependent on the slope of deflection, allowing for more realistic predictions of load transfer and rail deflection continuity (Kerr, 2000) ; (Furkan Esen, 2022).

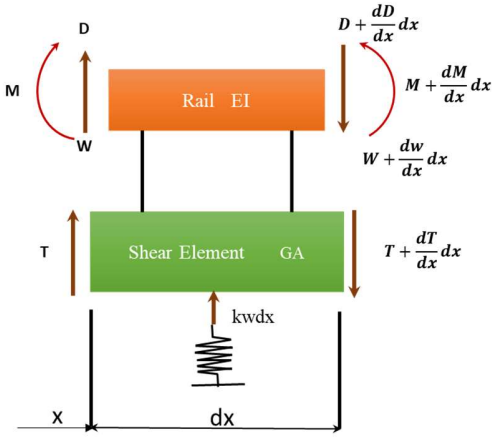

Figure 0.3 A rail beam on Winkler springs connected by a shear layer representing Pasternak's foundation

(Madshus & Kaynia, 2000) and (Kouroussis et al., 2011) further demonstrated that compared to Winkler's uncoupled springs, Pasternak's model better represents soil

continuity, avoids oversimplifications, and still retains analytical tractability. Recent studies highlight its usefulness in analyzing high-speed railway vibrations and dynamic track–soil interaction.

2.1.5 Wheel Rail Contact

The wheel–rail contact is the primary interface through which train loads are transmitted to the track structure. In most railway dynamics studies, this interaction is modelled using Hertzian contact theory, which idealizes the wheel and rail as two elastic bodies in non-conforming interaction. In this assumption, contact patch is elliptical, and normal force is related to elastic deformation at the interface.

According to Hertzian theory, contact force can be expressed as a nonlinear function of the indentation depth:

$$F_n(t) = K_H \delta(t)^{3/2} \tag{2.5}$$

where F_n (t) is contact force, δ(t)is the elastic approach (or vertical deflection) between the wheel and rail surfaces, and K_H is Hertzian contact stiffness. The stiffness K_H depends on the geometry of the wheel and rail profiles and their material properties, specifically the equivalent elastic modulus and combined radii of curvature (Fang et al., 2023; Kalker, 2013)

For dynamic analyses, this contact spring is often supplemented with a damping term to account for energy dissipation during impact and vibration transmission:

$$F_n(t) = K_H \delta(t)^{3/2} + c_n \dot{\delta}(t) \tag{2.6}$$

Where c_n is the damping coefficient. This spring–damper representation provides a convenient and widely accepted model for simulating the vertical wheel–rail interaction in railway vehicle–track systems (Patel et al., 2023; L. Xu & Zhai, 2019). Although simplified, the Hertzian spring–damper model effectively captures the fundamental physics of wheel–rail load transfer and is extensively used in high-speed rail studies, including the analysis of track performance. It serves as the foundation for more

advanced formulations that consider nonlinearities, time-dependent effects, and additional tangential contact mechanisms.

39

2.2 Static and Dynamic Response Analysis of Railway Slab Track

Slab track systems have emerged as a reliable and durable alternative to conventional ballasted tracks, particularly for high-speed railway applications. Their inherent advantages, enhanced stiffness, superior geometric stability, and reduced maintenance requirements have driven widespread adoption in modern rail infrastructure. Nevertheless, the structural performance of slab tracks must be evaluated not merely in terms of static strength but also through a comprehensive understanding of their behavior under moving loads, vibrations, and long-term fatigue demands. Consequently, a systematic review of existing research on the static and dynamic responses of slab track systems becomes essential. This section examines critical analytical, numerical, and experimental studies that investigate load transfer mechanisms, vibration characteristics, and the overall structural behavior of slab tracks. Special emphasis is placed on recent developments in slab track technologies and corresponding performance of intermediate layers such as CAM, which play a critical role in ensuring long-term durability. The review provides a critical synthesis of prevailing methodologies, identifies gaps in current knowledge, and establishes the foundation for subsequent investigation into the fatigue performance of CAM.

Ballasted track systems have been widely used due to their traditional construction methods and ease of maintenance. However, under increasing axle loads and high-speed train operations, their limitations in deformation control and long-term stability become evident. Slab track systems, particularly precast variants, have emerged as a more durable alternative offering superior stiffness and structural continuity.

Slab track systems, also referred to as ballastless tracks, have gained widespread application in modern high-speed railway (HSR) networks owing to their superior stiffness, geometric stability, durability, and reduced maintenance requirements compared to conventional ballasted tracks (Esveld, 2001). With the growing demand

for higher train speeds and heavier axle loads, slab track has become the preferred solution in countries such as Japan, Germany, and China, and more recently in India through the adoption of precast slab systems for projects like Mumbai–Ahmedabad High-Speed Rail corridor. The design, material properties, and interaction of their structural components strongly influence the performance, safety, and longevity of slab track systems. Consequently, researchers worldwide have extensively investigated ballasted and ballastless track systems under both static and dynamic loading conditions.

The primary reason for this development is the many structural and functional benefits slab track systems offer over conventional ballasted track. Before replacing ballasted tracks with slab tracks, it is essential to thoroughly understand the underlying mechanics and associated challenges. High mechanical stresses, inadequate load distribution, and ballast displacement at high speeds primarily drive track degradation in ballasted systems. One critical aspect is calculating the minimum ballast height required to maintain bearing stress within permissible limits. When designing slab tracks, several key factors must be addressed, including allowable rail bending stress and deflection, subgrade and concrete slab stress limits, and the permissible deflection of the concrete slab. Additionally, the inevitability of cracks on ballast less tracks, both during construction and operation of high-speed railways, underscores importance of analyzing factors that contribute to crack initiation and propagation. These considerations are crucial for ensuring the durability and performance of slab track systems (Jee et al., 2018). A dynamic analysis of the slab track is crucial to assess the impact of noise and vibration.

(Michas, 2012) Compared to ballasted tracks, slab tracks tend to generate higher noise levels at high speeds due to the limited vibration absorption capacity of the concrete slab and the decoupling effect of the rail fastening system. (Zoeteman & Esveld, 1999) claims that maintenance costs can be lowered by up to 70–90%.

(Zhai et al., 2010) As noted in the complex dynamics of high-speed train slab track systems, vibrations caused by irregularities in the rail track, deflections resulting from

railway dynamics, and variations in foundation settlement can all lead to significant damage to both the track infrastructure and the trains themselves.

(Kerr, 2000) The researcher utilized the Kerr method to ascertain the rail support modulus under static load conditions. The author advocated for the superiority of static testing over dynamic testing in yielding more accurate results for determining the track modulus.

(Lin & Trethewey, 1990) A dynamic analysis method was investigated for elastic beams under arbitrary dynamic loads. Derives governing equations using finite element formulation, solving efficiently with Runge-Kutta integration. Demonstrates accuracy and versatility with high-speed machining applications. In this context, the impact of vertical track stiffness on track performance is examined, with a focus on dynamic responses to parametric excitations.

(S. R. Matias & Ferreira, 2020) This article aims to provide an overview of current state of research on slab track system modelling, design, construction, and maintenance. According to this research article, Modelling techniques are fundamental for assessing most influential variables that affect structural performance of slab tracks, particularly dynamic and long-term behavior. Currently, main gap in the track modelling literature is related to research on fatigue analysis over a specified life period. The thermo-hydro-mechanical behavior of the soil is crucial in evaluating long-term settlements, highlighting the need for future researchers to focus on soil-water characteristics and water movement under extreme weather conditions.

(Vu, Jang et. al. 2021) A study of track structure under dynamic loading using the finite element program All-Purpose Analysis of Train Structure Interaction (APATSI), developed by the Korea Railroad Research Institute, was conducted to evaluate the structural response and running safety, thereby providing a precise understanding of the load transfer efficiency of precast slab track systems. (Güllü et al., 2021) A full-scale laboratory test procedure was proposed to evaluate the performance of slab tracks,

defining possible failure modes that reduce experimental costs and identify mechanical properties.

(H. Xie et al., 2020) The dynamic response of the train-track-bridge system on the Continuously Welded Rail was investigated under the dynamic load of a train on the HSR using finite element software ANSYS and dynamic analysis software SIMPACK. For analysis, the bridge model of the steel spring floating slab track and the CRTS III ballast less track was examined. The influence of the train's speed on the bridge, fasteners, and rail displacement, as well as vertical vibration acceleration and wheel-rail force response, was analyzed. The displacement and acceleration of the rail and track slab in the CRTS III ballast-less track are smaller than those in the floating slab track structure; however, the floating slab track structure exhibits better vibration reduction performance for bridges. The acceleration of the rail, track slab, and bridge increases significantly with the increase in train speed; the rail structure has the largest increment. Reducing the stiffness of fasteners could decrease the vertical acceleration response of the steel spring floating slab track system. The ability to absorb shock can be enhanced by reducing the stiffness of the fastener appropriately.

(X. W. Sheng et al., 2020) The use of rubber under ballast mat (UBM) as an isolation layer in ballastless tracks in high-speed train systems was investigated. Static, dynamic, and fatigue analyses were conducted to determine the basic material characteristics of the rubber UBMs.

(Connolly & Costa, 2020) A dynamic analysis was conducted to investigate the effect of multiple loads moving at speeds exceeding the critical velocity, and a numerical model was also developed for analysis. This model was finally validated using field data. According to the observation: 1). When vehicles operate at speeds greater than the critical velocity, vehicle axle spacing plays a dominant role in the displacement amplification of the track system. 2). Maximum track amplification occurs when the vehicle axle frequency is equal to the propagating wave vibration frequency of the track-ground system.

(Aggestam, et. al. 2018) The vertical dynamic vehicle track instruction analysis procedure has been presented and utilized to examine the impact of foundation stiffness gradients on the wheel-rail contact force. The amplitude of the wheel–rail contact force was found to be independent of the foundation stiffness gradient at high speeds in the slab track context; however, other dynamic responses, such as the bending moment in the slab and the load distribution on the foundation, were affected. It was also found that a geometrical rail imperfection, exemplified here by a dipped welded rail joint, has a significant impact on both the wheel–rail contact forces and the bending moment in the panels.

(X. Yang et al., 2015) Numerical simulations are performed to validate the theoretical model and gain insights into the dynamic behavior of the entire system. The results may lead to enhanced design guidelines for high-speed railway bridges and track systems, ensuring smoother train operations, reduced vibrations, and optimized structural integrity. Focused interaction between train's wheels and railway track influences vibrations transmitted to ground during train operations, including factors affecting wheel-rail dynamics, the mechanisms through which ground vibrations are generated, and impact on nearby structures and environment. The study provides a valuable understanding of the complex affiliation with wheel-rail dynamics and ground vibrations, offering a foundation for improving the design and operation of railway systems to minimize their environmental impact and enhance overall performance.

(Madshus & Kaynia, 2000) investigated the dynamic behavior of high-speed railway lines on soft ground, revealing that large dynamic amplifications occur when train speeds approach a critical velocity determined by the soil's Rayleigh wave characteristics. They found that below the critical speed, displacements are in phase with the train loads, while above it they become out of phase, and developed a computer code capable of accurately predicting such responses.

(Shamalta & Metrikine, 2003) presented an analytical study of an embedded railway track under moving loads, modelling the track as a flexible plate supported by beams and viscoelastic elements. Their dispersion analysis clarified the elastic system's

response, showing how rail and slab displacements vary with load velocity and frequency, and comparing a full 2D model with a simpler 1D representation.

(Y. Guo & Zhai, 2018) focused on dynamic analysis of vehicle-slab track system in China's high-speed railway network, particularly when subjected to differential subgrade settlement. Subgrade differential settlement refers to uneven settling of track's supporting foundation, which can lead to varying vertical displacements along track alignment. (Nielsen & Li, 2018) The researcher focused on the differential settlement in soil subgrade is unavoidable, and it has a direct influence on the services and performance of ballast-less railway slab track structures and the operational conditions for high-speed trains.

Charoenwong et al. 2023 compare how slab track systems and conventional ballasted track systems degrade in terms of track geometry over time under train loading. They develop or use models to simulate the progression of alignment, gauge, and vertical irregularities, and examine which track type is more resilient to geometric deterioration. Their results suggest that slab tracks tend to maintain better geometry over time, with slower rates of degradation, owing to their more rigid and stable structure, whereas ballasted tracks show more pronounced geometry decay under repeated loads. The study offers quantitative comparisons of degradation trends, sensitivity to loading, and implications for maintenance scheduling in railway design and asset management.

(L. Xu et al., 2021)present a computational platform designed to simulate the dynamic response of slab track systems under the passage of train loads. The platform integrates finite element (or related) models of track components (slabs, trackbed layers, and support structures) with moving load representations of vehicle axles. They use this platform to investigate how factors such as the spatial variability of support layers, parametric uncertainties, and dynamic coupling affect slab track performance. Through numerical experiments, they investigate the impact of variations in support stiffness, damping, slab properties, and load speed on track deflections, stresses, and vibration responses. The platform is validated against benchmark or reference results, and is used to run parametric studies to guide design and optimization of slab track systems.

(Long et al., 2024)propose a comprehensive dynamic model for integrated vehicle–track–bridge systems, with a particular focus on how track alignment (i.e., geometric layout) affects dynamic interaction in high-speed rail contexts. The model captures the coupling between vehicle dynamics, track structural behavior, and bridge response under the excitation of track irregularities and alignment deviations. They develop software to simulate ride comfort metrics (according to standards such as ISO or UIC), wheel–rail forces, and structural responses, and perform case studies on various alignment scenarios. Their results demonstrate how alignment choices (curvature, transition lengths, vertical/horizontal geometry) affect dynamic forces, comfort indices, and structural compatibility, and they propose optimized alignment parameters to enhance overall performance and safety.

(Zhai et al., 2009)Lay a foundational theory and modeling framework for analyzing the coupled dynamics of a vehicle and track system as an integrated entity. They propose a three-dimensional model in which a typical passenger vehicle (modeled as a 35-degree-of-freedom multi-body system) is coupled with a track subsystem, modeled as two continuous rails on discrete-elastic supports (for ballasted track) or via plate/viscoelastic foundations (for slab track). The coupling is mediated by a wheel–rail contact model accounting for vertical, lateral, and torsional interactions. Random track irregularities are input as excitations via spectral methods. They solve the nonlinear system dynamics in the time domain using an explicit integration method and validate model predictions via full-scale field tests (on Chinese railway lines). The authors also demonstrate that the coupled model yields different (often lower) dynamic indices compared to classical (vehicle-only) dynamics, particularly in curves, and emphasize the importance of considering track flexibility in dynamic design.

(M. Wang et al., 2017)Conduct a full-scale experimental investigation of the dynamic behavior of several China Railway Track System (CRTS) non-ballasted (slab and double block) track types using a 55.17 m long rig. They apply wheel-drop tests (a dropping wheelset) to induce impact excitations, and measure accelerations, velocities, and dynamic response across layers. Using those data, along with a mathematical track

model, they extract the dynamic stiffness and damping coefficients of the four studied track types under varying drop heights. Their comparisons reveal that different CRTS designs (CRTS I, II, and III) exhibit distinct vibration levels, transfer functions, and dynamic properties. This work is significant because it provides direct experimental quantification of dynamic stiffness and damping for slab track types in high-speed rail contexts, enabling calibration or validation of numerical vehicle–track models.

(X. Wang et al., 2024)analyze the nonlinear lateral stiffness behavior of rail fasteners and assess its influence on wheel–rail stick-slip phenomena (which can promote irregular wear or noise). They experimentally or semi-empirically characterize the lateral force–displacement relationships of fasteners under cyclic loading, showing hysteresis, stiffness degradation, and nonlinear segments. Then they embed this nonlinear fastener model into dynamic wheel–rail interaction simulations to examine how the nonlinearity influences stick-slip instabilities, vibration amplitudes, or transition thresholds. Their results highlight that fastener nonlinearity can significantly alter the onset and amplitude of stick–slip vibration under certain loading and speed conditions, implying that more refined fastener models should be used in predicting wear, noise, and dynamic stability.

(J. Yang et al., 2020) propose an enhanced dynamic model tailored for ballastless (slab) track systems with medium-thick slabs (i.e. slab thickness not extremely thin, not extremely thick). The model considers the coupling among rail, slab, fasteners, substructure layers, and support, with a focus on how slab thickness affects dynamic stiffness, damping distribution, and vibration behavior. They include irregularity excitation and derive responses such as deflections, stresses, and dynamic forces across components. The authors conduct parametric studies to assess the model's sensitivity to slab thickness, support stiffness, damping, and load speed, and validate the model against available data or prior models. Their findings reveal that medium-thick slabs exhibit intermediate dynamic behavior (neither fully rigid nor highly flexible), and optimal slab thickness (or support design) can mitigate vibration or stress peaks. This work bridges simpler thin-slab models and full thick-slab (rigid) approximations, offering more realistic modeling for many practical slab track systems.

(Y. Yang et al., 2019) investigate both static and dynamic structural behavior of prestressed concrete (PC) track beams used in straddle-type monorail transit systems. Their study includes finite element modeling of beam cross-sections, analysis of static load behavior (bending, shear, deflection) and dynamic vibration characteristics (natural frequencies, mode shapes, dynamic response). They may also consider interaction with the vehicle mass or wheel loads. The work helps in understanding how the PC track beams behave under service loads and dynamic excitations, which is crucial for monorail guideway design, vibration control, and durability considerations in elevated or urban contexts.

(Timoshenko et al., 1974) is a classical text on vibration theory and structural dynamics more generally. It covers fundamental principles such as mode shapes, natural frequencies, damping, forced vibration, continuous systems (strings, beams, plates), and coupling. In railway/track dynamics contexts, this text provides the theoretical underpinnings (e.g. beam theory, continuum dynamics, modal methods) upon which specialized vehicle–track and structural dynamics models are built.

(Tran et al., 2016)model the dynamic behavior of high-speed trains when subjected to sudden (abrupt) braking. They analyze deceleration transients, wheel–rail forces, vibration responses in car bodies, and coupling effects between carriages. Their results contribute to understanding safety, ride comfort, and dynamic loading during emergency braking scenarios in rail systems.

(Vesali et al., 2024) Focus on bridge–track dynamics in a scenario where trains enter a multi-span double-track bridge with a time delay (i.e. second train following the first). They develop or use models for bridge–track–train coupling and examine how the delayed entry of the second train affects dynamic interactions, resonance, amplification, and structural responses. Their findings are relevant for traffic scheduling, safety, and design in dense railway operations.

(Wanming Zhai, 2020) Monograph provides a comprehensive treatment of vehicle–track coupled dynamics theory, modeling approaches, solution methods, and engineering

applications. It covers multibody dynamics of vehicles, continuum and discrete track modeling (both ballasted and ballastless), contact models, coupling strategies, dynamic responses, validation studies, and case applications. This book is often a reference work summarizing the state-of-the-art in this field.

(X. Xiao et al., 2012) Investigate how seismic excitation (earthquake ground motions) may induce derailment or loss of wheel–rail contact in high-speed trains. They develop a dynamic model of vehicle–track interaction under earthquake inputs, simulate responses (displacements, contact forces), and propose criteria or mechanisms by which derailment may occur under severe ground motion. The work is relevant for the safety and design of high-speed lines in seismically active zones.

(Zhai et al., 2010) develop a coupled train–track–ground dynamic model to predict ground vibrations induced by high-speed train operations. The model integrates vehicle dynamics, track structural behavior, and ground (soil) response. They simulate the propagation of vibration into soil and estimate vibration levels at a specified distance from the track. This work is useful in environmental vibration prediction and in understanding how the track–ground coupling influences vibration transmission.

(Yousif Aziz, 2012) Examines the settlement behavior of high-speed railway bridges built over deep soft soil. He combines theoretical (analytical or semi-analytical) models with experimental or field measurement data to understand how bridge foundations settle over time under static loads. The work helps in understanding long-term deformations, differential settlement, and their influence on track geometry and structural integrity.

(Bastin, 2006) Detailed the development of German non-ballasted track forms, tracing the evolution of the Rheda system from its 1972 conception to the Rheda 2000 version, and described installation methods and transition arrangements between ballasted and slab track sections.

(Kaewunruen & Remennikov, 2007) provided a comprehensive review of the dynamic properties of ballasted tracks, summarizing vibration measurement methods and the influence of individual track components on system dynamics.

(Aggestam & Nielsen, 2020) simulated vertical dynamic vehicle–track interactions using a 3D slab-track model, coupling ABAQUS and MATLAB via Python scripts. They evaluated principal stresses and mesh convergence, demonstrating that simplified 2D models could reliably substitute for full 3D analyses.

(Ling et al., 2020) studied vibration-attenuating slab tracks for urban railways, comparing four elastic configurations—resilient-fastener, elastic-supporting-block, ladder-type sleeper, and floating-slab tracks—and found that the elastic-supporting-block design achieved the best vibration and noise reduction performance under varied loading conditions.

(Li & Berggren, 2010) Utilizes static and dynamic methods for calculating global track stiffness. Provides statistical analysis of results, offering insights into track stiffness and variations on typical Swedish tracks.

(J. Yang et al., 2020) proposed a novel dynamic model for medium-thick slab ballastless tracks based on Reissner-Mindlin plate theory. Utilizes an efficient computational algorithm for solving transverse deflection, avoiding shear-locking effects. Establishes a mathematical model for ballastless track dynamics considering shear deformation and moment of inertia in medium-thick track slabs. Experimental verification demonstrates accuracy and efficiency.

(Y. Yang et al., 2019) The author reports on in-situ tests of four pre-stressed concrete (PC) track beams in a monorail transit system. Static load tests measured strain and deflection to assess load-bearing capacity and stiffness. Dynamic tests studied strain, deflection, acceleration, and displacement under varying train speeds and loads. Results indicate the influence of curvature, span length, train speed, and load on dynamic responses. Dynamic loads impact PC track beams in curves. Still, appropriate train loads enhance riding comfort.

(Yousif Aziz, 2012) The study on the Beijing-Shanghai high-speed railway measures bridge settlement over time and load. The results of using a single-point settlement account and norm codes reveal a novel method for calculating compressed layer thickness. Corrections were made for conservative factors in pile foundation settlement measurements. The study suggests using a single-point settlement account with level joint monitoring for practical, profound soil observation and compression monitoring, especially in unstable base bottom layers.

(Ren et al., 2019)The author examines the impact of passenger and freight trains on mixed railway track damage. Concrete specimens tested under varied loads and speeds reveal differences in deterioration between the dynamic modulus of elasticity and flexural strength. Lower frequencies accelerate initial damage, while higher stress levels intensify later. Slower trains accelerate early damage, while faster trains worsen damage progression.

(Zhu & Cai, 2014) In numerous prior studies focusing on vehicle-track interactions, researchers commonly rely on the predetermined static material properties of the slab track components. These properties are typically derived from quasi-static loading tests conducted in laboratory settings. This approach provides a comprehensive understanding of how slab track components behave under various loads and conditions, thus providing valuable insights into their interaction with passing vehicles.

(M. Wang et al., 2017) For instance, the modulus of elasticity of the concrete slab, such as C60 concrete, is established at 3.6×1010 Pa based on compressive strength tests, with loading conditions primarily static. Similarly, the stiffness of rail pads in systems like the WJ-7B fastener system is measured at 2.5×107 N/m, also derived from static loading tests. These material properties are static benchmarks obtained through standardized test protocols. Hence, it is imperative to consider the accurate material properties of slab track components when conducting dynamic interaction simulations.

(X. Chen et al., 2013; Kaewunruen & Remennikov, 2007, 2008) Research indicates that the characteristics of concrete and cement-based materials can significantly differ

under dynamic loads compared to static or quasi-static loads, particularly regarding the modulus of elasticity.

(Z. Chen et al., 2018) The author investigates the track stresses and vehicle dynamics under pier settlement. A dynamic model validated against field data determines a safe settlement threshold for high-speed railways with CRTS II slab tracks. The vertical car body acceleration is most affected, and track stresses occur at settlements and adjacent piers. The safe settlement value is 11.5 mm, considering bridge pier settlement, vehicle load, prestressing impact, and self-weight.

(G. Guo et al., 2023) The researcher investigates how temperature loads affect the dynamic response of high-speed railway bridges with interlayer debonding. Using finite element simulations shows that increasing temperature loads lead to more significant deformation and dynamic response in the ballast, less-track structure. This highlights the importance of considering temperature effects in maintenance and repair planning for rail infrastructure.

(X. Wang et al., 2024) This study highlights the critical role of nonlinear lateral stiffness in fasteners for accurately predicting wheel-rail stick-slip vibrations on curved tracks. A new dynamic model, which combines the Kelvin-Voigt and Berg friction models, effectively captures fastener behavior across the shear, slip, and collision stages. Simulations and experimental validations show that lateral slip in fasteners significantly reduces damping, amplifying high-frequency oscillations in stick-slip forces. To mitigate such effects, preventing fastener lateral slip is recommended for improved rail performance and durability.

(Real et al., 2016) The author analyzed three types of railway tracks: ballasted, asphalt slab, and concrete slab. A Finite Elements model was calibrated with actual data. Static and dynamic analyses were conducted to evaluate three techniques for improving track behavior in transition zones: varying elastomer stiffness, adding additional rails, and using resilient mats. Results showed better performance in vertical stiffness transition, with minimal impact on dynamic response.

Moreover, compared to the traditional pre-cast slab system, the alternative system involves distinct structural dimensions, material properties, and manufacturing processes. However, the design of this pre-cast slab system remains relatively immature and lacks extensive testing to assess its engineering performance, including load-carrying capacity, structural integrity, deflection, and durability.

Early research by (Esveld, 2001) emphasised the geometric precision and long-term stability offered by ballastless track structures, making them well-suited for high-speed operations. Subsequent studies, such as those by Zhai et al. (2009), developed static loading models to investigate the deflection and stress distribution in slab track components. Comparative analyses between ballasted and slab tracks by Xu and Cai (2015) highlighted the latter's superior resistance to deformation and differential settlement under train loads. (Esveld et. al 2003)

Collectively, static studies suggest that slab tracks reduce settlement and improve stability, but their performance remains sensitive to slab geometry, CAM modulus, and bonding conditions. This highlights the need for further parametric studies tailored to Indian high-speed rail conditions.

In summary, dynamic studies confirm that slab tracks control deflections and vibrations more effectively than ballasted systems but face challenges related to resonance, settlement, and component flexibility. Further field-validated parametric studies are required, especially for Indian conditions.

Overall, resilient mats have proven effective in reducing vibration levels, but challenges remain regarding long-term degradation, optimized design, and their integration with CAM properties. Research gaps are especially evident in the Indian HSR context.

The reviewed studies show that slab tracks consistently outperform ballasted systems in both static and dynamic performance, offering reduced deflections, improved stiffness, and better vibration control. Static research has largely concentrated on deflection limits, bonding, and stiffness estimation, while dynamic studies have emphasized resonance, fatigue, and settlement effects. Vibration mitigation research highlights the promise of

slab mats, though their long-term behavior and adaptability to local soils remain uncertain.

Importantly, most prior research has focused on European and East Asian networks. Very limited work exists on Indian high-speed railway projects, particularly regarding fatigue of CAM layers, interface bonding, and vibration mitigation. This makes India-specific investigations, integrating experimental validation with numerical simulation, both timely and necessary.

61

In summary, research over the past decades has consistently shown that slab tracks outperform conventional ballasted systems in terms of stiffness, deflection control, and reduced maintenance demands. At the same time, studies also reveal that their performance is strongly dependent on design choices such as pad stiffness, slab thickness, and subgrade condition, as well as on external influences like settlement, temperature variation, and train speed. While static analyses provide a baseline understanding of stress limits and deformation, dynamic investigations highlight more complex issues of vibration transmission, resonance, and long-term deterioration. Nevertheless, one critical dimension that emerges across both static and dynamic studies is the need to address **fatigue performance**. With millions of load cycles expected during the service life of a high-speed corridor, understanding how repeated loading influences the durability of CAM and concrete slabs is fundamental. This recognition sets the stage for the next section, which reviews existing knowledge on the fatigue behavior of these materials and underscores why it forms a cornerstone of the present study.

2.3 Fatigue Performance of Cement Asphalt Mortar (CAM)

As highlighted in the previous section, both static and dynamic studies provide vital information on how slab track systems behave under load. However, the performance of these systems cannot be judged solely on short-term responses. High-speed rail infrastructure is expected to operate for decades, carrying millions of axles passes during its service life. Under such repeated loading, even small stresses can accumulate and gradually reduce the strength and stiffness of track components. This long-term process,

known as fatigue, is now recognised as one of the most critical factors governing the durability of slab track systems. Two components in particular demand attention: the cement asphalt mortar (CAM) layer, which acts as the resilient cushion beneath the slab, and the concrete slab itself, which forms the main structural layer. The long-term performance of slab track structures is closely governed by the fatigue resistance of their embedded cementitious layers, particularly cement mortar and cement–asphalt (CA) composites. Recent research has focused extensively on characterizing high-cycle deterioration mechanisms, defining constitutive laws for stiffness degradation, and developing predictive models that link microstructural evolution with macro-scale mechanical response.

The CAM layer has a dual role: it spreads vertical loads from the rail and slab to the sub-base while also helping to damp vibrations generated by passing trains. Due to its viscoelastic nature, CAM is sensitive to repeated loading and environmental factors, including temperature. Several laboratory investigations have indicated that the stiffness and modulus of CAM decrease when subjected to cyclic loads, leading to micro-cracking and eventual loss of performance (Qin et al., 2022; Tian & Yin, 2016). More recent work suggests that load frequency has a significant impact on fatigue life: lower frequencies tend to accelerate initial cracking, while higher loads at greater speeds intensify the later stages of damage (Ren et al., 2019).

One of the notable contributions in this domain is the experimental investigation of the high-cycle flexural fatigue behavior of cement mortar, reported by(Q. Xu & Wang, 2023). Using controlled flexural loading representative of high-speed rail environments, the study demonstrated that fatigue damage in plain cement mortar evolves in three identifiable stages: initial rapid stiffness attenuation, a relatively stable propagation stage, and an accelerated terminal degradation phase preceding failure. The authors highlighted the sensitivity of fatigue resistance to stress levels and microstructural integrity, indicating that even small defects can trigger premature cracking after millions of loading cycles.

Complementing this work, (M. Zhou et al., 2025) explored the damage evolution and service life prediction of CA mortars subjected to temperature fluctuations and high-frequency train loading. Their findings emphasized that the interplay between thermal cycles and cyclic mechanical loading significantly accelerates fatigue deterioration. A temperature-dependent viscoelastic constitutive model was proposed, capturing the combined effects of binder softening, aggregate debonding, and progressive microcracking within the asphalt–cement matrix. The study provided valuable insights for predicting CA mortar longevity under realistic operational conditions.

Further advances were made by (H. P. Chen et al., 2024)who employed mesoscale numerical modelling to forecast the fatigue life of CRTS-II slab-track CA mortars subjected to concurrent thermal gradients and vehicular stresses. By explicitly representing the mortar's internal phases aggregates, asphalt films, and voids – the model was able to reproduce localized stress concentrations and crack initiation sites. Their results confirmed that thermal mechanical coupling plays a critical role in accelerating modulus degradation. The numerical predictions corresponded effectively with laboratory fatigue tests, illustrating the efficacy of the mesoscale methodology for the long-term performance simulation of slab-track mortar layers.

Alongside studies on CA mortar, a significant amount of research has focused on the fatigue properties of asphalt mixtures. (Meng et al., 2024)examined international methodologies and obstacles related to fatigue tests for asphalt mixtures. Their review summarized key factors influencing repeatability, such as loading mode, specimen geometry, rest periods, and environmental conditioning, and emphasized the need for harmonized test protocols. The authors also highlighted mechanistic relationships between mix composition, binder ageing, and fatigue crack behavior, which are essential when comparing asphaltic layers with cement-based CA mortars.

The mechanistic distinction between tensile and compressive fatigue responses in asphalt materials was further examined by (Moghadas Nejad et al., 2017)who developed a fatigue damage model incorporating asymmetric modulus decay. Their research revealed that microcrack opening and binder debonding cause the tensile modulus to

deteriorate more quickly than the compressive modulus. The proposed model provides a more realistic framework for predicting fatigue life under mixed-mode loading conditions, which frequently occur in slab-asphalt track systems.

On the cementitious side, (Oneschkow & Timmermann, 2022) investigated how the varying compositions of high-strength concrete and mortar influence compressive fatigue behavior. Their findings revealed that aggregate distribution, binder stiffness, and water–cement ratio significantly affect fatigue endurance. Materials with denser microstructures and optimized aggregate packing exhibited slower stiffness degradation and longer fatigue life. This has direct implications for the design of mortar layers used in track systems where repeated high compressive loads dominate.

(Atalan et al., 2022) provide a broader perspective through their review of numerical models applied to slab–asphalt track railways. The review categorizes modelling strategies into analytical, finite-element, discrete-element, and coupled vehicle–track models. It discusses how advanced material models—incorporating viscoelasticity, thermo-mechanical effects, and fatigue damage—are progressively being integrated to improve prediction fidelity. The authors note that numerical models are increasingly used not only for performance assessment but also for optimizing design parameters of slab track systems.

The practical relevance of CA mortar performance was reinforced by (Le et al., 2020) who evaluated the full-scale testbed behavior of CA mortar for ballasted track stabilization. The study demonstrated how CA mortar can effectively enhance track stability by redistributing loads and reducing settlement. Fatigue resistance emerged as a critical determinant of long-term performance, with microstructural observations confirming patterns of crack initiation and binder degradation similar to those reported in high-speed slab-track studies.

Environmental effects also play a part. Studies on slab track systems in China have reported that thermal stresses and settlement conditions can amplify fatigue in the CAM layer (Chen, Zhai, and Yin, 2018; Guo, Hao, and Du, 2023). Despite these advances, most fatigue data for CAM are derived from Japanese and Chinese slab track designs, indicating a limited understanding of how CAM materials behave under Indian conditions. Given that material properties and climate can significantly affect fatigue life, generating India-specific data remains a clear gap.

Early efforts to characterize time-dependent deformation of cement–asphalt mortar (CA mortar) were presented by (Y. J. Xie et al., 2014) Their research methodically assessed the creep behavior of CA mortar, revealing that the asphalt component is essential for decreasing stiffness and improving viscoelastic deformation under continuous load. The study showed that creep strains keep building up even when stress ratios are low. This means that long-term deformation needs to be taken into account when designing slab-track systems that use CA mortar as a flexible support layer.

To complement mechanical characterization, (Qiu et al., 2014) proposed an ultrasonic pulse velocity (UPV)–based methodology for determining the mechanical properties of CA mortar. Their results indicated that wave propagation characteristics correlate strongly with stiffness degradation, allowing non-destructive identification of early damage. This provides a practical diagnostic tool for in situ assessment of mortar layers without disturbing track operations.

Regarding damage assessment and repair decisions, (Ren et al., 2016) established criteria for repairing CA mortar used in prefabricated slab-track systems. By examining the relationship between surface defects, internal voids, modulus deterioration, and service-level displacements, the study defined threshold values beyond which replacement or injection repair becomes necessary. Their work is particularly relevant for maintenance planning in ageing slab-track infrastructures.

(H. Xiao et al., 2019) examined the initiation and evolution of fatigue cracking in CRTS-II interlayers using advanced finite-element approaches. Using FE-SAFE and the extended finite element method (XFEM), the authors simulated localized crack nucleation under cyclic train loads and identified stress concentrations near interface discontinuities. Their findings showed that crack growth paths are strongly influenced by local adhesion quality and layer stiffness mismatch, offering insights for improving interlayer bonding and reducing premature failures.

Efforts to distinguish tensile and compressive fatigue responses in cement-stabilized materials were carried out by (Lv et al., 2019) They demonstrated that compressive modulus degradation occurs more gradually, while tensile modulus deteriorates rapidly due to microcrack opening. This asymmetry forms the basis for more accurate models that predict fatigue life, particularly in flexural scenarios where alternating tension–compression states dominate.

Comprehensive fatigue laws for CRTS-II slabs were later developed by (Y. Yang et al., 2022) who examined damage accumulation across millions of loading cycles. Their methodology integrated stiffness decay curves, energy dissipation characteristics, and empirical fatigue-life models in their methodology to predict slab failure under repeated train loads. The study reinforced the importance of describing fatigue damage as a multi-stage process rather than relying solely on Wöhler-type relationships.

At a structural scale, (Tarifa et al., 2015) conducted full-scale fatigue tests on precast reinforced-concrete slabs used in railway track systems. Their findings demonstrated that slab fatigue performance depends heavily on reinforcement detailing, aggregate distribution, and boundary conditions that replicate field support conditions. The experimental data provide valuable benchmarks for validating numerical models of slab-track behavior under operational loads.

Material-level innovations were explored by (Junco et al., 2018) who embedded polyurethane foam waste into mortar matrices and evaluated fatigue resistance. The modified mortar exhibited enhanced energy absorption and delayed crack propagation,

suggesting that microstructural lightweight inclusions can improve fatigue life under bending loads.

In the domain of high-ductility cementitious composites, (Q. Li et al., 2016) investigated the compressive fatigue behavior of fibre-reinforced materials. Their results revealed that fibre- bridging mechanisms slow down crack growth and postpone the rapid degradation phase typically observed in plain cementitious materials. The study emphasized the role of ductile microstructures in improving long-term performance of structural layers subjected to repetitive loading.

(W. Li et al., 2011)looked at how environmental coupling affects concrete that is exposed to both flexural fatigue and freeze-thaw cycles at the same time. The combined deterioration mechanism accelerated stiffness reduction and early microcrack coalescence, underscoring the importance of considering environmental impacts in cold-region track design.

Further exploring operational environments, (Z. qiang Li et al., 2022) analyzed fatigue damage in ballastless slab tracks used in heavy-haul railway tunnels. Their research demonstrated that elevated axle loads and tunnel-induced thermal stability intensify fatigue stresses within the slab and mortar layers. The results indicated that tunnel environments demand stricter fatigue performance requirements compared to open-air high-speed rail sections.

The general fatigue behavior of concrete was also summarized by (F. Liu & Zhou, 2017a) who provided experimental evidence on fatigue strain evolution and modulus degradation patterns. Their findings provided baseline data for comparative research, echoing the three-stage fatigue process often reported in cementitious and composite materials.

(X. Liu et al., 2019) examined the composite behavior of track slabs and self-compacting concrete layers under train-induced fatigue loads. Their experiments demonstrated that the interaction between layers significantly modifies strain distribution, resulting in stress transfer patterns that simplified single-layer fatigue models fail to capture. Proper

characterization of this composite action is essential for accurate structural modelling and life prediction of slab tracks.

The evidence from international research makes clear that both CAM and the concrete slab are vulnerable to fatigue. While static and dynamic responses provide important indicators of performance, they cannot capture the long-term degradation that occurs due to repeated loading. For Indian high-speed rail applications, this issue is particularly important because local material compositions, environmental conditions, and mixed traffic demands may not align with existing fatigue data from Europe, Japan, or China.

To bridge this gap, the present study adopts the fatigue performance of CAM is investigated experimentally, generating S–N curves that reflect the behavior of materials likely to be used in Indian slab tracks, which enables the prediction of stress distributions, crack initiation, and long-term deterioration under realistic loading scenarios. Together, these approaches provide a more representative framework for assessing fatigue in slab tracks and form an essential foundation for improving the design and durability of Indian high-speed railway infrastructure.

The review of existing studies makes it clear that fatigue is not just an academic concern but a practical challenge that will determine the long-term success of slab track systems. While CAM has been shown to suffer from gradual deterioration under repeated train loads, most of the available knowledge has been developed in the context of European, Japanese, or Chinese high-speed networks. The absence of fatigue data tailored to Indian materials and service conditions leaves a significant gap, especially as the country prepares to expand its high-speed rail infrastructure. These limitations highlight the need for focused research that combines experimental evidence with advanced simulations, ensuring that slab track designs are not only structurally efficient but also resilient over decades of service. Building on this recognition, the next section identifies the key research gaps that remain unresolved and explains how the present study is positioned to address them.

2.4 Research Gaps

The comprehensive literature review has identified the following major research gaps:

1. **Lack of localized data:** Most existing slab track models are based on foreign materials and construction practices, which differ significantly from Indian conditions.
2. **Unexplored vibration mitigation approaches:** The influence of slab mats and damping layers using locally available materials remains under-studied.
3. **The need for comprehensive parametric analysis: Slab thickness, CAM stiffness, and pad modulus require detailed evaluation to optimize the** cost–performance balance.
4. **Insufficient characterization of fatigue for CAM:** Although several international studies have proposed fatigue laws, there is no systematic experimental database for CAM used in Indian projects.
5. **Service life prediction:** Existing design methodologies lack fatigue-based service life predictions under Indian HSR loading scenarios.

65

2.5 Objectives of the Study

The specific objectives of the present study are formulated as follows:

1. The study aims to evaluate the static response of the precast railway slab-track system through a detailed finite-element-based parametric study, with a focus on stress distribution, deflection profiles, and load transfer efficiency under standard wheel loading conditions.
2. The study aims to mitigate vibrations in the high-speed railway slab-track system by introducing a resilient slab-mat layer and evaluating its effects on vibration amplitude, damping behavior, and resonance frequency characteristics.

3. The study also aims to investigate the dynamic vehicle-track interaction of the precast slab-track system, evaluating the influence of key structural and operational parameters such as train speed, axle load, and rail-pad stiffness.
4. The aim is to analyze the fatigue behavior of the Cement-Asphalt Mortar (CAM) layer of the precast slab-track structure through cyclic laboratory testing, and to develop an empirical relationship between stress level and fatigue life under repetitive load conditions.

turnitin Page 68 of 200 - Integrity Submission Submission ID trn:oid:::27535:124127336

CHAPTER 3: NUMERICAL SIMULATION AND METHODOLOGY

1.1 General

The current chapter is focused on the numerical modelling, as a technical frame, and the steps, as a methodology, for the evaluation of static behavior, vibration characteristics, vehicle-track interaction, and the fatigue performance of a slab-track system. The simulation method, which is based on the weaknesses that were found in Chapter 2, combines finite-element modelling, dynamic analysis, and fatigue evaluation to get a realistic picture of the track under high-speed railway loading.

In Section 3.1, the general modelling philosophy is presented, while Section 3.2 describes the simulation techniques, including the model formulation, meshing, boundary conditions, and geometric parameters of the slab track. Sections 3.4 and 3.5 describe the methods for static response and vibration characteristic analyses. Section 3.6 introduces the model for the dynamic vehicle–track interaction, which deals with nonlinear wheel-rail contact, rail-pad behavior, vehicle subsystem modelling, and the coupled FE equations. Finally, Section 3.7 discusses the methodology for the fatigue study of CAM, which includes damage modelling and service life predictions.

The numerical results and discussions presented in subsequent chapters are based on this structured methodology.

3.2 Simulation Technique

The performance of the precast railway slab track system was assessed under static, dynamic, and fatigue conditions using advanced numerical simulation techniques. The Finite Element Method (FEM), implemented using ANSYS software, was the primary tool employed to capture the mechanical behavior of the structural components under loads and boundary conditions. The simulation framework was carefully developed to ensure accuracy, reliability, and computational efficiency, with appropriate consideration for material nonlinearity, geometric discretization, and contact interfaces. Each step of

the simulation, ranging from model formulation to post-processing, was executed in accordance with international railway engineering guidelines and validated against published studies, thereby ensuring the robustness of the adopted methodology.

3.2.1 Modelling

54

The model consisted of the main components of the slab track system: rail, rail pad, precast concrete slab, cement asphalt (CA) mortar layer, and supporting foundation as illustrate in Figure 3.1. The rails were represented using beam elements, which provided an efficient yet accurate description of longitudinal stiffness and bending behavior. The slab and CAM layer were represented using three-dimensional solid elements (SOLID185 in ANSYS), ensuring that both flexural and shear effects could be captured. Special attention was given to material properties: the rail was modeled as elastic steel, the slab as high-strength reinforced concrete, and the CAM layer as viscoelastic material. To reduce end-boundary effects, three slab units were considered, and the central unit was selected for detailed analysis.

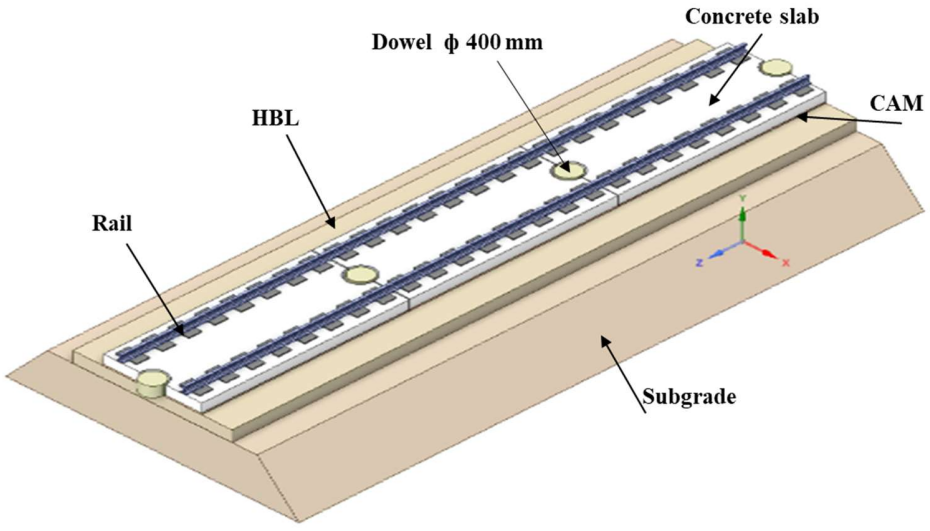

Figure 0.1Three-dimensional schematic of the slab track FEM model

3.2.2 Computational Domain

The computational domain was defined as a realistic segment of the slab track sufficient to capture stress distribution and deformation without artificial boundary influences. The slab length was modeled as 14.85 m, with a width of 2.35 m, corresponding to typical slab dimensions used in precast systems. The CAM layer was defined with a length of 4.95 m and a width of 2.35 m, matching construction practice for embedded support layers. The rail pad was included as a thin elastic layer to transmit load between the rail and the slab. This domain size was carefully selected to minimize computational cost while ensuring that the middle slab unit realistically represented the structural response under applied loads as shown in Figure 3.2.

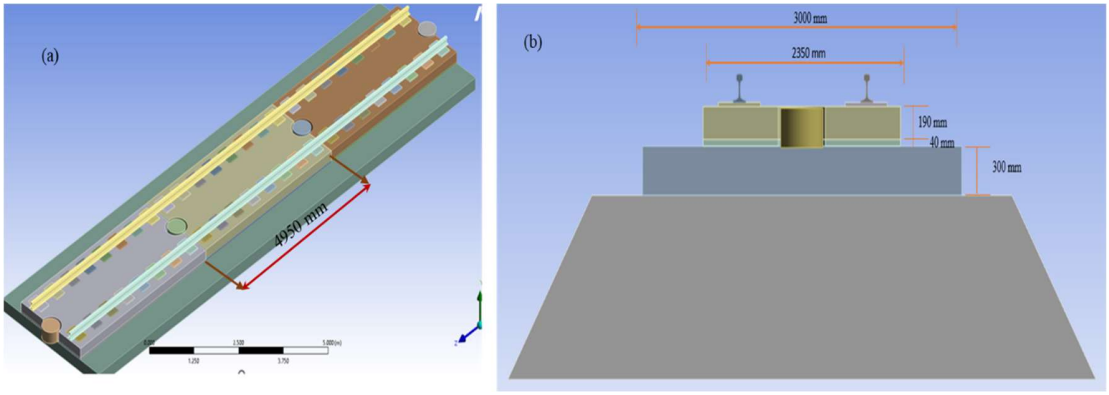

(a) Iso metric view of slab track (b) Front view of slab track

Figure 0.2 Dimensions of the computational domain of the slab track

3.2.3 Meshing

Meshing played a critical role in ensuring numerical accuracy. A multi-zone meshing strategy was adopted, in which fine mesh density was utilized in regions of high stress gradients, such as the rail–pad interface and slab–CAM interface, whereas coarser meshes were employed for the foundation. Hexahedral elements were used wherever possible to minimize element distortion, and mesh convergence tests were conducted to determine an optimal mesh density that balanced solution accuracy and computational time. In computer engineering, the simulation approach relies heavily on meshing as a fundamental building block as shown in Figure 3.3. The accuracy, convergence, and

velocity of the solution are all influenced by the mesh. In addition, the amount of time necessary to develop a model and its mesh often constitutes a significant fraction of the total amount of time necessary to acquire results through a CAE solution. As a result, the quality of the response will depend on how exact and automatic the meshing instruments are. The process of dividing a continuous structure into a series of discrete components is referred to as meshing. The mesh may be defined as the technique of breaking a whole component into a group of components. As a result, the load is distributed uniformly over the component whenever it is subjected to loading due to the meshing.

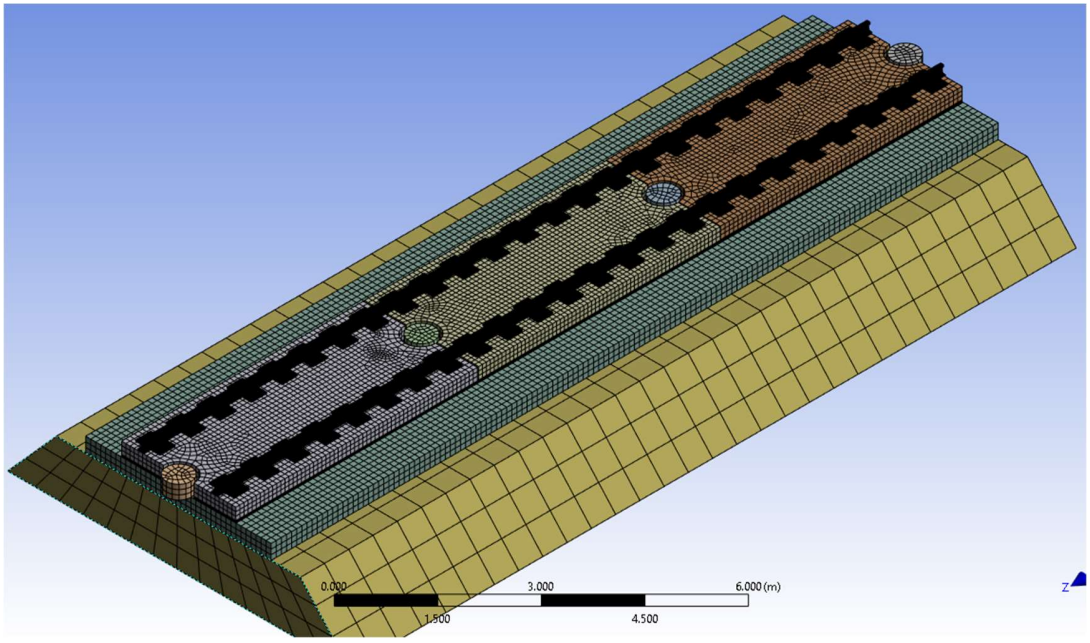

Figure 0.3 FEM mesh of slab track model

3.2.5 Boundary Conditions

Boundary conditions were applied to replicate realistic field constraints. The bottom of the CAM layer and foundation was restrained in the vertical direction to represent rigid support. Symmetry conditions were applied along the lateral edges to reduce computational cost while retaining realistic stress distributions. At the rail top, loading was applied as a series of point forces representing axle loads of 250 kN distributed over four axles for static response study. These loads were shifted sequentially across the rail

to simulate the quasi-static passage of the wheel. Contact interactions between rail pad, slab CAM, and foundation were modeled using frictional or bonded contact pairs depending on their construction properties.

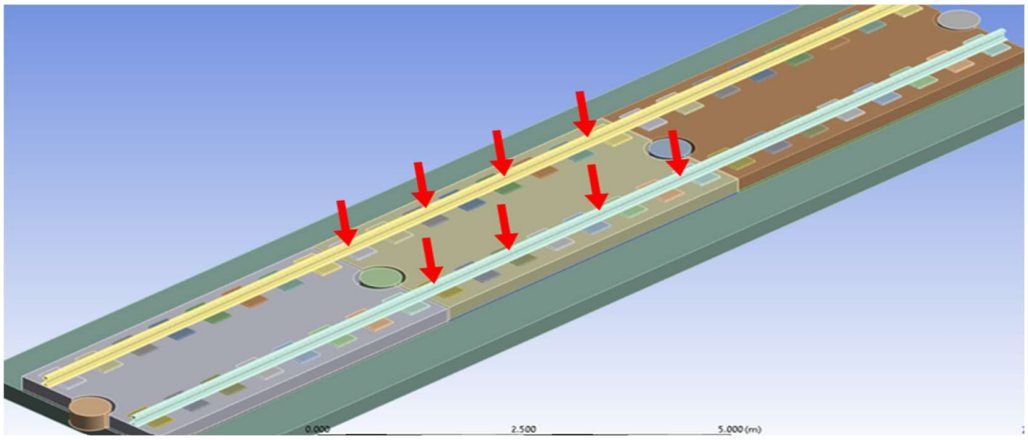

Figure 0.4 Application of loading on the slab track FEM model

This research presents a comprehensive evaluation of the static, dynamic, vibration, and fatigue behaviors of slab track systems, which are increasingly adopted in high-speed rail worldwide. Proven in Japan's Shinkansen, slab tracks are also in use in India through the Rheda system on the Delhi Airport Metro Express, the Porr system in Jammu & Kashmir tunnels, and the Shinkansen-type track on the Mumbai–Ahmedabad High-Speed Rail (MAHSR) project. While conventional ballasted tracks face settlement and durability issues at high speeds, slab tracks offer stiffness and longevity, but raise concerns about higher costs, fatigue in concrete and CAM layers, and dynamic amplification. To address these trade-offs, the study employs FEM for static and quasi-static responses under Static load, MEM for vehicle–track dynamics with wheel–rail nonlinearities, modal and harmonic analyses for slab mat-based vibration control, and Miner's hypothesis for CA mortar fatigue life. The sequential methodology integrates these approaches to meet the research objectives.

3.3 Methodology for Objective 1: Static Response

"To evaluate the static response of the precast railway slab track system through a detailed parametric study"

The evaluation of the static response of the precast slab track system forms the foundation of the present research. The primary aim is to capture stress distribution, deformation, and load transfer mechanisms under standardized loading conditions. For this purpose, the Finite Element Method (FEM) was adopted using ANSYS. The simulation employed the UIC LM71 load model, which is widely recognized in European railway standards for representing the static load effect of four axles with an equivalent axle load of 250 kN. The model domain consisted of a rail, rail pad, concrete slab, cement asphalt (CA) mortar layer, and the supporting base, each defined by an appropriate elastic or viscoelastic constitutive law. The rails were modeled as beam elements, whereas the slab and CAM layers were discretized as three-dimensional solid elements.

The train load configuration shown in Figure 3.5 follows the UIC Load Model LM 71 specifications, as defined in Eurocode 1: Actions on Structures - Part 2 (Traffic Loads on Bridges) (En, 2003), to simulate the static vertical effects of high-speed and mixed-traffic railway operations. This load model comprises four concentrated axle loads of 250 kN each, arranged to represent standard bogie spacing, combined with a uniformly distributed load (UDL) of 80 kN/m applied along the loaded track length. In the FEM simulations, axle loads were applied as point forces at railhead nodes corresponding to wheel–rail contact locations, while the UDL was applied along the intermediate rail elements to represent the continuous influence of the car body mass and ancillary equipment. This combined loading captures both the localized effects of wheel loads and the distributed weight of the train, ensuring realistic load transfers from the rail to the slab and supporting layers. The load distribution method strictly follows the UIC LM 71 specifications and reflects vertical load patterns observed in actual high-speed rail operations.

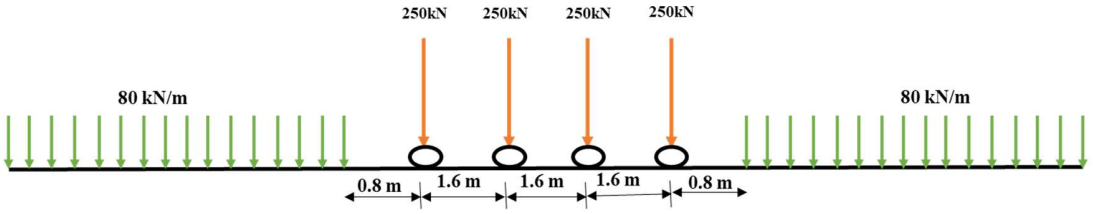

Figure 0.5 Static load condition UIC LM 71

To minimize the boundary effects, three slab units were included in the computational domain, with the central slab being the main focus of analysis. The model was meshed with a finer element density in the contact and interface zones to ensure accurate stress calculations, while coarser meshes were used in less critical regions to reduce computational demand. The static response was evaluated in terms of slab mid-span deflection, stress contours in the concrete and CAM layers, and load distribution patterns. This analysis provided the benchmark against which subsequent dynamic and fatigue analyses were compared.

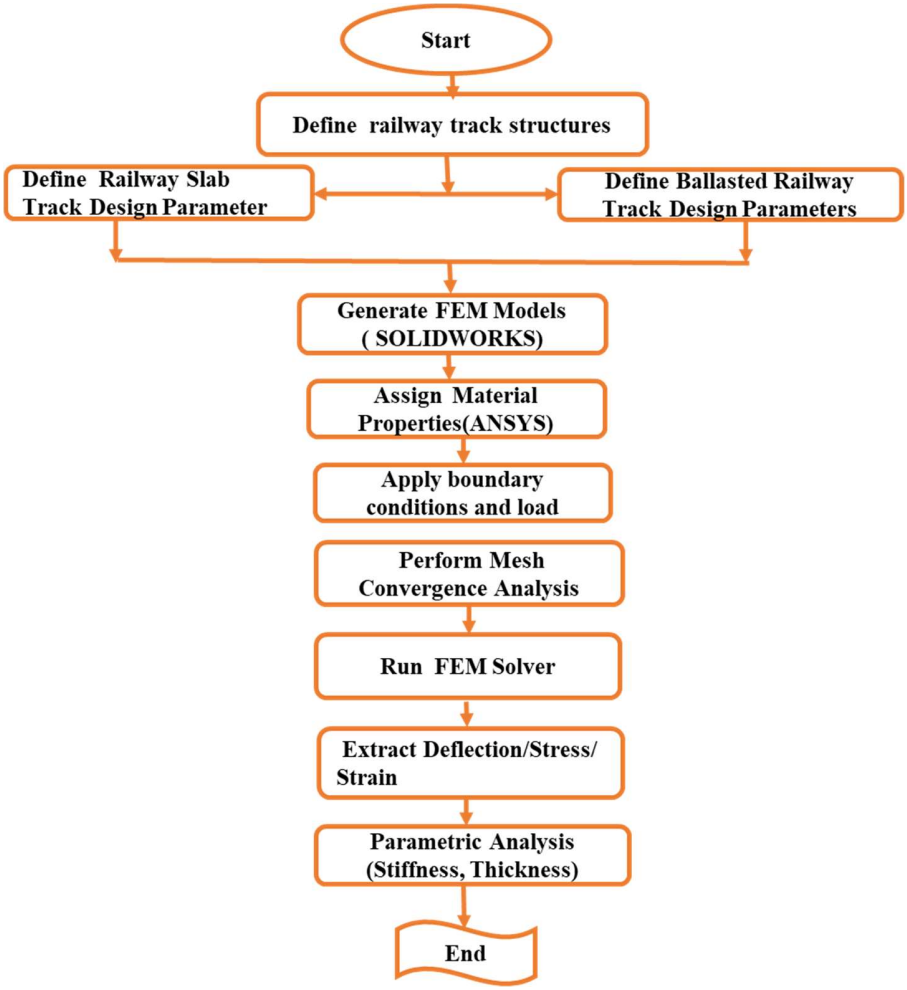

Figure 0.6 Flow chart for methodology of static response study

Table 0.1 Mechanical properties of the ballast track structure (Singh Jitendra, 2023)

Track components	Unit weight kN/m^3	Elastic modulus GPa	Poisson's ratio
Rail	7850	210	0.30
Rail Fastener	1800	0.22	0.30
Ballast Sleeper	2050	75	0.20
Ballast layer	1800	0.273	0.30
Sub Ballast layer	2100	0.20	0.20
Soil subgrade	2000	0.01	0.35

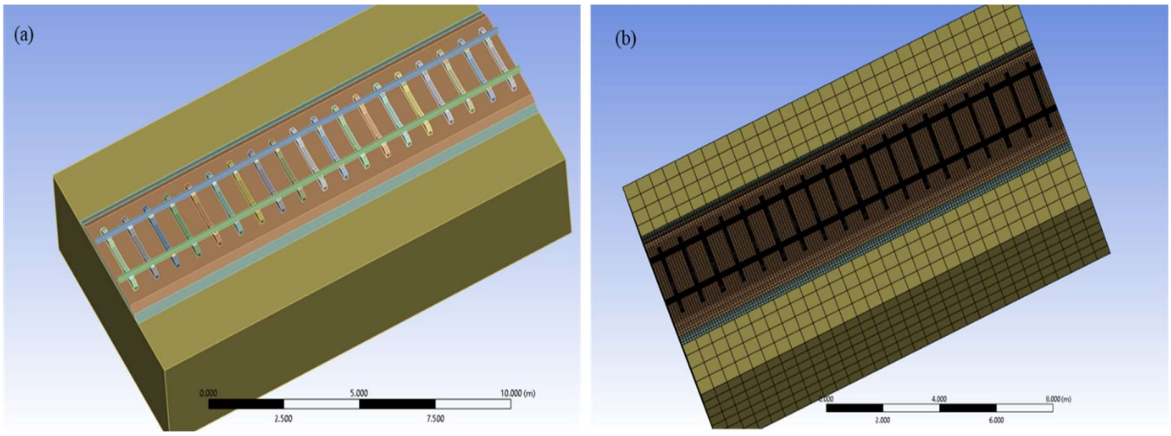

Figure 0.7 Isometric view of railway track structure and meshing model: a) FEM Ballast track model; b) Meshing ballast track model

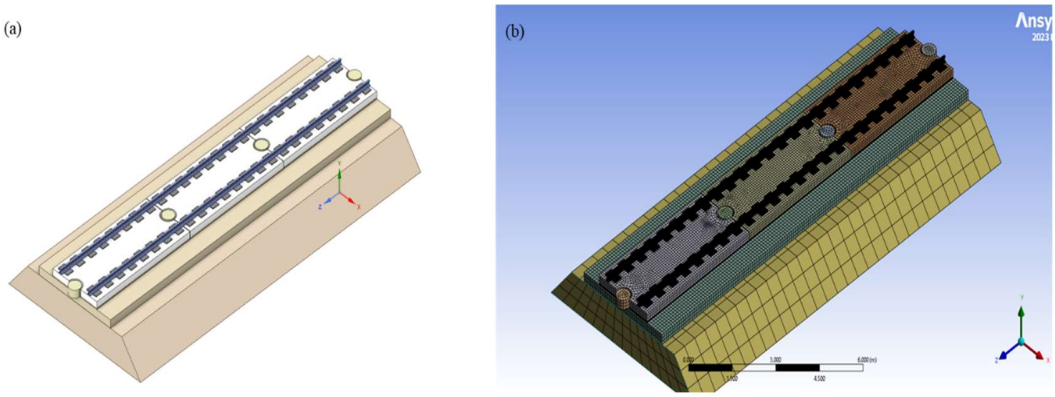

Figure 0.8 Isometric view of railway track structure and meshing model: a) FEM Slab track model; b) Meshing slab track model

Table 0.2 Parameters of Shinkansen slab track structure *(JICA & MOR, 2015)*

Track Component	Parameter	Value	Units
Rail profile	Inertia	3.52×10^{-5}	m^4
	Mass of rail	60	kg/m
	Modulus of elasticity	2.1×10^5	MPa
Rail pad	Damping	48.5	kN.s/m
	Stiffness	65	MN/m
Concrete slab	Inertia	8.65×10^{-5}	m^4

	Mass of Concrete slab	1380	kg/m
	Modulus of elasticity	5.47×10^5	MPa
Cement asphalt Mortar	Damping	85	kN.s/m
	Stiffness	900	MN/m
Concrete supporting layer	Inertia	3.5×10^{-3}	m^4
	Mass of HBL	2450	kg/m
	Modulus of elasticity	5.47×10^5	MPa
Subgrade layer	Damping	90	kN.s/m
	Stiffness	70	MN/m

3.4 Methodology for Objective 2: Vibration Response

"Study of vibration mitigation by slab mat layer in a precast high-speed railway slab track system"

The vibration analysis was conducted to investigate the dynamic characteristics of the slab track system under harmonic excitations. This study employs two slab-track models for vibration analysis. The first model comprises a rail, rail pad, fastening system, concrete slab layer, composite asphalt layer, and subgrade layer. Additionally, the second slab track model is utilized to evaluate the impact of the elastic material layer on the vibration response. This second model incorporates an elastic material slab mat layer positioned between concrete slab layer and composite asphalt layer. The modeling of these slab track models is conducted using SOLIDWORKS. In this study, it is assumed that the vehicle is moving on a tangent track, where the magnitude of lateral forces is negligible compared to the magnitude of vertical forces. As a result, lateral forces are not considered to have a significant impact on the findings of this study, allowing the analysis to focus primarily on the effects of vertical forces. The sequence of the simulation is shown in flow chart form in Figure 3.9, which can be seen below. ANSYS design modeler program has received model geometry from SOLIDWORKS STEP file formats, and it has been loaded.

3.4.1 Mesh independence

In the numerical simulation of a high-speed slab track structure for vibration analysis, a well-designed meshing strategy is crucial to ensuring accurate and reliable results. Optimize the mesh to balance computational efficiency and precision with a focus on capturing critical vibration characteristics. Fine meshing applies to key areas, such as the rail, the top layer of the concrete slab, and the interface between the slab and the mat layer.

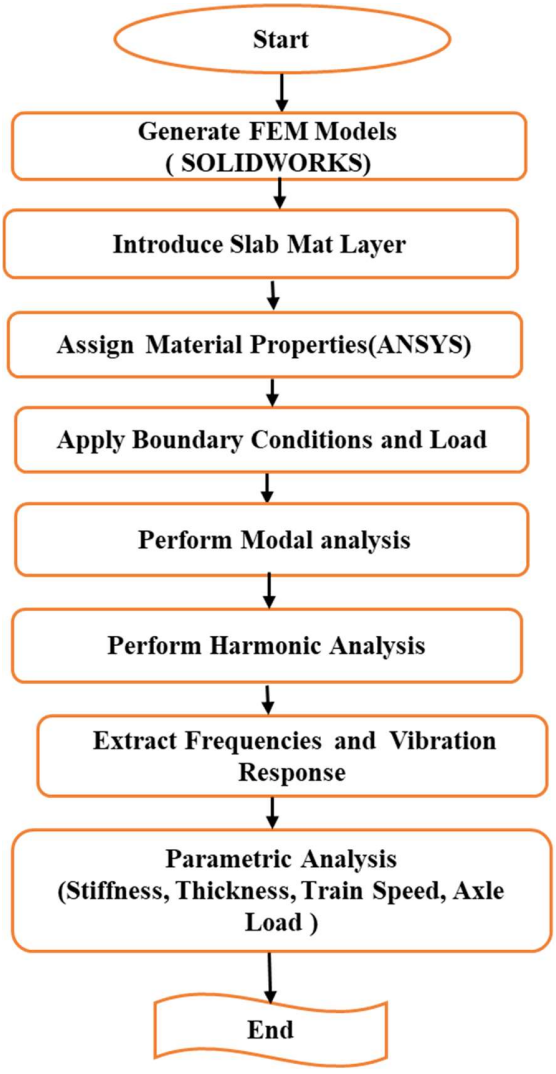

Figure 0.9 Flow chart for methodology of vibration response study

These regions are critical for accurately modeling dynamic responses, vibration propagation, and energy dissipation mechanisms. The subgrade layer employs a medium-sized mesh to accurately depict the wider interaction with the slab, thereby minimizing computational demands. The subgrade layer employs inflation layers at interfaces and along key surfaces to enhance the modeling of vibration behavior, particularly near transitions between the slab, mat, and subgrade. The mesh sizes follow the guidelines from the ANSYS Meshing User's Guide (ANSYS, n.d.), with fine meshes set to 0.0125 m for the rail, slab top, and slab-mat interface, and medium meshes set to 0.05 m for the subgrade layer. Mesh independence test result of this study is discussed in table 3.3. This meshing method ensures accurate recording of displacement and vibration characteristics, particularly in critical areas. It also shows how important the slab mat layer is for reducing vibrations. By carefully improving the mesh in these places, the study is able to make a realistic simulation of vibration attenuation. This aids in devising effective strategies to reduce vibrations in high-speed slab track structures. For vibration response study meshing of track model is used as shown in Figure 3.10 and 3.11.

Table 0.3: Mesh independence test result for slab track model

Type of meshing	**No of elements**	**Rail Acceleration**	**Slab Acceleration**
Coarse	853654	1.45	0.92
Medium1	125879	1.22	0.85
Medium 2	155974	1.08	0.78
Fine 1	189752	1.02	0.72
Fine 2	259716	1.01	0.71
Fine 3	286715	1.01	0.71

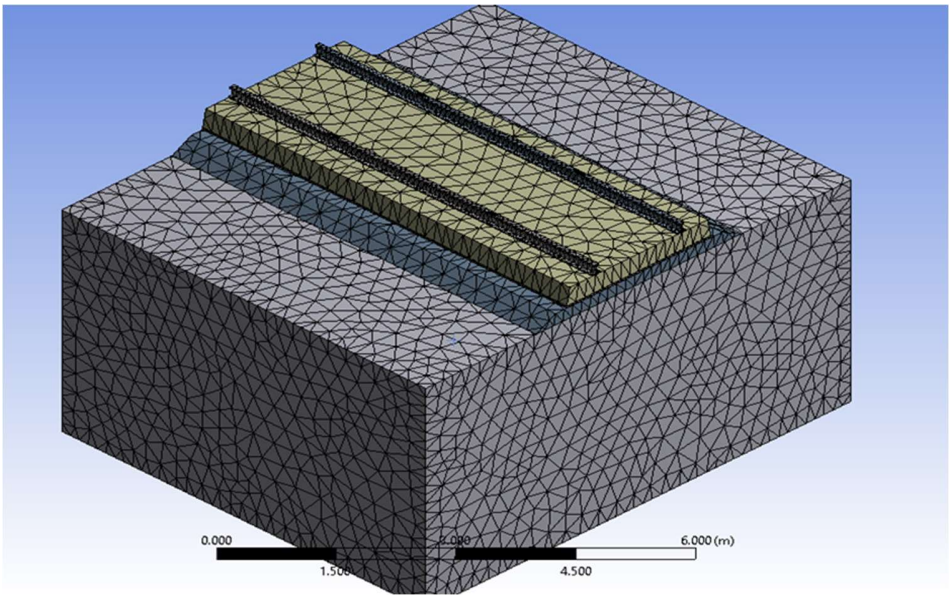

Figure 0.10 Tetrahedral medium meshing of the 3D model

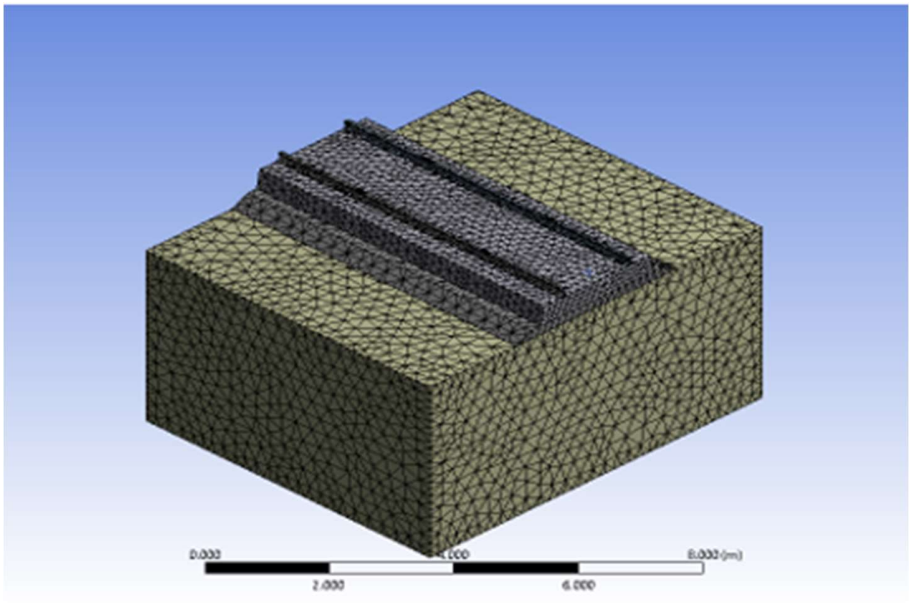

Figure 0.11 Tetrahedral fine meshing of the 3D track model

The study was divided into two parts: modal analysis and forced vibration response analysis. Using the finite element method, the simulation results show the vibration response and how the layer of slab mat affects the response of the Precast slab track system to vibration.

3.4.2 Modal analysis

Modal analysis is a fundamental technique used to determine the natural frequencies and mode shapes of a structural system, such as a slab track structure. These properties are essential for understanding the dynamic behavior of the system and ensuring its stability under operational loads. The natural frequencies indicate the resonance points, while the mode shapes describe the deformation patterns at these frequencies.

For a slab track structure, modal analysis is particularly important to evaluate its dynamic performance under train-induced vibrations, environmental effects, or other external disturbances. The modal analysis is based on the free vibration equation of motion for a structure:

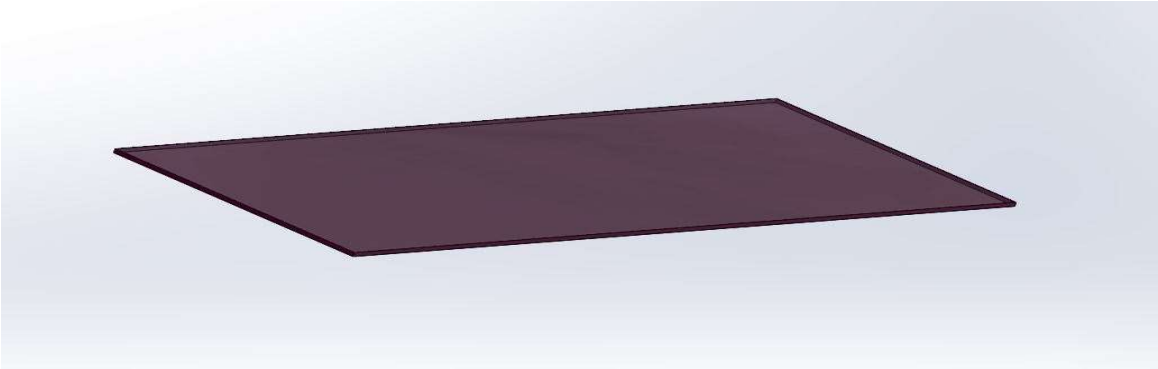

Figure 0.12 : 3D model of slab mat in SOLIDWORKS with 35 mm thickness

$$M\ddot{a} + Ka = 0 \qquad (3.1)$$

Where:

M: Mass matrix,

K: Stiffness matrix,

ä: Nodal acceleration vector,

a: Nodal displacement vector.

By assuming a harmonic solution for displacement:

$a(t) = \phi e^{i\omega t}$

Where:

ϕ: Mode shape (eigenvector),

ω: Circular natural frequency,

t: Time.

Substituting $a(t)$ into the vibration equation results in:

$$(-\omega^2 M + K)\,\phi = 0 \qquad (3.2)$$

This is a standard eigenvalue problem, where:

ω^2represents the eigenvalue (square of the natural frequency),

Φ represents the corresponding eigenvector (mode shape).

Rewriting:

$$\omega^2 M\phi = K\phi$$

These results provide insights into the dynamic characteristics of the slab track structure. For example: Low-frequency modes typically represent global movements (e.g., bending of the entire slab). High-frequency modes reflect local deformations or vibrations of specific components.

Finite Element Analysis (FEA) tools such as ANSYS are often used for modal analysis. The procedure involves:

Modeling the slab track structure: Incorporating materials, boundary conditions, and geometry.

Meshing: Dividing the structure into finite elements for numerical computations.

Solving the eigenvalue problem: Using numerical methods to extract natural frequencies and mode shapes.

3.4.3. Harmonic response analysis

The method of harmonic response analysis determines the steady-state response of linear structural systems under harmonic loading. This study compared two types of slab tracks, one with an anti-vibration slab mat layer and one without, to evaluate their vibration-reducing effects at a running speed of 280 km/h. The stiffness of the slab mat layer used in the comparison is k_m = 25 MN/m3. The primary function of this slab mat layer is to mitigate vibrations, particularly when trains are passing at high speeds. The acceleration of the concrete slab and subgrade layer serves as the key index to evaluate the effectiveness of vibration reduction. The simulation results from the mid-span section of the track shed light on the vibration-reducing effects in both the time and frequency domains. The results not only quantified the effectiveness of slab mats in reducing vibration transmission but also established safe operating frequency ranges for high-speed railway operation in the Indian context.

The analysis relies on solving the structure's vibration equation.

$$M\ddot{a} + C\dot{a} + Ka = F \qquad (3.3)$$

Here:

M is the mass matrix.

C is the damping matrix.

K is the stiffness matrix.

$\ddot{a}, \dot{a}$, and a are the nodal acceleration, velocity, and displacement vectors, respectively.

F is the load vector acting on the track structure.

Harmonic response analysis expresses the load F and displacement a as complex vectors, unlike typical scenarios:

$$F = F_{max}e^{i\omega t} = (F_1 + iF_2)e^{i\omega t}$$

$$a = a_{max}e^{i\omega t} = (a_1 + ia_2)e^{i\omega t}$$

Substitute these values into the vibration equation to obtain:

$$(-\omega^2 M + i\omega C + K)(a_1 + ia_2) = (F_1 + iF_2) \quad (3.4)$$

Where:

F_{max} and a_{max} are the amplitudes of the load and displacement, respectively.

96 ω is the circular frequency,

i is the imaginary unit ($\sqrt{-1}$)

t is time,

F_1, F_2, a_1, and a_2 represent the real and imaginary components of the load and displacement, respectively.

The concept of admittance in this context is crucial, as it characterizes the structure's vibration response. Harmonic response analysis enables a detailed examination of the admittance properties.

3.5 Methodology for Objective 3: Dynamic Vehicle -Track Interaction

"To investigate the dynamic vehicle–track interaction of the precast railway slab track system and evaluate the influence of key parameters through a parametric study"

The dynamic vehicle–track interaction analysis was designed to replicate the coupled behavior of trains running at high speed on the slab track system. To achieve this, a Moving Element Method (MEM) was developed, where the vehicle was represented as a multi-degree-of-freedom system comprising the car body, bogies, and wheelsets. Each subsystem was connected through suspension elements modeled as linear springs and

dampers. The track subsystem was represented by the FEM model developed earlier, and the wheel–rail interface was incorporated using nonlinear Hertzian contact theory.

This study utilizes numerical analysis to examine the precast slab system's dynamic responses, utilizing actual design parameters from the Mumbai-Ahmedabad high-speed railway(JICA & MOR, 2015). Dynamic simulation of rail slab and track-coupled system will be performed in this work by implementing finite elements method in moving reference frame. The vehicle is exhibited as a multi-body system, considering the interaction between wheels and rails through a nonlinear Hertz contact mode, and also considering the nonlinear friction force concept of the rail pad. The slab track's three-layer beam model can be used to determine the significant parameters, including mass, damping, and stiffness matrices in moving reference frames. Comparison with existing literature findings evaluates the correctness of the presented computational model. Parametric research is also carried out in addition to inspecting and addressing the dynamic performance of the coupled rail track system, which includes track imperfections and vehicle speeds. In this context, use of MEM in dynamic modeling and vehicle-track analysis has increased.

Two different components make up the vehicle-slab track coupled structure. The first one considers the vehicle, which comprises a coach body, two bogies, four wheels, and two-stage suspension system. This second component is made up of rail and supporting structures. Figure 3.13 shows a representation of coupled system, including vehicle being simulated as multi-body system and rack represented by triple-layered Euler's beam model. The vehicle is presumed to be moving forward along positive x-axis with speed (v). In the coordinate system being used, it is essential to consider that displacement of upright direction and load is positive in an upward direction. The following assumptions are used to create an analytical model for the slab track system:

- The vehicle is modeled as a multi-body system with 26 degrees of freedom (DOFs), including vertical and pitching motions of the car body, bogies, and wheelsets.
- Primary and secondary suspensions are modeled using spring-dashpot systems.

- Wheel–rail contact is governed by a nonlinear Hertzian contact model.
- The vehicle moves at a constant speed along the x-direction.
- The system is assumed to be symmetric; only half of the track-vehicle system is modeled.
- Track boundaries are assumed to be sufficiently distant, with zero end forces and moments.
- Only vertical dynamics are considered; lateral and longitudinal effects are neglected.
- Vertical rail irregularities are considered determinants of function in the sinusoidal form
- A high-speed slab track is modeled as three-layer track system that includes rail cushions, subgrade, concrete slab, cement asphalt mortar (CAM) layer, and rail beam.
- Non-linear frictional behavior of the rail pad is considered in the model. Discrete pads with elastic stiffness and dampening qualities support elastic beam, representing rail.
- The concrete base and track slab have been designed as elastic beams held up by CA mortar and subgrade. The damping qualities and elastic stiffness of CAM and subgrade are the only variables considered.

By assumption, the modeling high-speed vehicle-slab track model has been done. The rigid bodies using shell and beam components characterize the coach's body, the train's bogies, and wheel sets. Each coach part is linked to others by dashpots and suspension springs. The vehicle model comprises 26 DOF, encompassing vertical and pitch motion of coach body, bogies, and wheelsets. The slab track comprises concrete foundation, rails, rail pads, concrete, and CAM. In this model, rail is represented as Euler beam that is held up by rail pads.

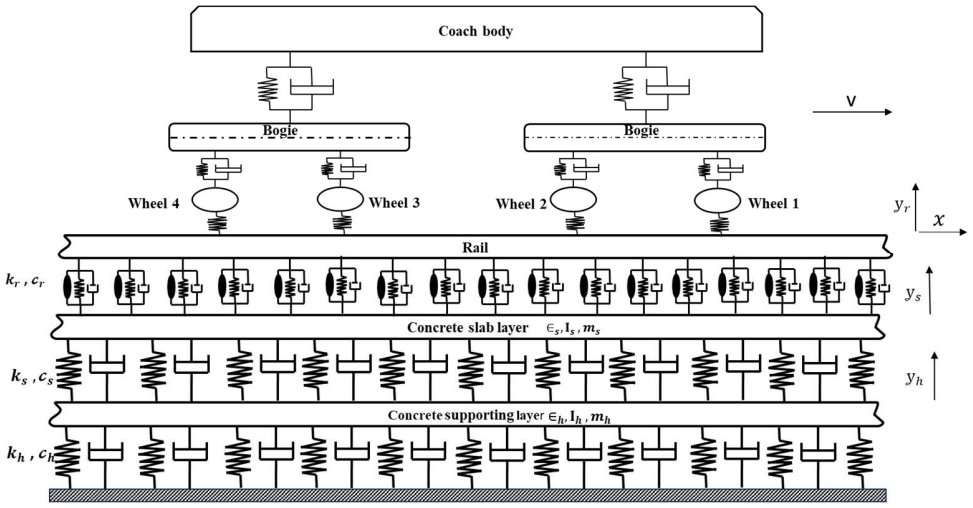

Figure 0.13 The model of system for vehicle-track coupling

These rail pads have been modelled as springs and dashpots. To obtain the complex 3D mechanical condition, concrete base, CAM, and slab are modelled using solid parts. In many simulation models, subgrade is often called spring-damping system. A common name for subgrade in several simulation models is spring-damping system.

3.5.1 Non-linear wheel-rail contact model

An integral part of train-slab track coupling system, dynamic coupling model connects vehicle and slab track subsystem at wheel-rail interface. The car and slab track are vertically coupled when wheels and rails make contact. In the present study, the interaction between the high-speed train wheel and the slab track system is modelled by coupling the wheel and rail components through a non-linear contact formulation based on the Hertzian contact theory. This theory provides an effective and computationally efficient method to capture the vertical contact force generated at the wheel–rail interface as a function of their relative vertical displacement. The wheel–rail contact area is idealized as an elliptical region, and the contact pressure is assumed to follow a semi-ellipsoidal distribution. The normal force of contact between wheels and rails is calculated at their interface applying nonlinear Hertzian elastic contact theory. The following assumptions are adopted in accordance with classical Hertzian theory:

- Both the wheel and rail bodies are considered elastic half spaces in the vicinity of contact.
- Elastic strains are assumed to be small and within the linear range.
- Stresses are assumed to dissipate away from the contact zone.
- The contact interaction is modelled as frictionless to focus on normal force dynamics.
- The materials of both wheel and rail are assumed to be homogeneous and linearly elastic.

As per the Hertzian contact theory (Axinte, 2014; Patel et al., 2023; X. Xiao et al., 2012; Yan & Fischer, 2000)the contact force at the interface between the rail and wheel is related to their vertical deformation through a non-linear expression, where the force is proportional to the deflection raised to the power of 3/2. Based on these assumptions, the vertical contact force is computed using the following non-linear expression provided by (Wanming Zhai, 2020)as:

$$P_j = \begin{cases} [1/G \ (y_{td} - \eta_x + y_{wj})]^{1.5} & y_{td} - \eta_x + y_{wj} \geq 0 \\ 0 & y_{td} - \eta_x + y_{wj} < 0 \end{cases} \quad (3.5)$$

Here, P_j is Hertz normal contact force at interface between jth wheelset and rail, and G is wheel-rail contact coefficient for wheels with worn or cone tread, measured in units of $[\, m/N^{2/3}]$.

$$G = \frac{2\,E\,\sqrt{R_e}}{3(1-v^2)} \quad (3.5a)$$

In the above expression: E is the modulus of elasticity, Poisson's ratio of the contact material, and Re is the equivalent contact radius expressed as: $R_e = \sqrt{rR}$, where

$$R = \frac{R_w R_r}{R_w - r} \quad (3.5b)$$

In the above expressions, the parameter r denotes the rolling radius of the wheel, while Rw and Rr correspond to the curvature radii of the wheel and rail profiles, respectively. The Hertzian contact stiffness G, for specific values of R_w and R_r, is calculated using the techniques proposed by Newton and Clark (Newton & Clark, 1979) and later enhanced by Uzzal(Ul & Uzzal, 2012). One possible value for G is $4.75R^{-0.149} \times 10^{-8}$. where R

is the wheel's radius in meters, y_{td} is track's displacement at interface point, $\eta_{\varkappa}$ is track's surface irregularity's amplitude, and y_{wj} is jth wheel's displacement to rail.

3.5.2 Nonlinear friction force model of rail pad

The proposed model of vehicle track considers nonlinear behavior of rail pads. This model considers elastic and nonlinear frictional force as shown in Figure 3.14. Rail pads are often made of rubber with carbon-black filler added to them, which gives them a frictional quality. Therefore, a nonlinear friction model is required to represent this behavior (Berg, 1997). The model primarily consists of two parameters: the maximum frictional force, $Q_{f\,max}$and the displacement x_2, which corresponds to $\frac{1}{2}Q_{f\,max}$under applied load. During calculation process, a reference state x_s i.e., state at which contact condition is about to change must be established (X. Wang et al., 2024). By comparing relative movement direction of fastener at each moment with reference state, corresponding frictional force $Q_f$is then calculated using Eqs. (3.6). Figure 3.14 shows the current model, which factors in both component displacement and an equivalent condition in friction force vs. displacement curve; nonlinear friction force of rail pads is thus dependent on this reference state. In this model, friction force is represented by:

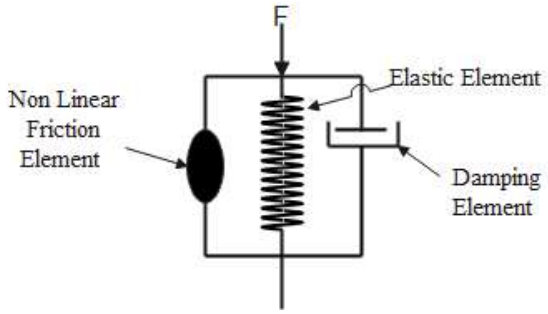

Figure 0.14 Rail pads nonlinear model

$$Q_f = \begin{cases} Q_{fr} & for\ x = x_s \\ Q_{fr} + \dfrac{x - x_2}{x_s(1 - \beta) + (x - x_s)}\left(Q_{f\,max} + Q_{fr}\right) & for\ x < x_s \\ Q_{fr} + \dfrac{x - x_2}{x_s(1 - \beta) + (x - x_s)}\left(Q_{f\,max} - Q_{fr}\right) & for\ x > x_s \end{cases} \quad (3.6)$$

$$\beta = \frac{Q_{fr}}{Q_{f\,max}} \tag{3.6a}$$

The rail pad supporting force is represented by the vertical dynamic force of the ith rail pad. It is possible to express it using the model's equations of motion.

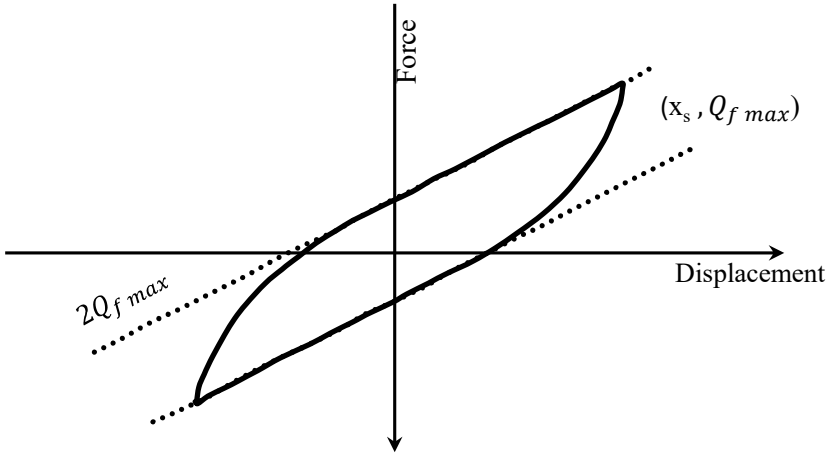

Figure. 0.15 Mechanical characteristics of nonlinear frictional rail pad model

3.5.3 Vehicle element model

The vehicle element model comprises several components, including a coach body supported by two bogies, each equipped with four-wheel setups. As illustrated in Figure 3.16, the symmetrical vehicle–track interaction model consists of total of 26 degrees of freedom (DOFs). The vehicle model includes 10 DOFs: 2 for car body (vertical displacement and pitch rotation), 4 for bogies (each with vertical displacement and pitch rotation), and 4 for wheelsets (vertical displacements only). The remaining 16 DOFs represent vertical displacements of rail at the wheel–rail contact points. This configuration enables detailed, dynamic interaction modelling between vehicle and track, capturing both rigid body motions of vehicle and rail deformations. In the vehicle element model, $2M_c$ and $2J_c$ represent rigid body's total mass and pitch inertia; $2M_b$ and $2J_b$ represent bogie's mass and pitch inertia; and $2k_{s1}, 2k_{s2}$ and $2c_{s1}, 2c_{s2}$ represent primary as well as secondary suspension systems of vehicle stiffness and damping coefficients, respectively. M_{wj} $(j = 1,2,3,4)$ value is mass of jth wheel, while k_c is

contact stiffness between wheel and rail supports it. Due to symmetric nature of the vehicle–track system, only one half of vehicle model is shown in Figure 4. Here, $2M_c$ and $2J_c$ represent the mass and pitch moment of inertia of one half of car body. Accordingly, the total mass and pitch inertia used in dynamic equations are $2M_c$ and $2J_c$ respectively. This modeling approach is adopted to reduce computational complexity while preserving the dynamic behaviour of the full system.

Table 0.4 Generalized high-speed train model coordinates

Parameter	Vertical motion	Pitch motion	No. of DOFs
Car	y_c	ϕ_c	2
Front bogie	y_{b1}	ϕ_{b1}	2
Rear bogie	y_{b2}	ϕ_{b2}	2
Wheelset 1	y_{w1}		1
Wheelset 2	y_{w2}		1
Wheelset 3	y_{w3}		1
Wheelset 4	y_{w4}		1

Here is the method by which this vehicle element's nodal displacement vector is defined:

$$u_v^e = \left\{ \begin{matrix} y_{r1}\ \phi_{r1}\ y_{r2}\ \phi_{r2}\ y_{r3}\ \phi_{r3}\ y_{r4}\ \phi_{r4}\ y_{r5}\ \phi_{r5}\ y_{r6}\ \phi_{r6}\ y_{r7}\ \phi_{r7}\ y_{r8}\ \phi_{r8} \\ y_c\ \phi_c\ y_{b1}\ y_{b2}\ \phi_{b1}\ \phi_{b2}\ y_{w1}\ y_{w2}\ y_{w3}\ y_{w4} \end{matrix} \right\}^T \quad (3.7)$$

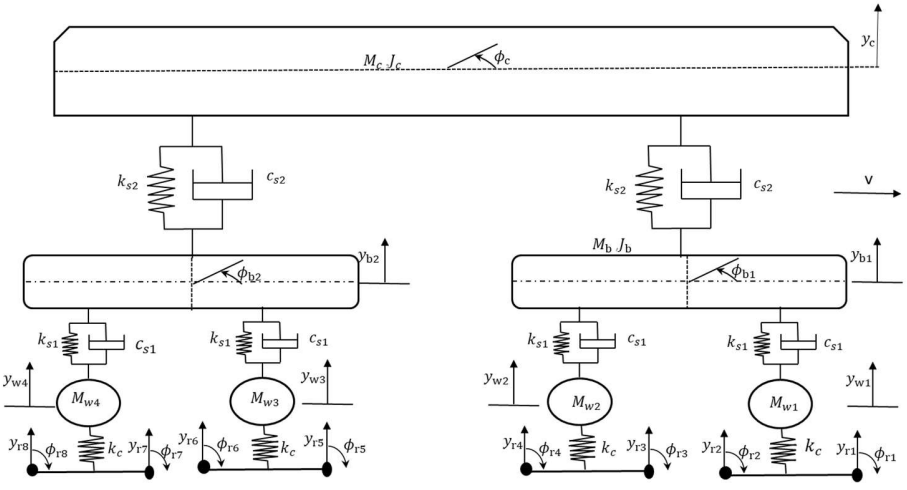

Figure. 0.16 Symmetrical vehicle–track interaction

For node j, the vertical rail displacement and rail slope can be obtained by y_{rj} and ϕ_{rj} (, 2..., 8); Figure3.16 displays vertical displacement of rail at each wheel-rail contact point, labeled as y_{cj} for (j = 1, 2, 3, 4). Additionally, y_c represents vertical motion of coach body, while ϕ_c denotes its pitch motion. The vertical and pitch motions of two bogies are denoted as y_{bj} and ϕ_{bj} for (j = 1, 2), respectively. Lastly, y_{wj} for (j = 1,2,3,4) represents vertical displacement of each wheel in contact with rail.

The following Lagrange equation may have been applied in the process of formulating an equation for finite element that represents vehicle element:

$$\frac{d}{dt}\frac{\partial L}{\partial \dot{u}} - \frac{\partial L}{\partial u} + \frac{\partial R}{\partial \dot{u}} = 0 \tag{3.8}$$

In Equation (3.8), R is dissipation energy, and L stands for the Lagrange function, it is represented as $L = T - \Pi$; T and Π symbolize kinetic and potential energies, respectively; u and $\dot{u}$ are nodal displacement and velocity vectors, respectively.

The following Equation describes kinetic energy of this vehicle element:

$$T = 0.5\ \dot{u}_v^{eT}\ M_v^e \dot{u}_v^e \tag{3.9}$$

Where M_v^e stands for vehicle element's mass matrix, vehicle has symmetric stiffness matrix, which can be determined as:

$$M_v^e = \begin{bmatrix} 0_{16\,X16} & \vdots \\ \cdots & M_{ve} \end{bmatrix}_{26X26} \tag{3.10}$$

$$M_v^e = \\ diag[\ M_c \quad J_c \quad M_b \quad M_b \quad J_b \quad J_b \quad M_{w1} \quad M_{w2} \quad M_{w3} \quad M_{w4}\ ] \tag{3.11}$$

The following Equation describes the potential energy of this vehicle element:

$$\Pi = 0.5\ u_v^{eT}\ K_v^e + \ u_v^{eT}\ F_v^e \tag{3.12}$$

K_v^e stands for vehicle element's stiffness matrix, and F_v^e is for nodal load vector.

$$K_v^e = K_c + K_v \tag{3.13}$$

The vehicle has symmetric stiffness matrix, which can be determined as:

$$K_v = \begin{bmatrix} 0_{16\,X16} & \vdots \\ \cdots & K_{ve} \end{bmatrix}_{26X26} \tag{3.14}$$

$$K_{ve} = \begin{bmatrix} 2k_{s2} & 0 & k_{s2} & 2k_{s2} & 0 & 0 & 0 \\ \square & 2k_{s2}\,l_b^2 & k_{s2}\,l_b & -k_{s2}\,l_b & 0 & 0 & 0 \\ \square & \square & 2k_{s1}+k_{s2} & 0 & 0 & 0 & -k_{s1} \\ \square & \square & \square & 2k_{s1}+k_{s2} & 0 & 0 & 0 \\ \square & \square & \square & \square & 2k_{s1}\,l_w^2 & 0 & k_{s1}\,l_w \\ \square & \square & \square & \square & \square & 2k_{s1}\,l_w^2 & 0 \\ \square & \square & \square & \square & \square & \square & k_{s1} \\ \square & symmetry & \square & \square & \square & \square & \square \\ \square & \square & \square & \square & \square & \square & \square \\ \square & \square & \square & \square & \square & \square & \square \end{bmatrix}$$

Where $2l_w$ is length of wheelbase, and $2l_b$ is space between centers of two bogie axles.

$$K_c = \begin{bmatrix} NN_{c4} & 0 & 0 & 0 & 0 & NI_{c4} \\ \square & NN_{c3} & 0 & 0 & 0 & NI_{c3} \\ \square & \square & NN_{c2} & 0 & 0 & NI_{c2} \\ \square & \square & \square & NN_{c1} & 0 & NI_{c1} \\ \square & Symmetry & \square & \square & 0_{6X6} & 0 \\ \square & \square & \square & \square & \square & I_{4X4} \end{bmatrix}_{26X26} \quad (3.15)$$

I_{4X4} represents identity matrix at rank 4.

$$NN_{ci} = \begin{bmatrix} N_1^2 & N_1N_2 & N_1N_3 & N_1N_4 \\ \square & N_2^2 & N_2N_3 & N_2N_4 \\ \square & \square & N_3^2 & N_3N_4 \\ \square & symmetry & \square & N_4^2 \end{bmatrix}_{x_{ci}} \quad (3.15a)$$

$$NI_{c1} = \begin{bmatrix} -N_1 & 0 & 0 & 0 \\ -N_2 & 0 & 0 & 0 \\ -N_3 & 0 & 0 & 0 \\ -N_4 & 0 & 0 & 0 \end{bmatrix}_{x_{c1}} \quad NI_{c2}$$

$$= \begin{bmatrix} 0 & -N_1 & 0 & 0 \\ 0 & -N_1 & 0 & 0 \\ 0 & -N_3 & 0 & 0 \\ 0 & -N_4 & 0 & 0 \end{bmatrix}_{x_{c2}} \quad (3.15b)$$

$$NI_{c3} = \begin{bmatrix} 0 & 0 & -N_1 & 0 \\ 0 & 0 & -N_2 & 0 \\ 0 & 0 & -N_3 & 0 \\ 0 & 0 & -N_4 & 0 \end{bmatrix}_{x_{c3}} \qquad NI_{c4}$$
$$= \begin{bmatrix} 0 & 0 & 0 & -N_1 \\ 0 & 0 & 0 & -N_2 \\ 0 & 0 & 0 & -N_3 \\ 0 & 0 & 0 & -N_4 \end{bmatrix}_{x_{c4}} \qquad (3.15c)$$

The Hermitian cubic polynomials compute the $N_1, N_2, N_3, and\ N_4$ interpolation functions. Wheel-rail contact occurs at certain location along the element; hence, interpolation functions are calculated for $x = x_{ci}$

$$N_1 = 1 - 3\left(\frac{x^2}{l_e^2}\right) + 2\left(\frac{x^3}{l_e^3}\right) \; ; \; N_2 = -x + \left(\frac{2x^2}{l_e}\right) - \left(\frac{x^3}{l_e^2}\right) ;$$
$$N_3 = 3\left(\frac{x^2}{l_e^2}\right) - 2\left(\frac{x^3}{l_e^3}\right) \; ; N_4 = \left(\frac{x^2}{l_e}\right) - \left(\frac{x^3}{l_e^2}\right) \qquad (3.15d)$$

F_v^e for the nodal load vector

$$F_v^e = F_v + F_\eta \qquad (3.16)$$

$$F_v = \{0_{1X16} \; -M_C g \; 0 \; -M_S g \; -M_S g \; 0 \; 0 \; -M_{w1} g \; -M_{w2} g \; -M_{w3} g \; -M_{w4} g\}^T \qquad (3.17)$$

$$F_\eta = k_c \eta_1 N_{1c} + k_c \eta_2 N_{2c} + k_c \eta_3 N_{3c} + k_c \eta_4 N_{4c} \qquad (3.18)$$

Where η_i $\{i = 1, 2, 3, 4\}$ symbolizes track vertical profile irregularity at rail point of contact with i^{th} wheel.

Where interpolation functions N_i (i = 1,2,3,4) are represented by (Eq. 3.15d), N_{1c} may be obtained by first substituting local coordinate of wheel-rail contact point into $N_1 - N_4$. Similarly, N_{2c}, N_{3c}, and N_{4c} may be obtained by replacing local coordinates x_{c2}, x_{c3} and x_{c4} into the interpolation functions.

$$N_{1c} = \{0_{1X12} \; -N_1 \; -N_2 \; -N_3 \; -N_4 \; 0_{1X6} \; 1 \; 0_{1X3}\}^T \qquad (3.19)$$

$$N_{2c} = \{0_{1X8} \; -N_1 \; -N_2 \; -N_3 \; -N_4 \; 0_{1X11} \; 1 \; 0_{1X3}\}^T \qquad (3.20)$$

$$N_{3c} = \{0_{1X4} \; -N_1 \; -N_2 \; -N_3 \; -N_4 \; 0_{1X16} \; 1 \; 0\}^T \qquad (3.21)$$

$$N_{4c} = \{-N_1 \; -N_2 \; -N_3 \; -N_4 \; 0_{1X21} \; 1\}^T \qquad (3.22)$$

The following Equation describes dissipation energy of this vehicle element:

$$R = 0.5\ \mathring{u}_v^{eT}\ C_v^e\ \mathring{u}_v^e \tag{3.23}$$

$$C_v^e = \begin{bmatrix} 0_{16\,X16} & \square \\ \square & C_{ve} \end{bmatrix}_{26X26} \tag{3.24}$$

$$C_{ve} = \begin{bmatrix} 2c_{s2} & 0 & -c_{s2} & -c_{s2} & 0 & 0 & 0 & 0 & 0 \\ \square & 2c_{s2}\,l_b^2 & c_{s2}\,l_b & -c_{s2}\,l_b & 0 & 0 & 0 & 0 & 0 \\ \square & \square & 2c_{s1}+c_{s2} & 0 & 0 & 0 & -c_{s1} & -c_{s1} & 0 \\ \square & \square & \square & 2c_{s1}+c_{s2} & 0 & 0 & 0 & 0 & -c_{s1} \\ \square & \square & \square & \square & 2c_{s1}\,l_w^2 & 0 & c_{s1}\,l_w & -c_{s1}\,l_w & 0 \\ \square & \square & \square & \square & \square & 2c_{s1}\,l_w^2 & 0 & 0 & c_{s1}\,l_w \\ \square & \square & \square & \square & \square & \square & c_{s1} & 0 & 0 \\ \square & symmetry & \square & \square & \square & \square & \square & c_{s1} & 0 \\ \square & \square & \square & \square & \square & \square & \square & \square & c_{s1} \\ \square & \square & \square & \square & \square & \square & \square & \square & \square \end{bmatrix} \tag{3.24a}$$

3.5.4 Slab track element model

Figure 3.17 shows a three-layer continuous beam railway slab track structure. The railway slab track element model has three parts: rail beam supported by discrete rail pad, concrete slab layer beam, and concrete supporting layer as hydraulically bonded bearing layer (HBL). These parts are linked by spring dashpot units. In Figure 3.17 , the parameters m_r, m_s and m_h represent mass per unit of length of rail, concrete track slab, and concrete support layer, and I_r, I_s and I_h denote moment of inertia of rail, track slab, and concrete support layer, and $\in_r$, $\in_s$ and $\in_h$ stand for elasticity modulus of rail, concrete slab layer, and concrete support layer c_r and k_r are damping coefficients and stiffness of railway slab track panel per unit length of slab track caused by rail pad and fastening, respectively. c_s and k_s CA mortar caused damping coefficients and stiffness per unit length of railway slab track. c_h and k_h are damping coefficients and stiffness per unit length of railway slab track caused by subgrade, respectively. In this study, the rail beams are modelled as Euler–Bernoulli beams with free–free boundary conditions at both ends. The rail beam is extended sufficiently far from the moving load to ensure that boundary effects are negligible. This formulation captures bending-dominated

vertical vibration modes, and the system's dynamic response is computed in the time domain using direct integration (Newmark method), inherently accounting for all relevant vibration modes without requiring explicit modal decomposition.

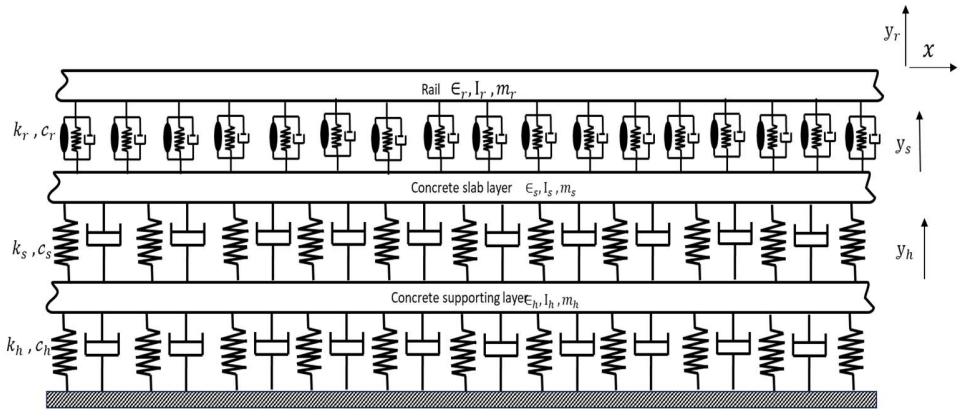

Figure 0.17 Simplified three-layer beam railway slab track model

3.5.4.1 Governing equation for element model of slab track

The governing equations that dictate the behavior of slab track subsystems can be delineated as follows: specifically, Describe vertical displacements of concrete support layer, railroad slab track, and rail as y_r, y_s and y_h.

$$\in_r I_r \frac{\partial^4 y_r}{\partial x^4} + m_r \frac{\partial^2 y_r}{\partial t^2} + c_r \left[\frac{\partial y_r}{\partial t} - \frac{\partial y_s}{\partial t}\right] + k_r(y_r - y_s) = \sum_{i=1}^{m} Q_{fi}(t)\delta(x - Vt) + \sum_{i=1}^{4} P_i(t)\delta(x - Vt) \quad (3.25)$$

$$\in_s I_s \frac{\partial^4 y_s}{\partial x^4} + m_s \frac{\partial^2 y_s}{\partial t^2} + c_s \left[\frac{\partial y_s}{\partial t} - \frac{\partial y_h}{\partial t}\right] - c_r \left[\frac{\partial y_r}{\partial t} - \frac{\partial y_s}{\partial t}\right] + k_s(y_s - y_h) - k_r(y_r - y_s) = 0 \quad (3.26)$$

$$\in_h I_h \frac{\partial^4 y_h}{\partial x^4} + m_h \frac{\partial^2 y_h}{\partial t^2} + c_h \left[\frac{\partial y_r}{\partial t}\right] - c_s \left[\frac{\partial y_s}{\partial t} - \frac{\partial y_h}{\partial t}\right] + k_h y_h - k_s(y_s - y_h) = 0 \quad (3.28)$$

The force that acts as force that comes into contact with rail and wheel set is P_i (i=1,2,3,4). V as speed, and δ (s + xi) as function of Dirac delta. The vertical dynamic force acting on the ith rail pad, referred to as Q_{fr} is the force supporting the rail.

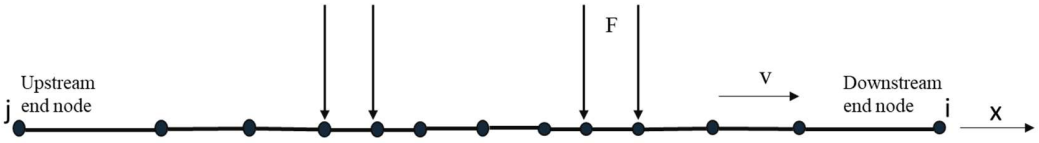

Figure 0.18 Discretization of rail beam of slab track into moving elements

The rail beam is discretized into limited number of moving components for numerical modeling, as depicted in Figure 3.19. Presumably, end forces and moments at both downstream and upstream terminals of beam are zero since they are sufficiently removed from contact force. When using MEM, correlation between moving coordinate w-axis and fixed x-axis. A moving coordinate is defined as follows for movable element of length l_e with nodes i and j:

$$w = x - x_l - Vt \tag{3.29}$$

The stationary coordinate of node ith is x_l. Therefore, the origin of z coordinates travels with a moving train or force. By substituting the aforementioned simple transformation into the equations (3.25- 3.28), governing equations for beam model of slab track in MEM have been derived.

$$\begin{aligned} &\in_r I_r \frac{\partial^4 y_r}{\partial w^4} + m_r \left[V^2 \frac{\partial^2 y_r}{\partial w^2} - 2V \frac{\partial^2 y_r}{\partial w \partial t} + \frac{\partial^2 y_r}{\partial t^2}\right] + c_r \left[\frac{\partial y_r}{\partial t} - V \frac{\partial y_r}{\partial w}\right] - c_r \left[\frac{\partial y_s}{\partial t} - V \frac{\partial y_s}{\partial w}\right] \\ &+ k_r(y_r - y_s) = \sum_{i=1}^{4} P_i(t)\delta(w + x_i) + \sum_{i=1}^{m} Q_{fi}(t)\delta(w + x_i) \end{aligned} \tag{3.30}$$

$$\begin{aligned} &\in_s I_s \frac{\partial^4 y_s}{\partial w^4} + m_s \left[V^2 \frac{\partial^2 y_s}{\partial w^2} - 2V \frac{\partial^2 y_s}{\partial w \partial t} + \frac{\partial^2 y_s}{\partial t^2}\right] + c_s \left[\frac{\partial y_s}{\partial t} - V \frac{\partial y_s}{\partial w}\right] \\ &- c_s \left[\frac{\partial y_h}{\partial t} - V \frac{\partial y_h}{\partial w}\right] - c_r \left[\frac{\partial y_r}{\partial t} - V \frac{\partial y_r}{\partial w}\right] + c_r \left[\frac{\partial y_s}{\partial t} - V \frac{\partial y_s}{\partial w}\right] + k_s(y_s - y_h) \\ &- k_r(y_r - y_s) \\ &= 0 \end{aligned} \tag{3.31}$$

$$\begin{aligned} &\in_h I_h \frac{\partial^4 y_h}{\partial w^4} + m_h \left[V^2 \frac{\partial^2 y_h}{\partial w^2} - 2V \frac{\partial^2 y_h}{\partial w \partial t} + \frac{\partial^2 y_h}{\partial t^2}\right] + c_h \left[\frac{\partial y_h}{\partial t} - V \frac{\partial y_h}{\partial w}\right] - c_s \left[\frac{\partial y_s}{\partial t} - \frac{\partial y_s}{\partial t}\right] \\ &+ c_s \left[\frac{\partial y_h}{\partial t} - V \frac{\partial y_h}{\partial w}\right] + k_h y_h - k_s(y_s - y_h) \\ &= 0 \end{aligned} \tag{3.32}$$

Matrix elements of railway slab track: mass, damping, and stiffness

Figure 3.20 illustrates track element model of three layers of continuous elastic beams are generate as moving element matrices of slab track. Where y1, y_4 and ϕ_1,$\phi_4$are vertical displacements of rails and their corresponding angle of rotation for nodes 1 and 4, respectively; y_2, y_5, and ϕ_2, ϕ_5 are vertical displacements and angle of rotation of

concrete slab for nodes 2 and 5, respectively; and y_3, y_6 and ϕ_3, ϕ_6 are vertical displacements and angle of rotation of HBL for nodes 3 and 6, respectively.

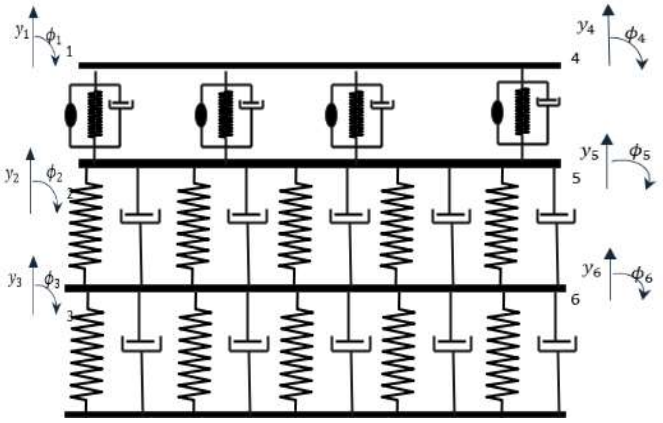

Figure 0.19 Moving three-layer slab track element model

The model includes rail pads as discrete viscoelastic supports. At the same time, CAM and subgrade are represented as continuous viscoelastic spring-dashpot units, which account for their elastic stiffness and damping qualities. In case of discrete rail pads, it is essential to remember that rail's support stiffness will always fluctuate regularly with duration depending on moving position and must be updated continuously. Hence, this dynamic element differs from continuously supported dynamic element (Lei & Wang, 2014). The concrete slab and HBL are modelled as 2D beam elements with continuous elastic support. To correctly show how the CAM layer and the subgrade affect elasticity and damping, use specific equivalent stiffness and damping coefficients. As a result, the nodal displacement vector corresponding to the dynamic track element can be expressed as follows:

$$u_l^e = \{y_1\ \phi_1\ y_2\ \phi_2\ y_3\ \phi_3\ y_4\ \phi_4\ y_5\ \phi_5\ y_6\ \phi_6\}^T \quad (3.33)$$

Hermitian cubic polynomials are used to compute the interpolation functions (Ni = 1,2,3,4):

$$N_1 = 1 - 3\left(\frac{w^2}{{l_e}^2}\right) + 2\left(\frac{w^3}{{l_e}^3}\right) \quad ; \quad N_2 = -w + \left(\frac{2w^2}{l_e}\right) - \left(\frac{w^3}{{l_e}^2}\right) \quad (3.34)$$

$$N_3 = 3\left(\frac{w^2}{l_e^{\,2}}\right) - 2\left(\frac{w^3}{l_e^{\,3}}\right) \quad ; \quad N_4 = \left(\frac{w^2}{l_e}\right) - \left(\frac{w^3}{l_e^{\,2}}\right)$$

Rail displacements (y_r) in moving track element can be described by using interpolation functions:

$$\begin{aligned} y_r &= N_1 y_1 + N_2 \phi_1 + N_3 y_4 + N_4 \phi_4 \\ &= [N_1 \;\; N_2 \;\; 0_{1X4} \;\; N_3 \;\; N_4 \;\; 0_{1X4}]\, r u_l^e \\ y_r &= N_r u_l^e \end{aligned} \tag{3.35}$$

Concrete slab displacements (y_s) in moving track element can be described by using interpolation functions.

$$\begin{aligned} y_s &= N_1 y_2 + N_2 \phi_2 + N_3 y_5 + N_4 \phi_5 \\ &= [0 \;\; 0 \;\; N_1 \;\; N_2 \;\; 0_{1X4} \;\; N_3 \;\; N_4 \;\; 0 \;\; 0]\, u_l^e \\ y_s &= N_s u_l^e \end{aligned} \tag{3.36}$$

HBL displacements (y_h) in moving track element can be described by using interpolation functions

$$\begin{aligned} y_h &= N_1 y_3 + N_2 \phi_3 + N_3 y_6 + N_4 \phi_6 \\ &= [0_{1X4} \;\; N_1 \;\; N_2 \;\; 0_{1X4} \;\; N_3 \;\; N_4]\, u_l^e \\ y_h &= N_h u_l^e \end{aligned} \tag{3.37}$$

Nr, N_s and N_h are matrix of interpolation functions for displacement of rails, concrete slab layer, and concrete supporting layer HBL and N_1, N_2, N_3, and N_4 are displacement interpolation functions for slab track element. The variational (or weak) form is obtained by multiplying equations (3.30- 3.32) with weighting functions (variations) y_r, y_s and y_h and integrating the result over element length.

$$\begin{aligned} \int_0^{l_e} y_r(w) \Bigg\{ & \in_r I_r \frac{\partial^4 y_r}{\partial w^4} + m_r \left[V^2 \frac{\partial^2 y_r}{\partial w^2} - 2V \frac{\partial^2 y_r}{\partial w \partial t} + \frac{\partial^2 y_r}{\partial t^2} \right] \\ & + c_r \left[\frac{\partial y_r}{\partial t} - V \frac{\partial y_r}{\partial w} \right] - c_r \left[\frac{\partial y_s}{\partial t} - V \frac{\partial y_s}{\partial w} \right] + k_r (y_r - y_s) \\ = & \sum_{i=1}^{4} P_i(t) \delta(w + x_i) + \sum_{i=1}^{m} Q_{fi}(t) \delta(w + x_i) \Bigg\} dw \end{aligned} \tag{3.38}$$

$$\int_0^{l_e} y_s(w)\left\{\in_s I_s \frac{\partial^4 y_s}{\partial w^4} + m_t\left[V^2\frac{\partial^2 y_s}{\partial w^2} - 2V\frac{\partial^2 y_s}{\partial w \partial t} + \frac{\partial^2 y_s}{\partial t^2}\right] + c_s\left[\frac{\partial y_s}{\partial t} - V\frac{\partial y_s}{\partial w}\right] - c_s\left[\frac{\partial y_h}{\partial t} - V\frac{\partial y_h}{\partial w}\right] - c_r\left[\frac{\partial y_r}{\partial t} - V\frac{\partial y_r}{\partial w}\right] + c_r\left[\frac{\partial y_s}{\partial t} - V\frac{\partial y_s}{\partial w}\right] + k_s(y_s - y_h) - k_r(y_r - y_s)\right\} dw = 0 \quad (3.39)$$

$$\int_0^{l_e} y_h(w)\left\{\in_h I_h \frac{\partial^4 y_h}{\partial w^4} + m_h\left[V^2\frac{\partial^2 y_h}{\partial w^2} - 2V\frac{\partial^2 y_h}{\partial w \partial t} + \frac{\partial^2 y_h}{\partial t^2}\right] + c_h\left[\frac{\partial y_h}{\partial t} - V\frac{\partial y_h}{\partial w}\right] - c_s\left[\frac{\partial y_s}{\partial t} - \frac{\partial y_s}{\partial t}\right] + c_s\left[\frac{\partial y_h}{\partial t} - V\frac{\partial y_h}{\partial w}\right] + k_h y_h - k_s(y_s - y_h)\right\} dw = 0 \quad (3.40)$$

The element mass, damping, and stiffness matrices for first layer of slab track in MEM can be determined using Equation (3.38), Galerkin's method, and Nr be the displacement interpolation shape function, expressed as:

$$\int_0^{l_e} y_h(w)\left\{\in_h I_h \frac{\partial^4 y_h}{\partial w^4} + m_h\left[V^2\frac{\partial^2 y_h}{\partial w^2} - 2V\frac{\partial^2 y_h}{\partial w \partial t} + \frac{\partial^2 y_h}{\partial t^2}\right] + c_h\left[\frac{\partial y_h}{\partial t} - V\frac{\partial y_h}{\partial w}\right] - c_s\left[\frac{\partial y_s}{\partial t} - \frac{\partial y_s}{\partial t}\right] + c_s\left[\frac{\partial y_h}{\partial t} - V\frac{\partial y_h}{\partial w}\right] + k_h y_h - k_s(y_s - y_h)\right\} dw = 0 \quad (3.41)$$

$$C_r = -2m_r V\int_0^{l_e} N_r^T N_{r,w}\, dw + c_r\int_0^{l_e} N_r^T N_r\, dw - c_r\int_0^{l_e} N_r^T N_t\, dw \quad (3.42)$$

$$K_r = \in_r I_r \int_0^{l_e} N_{r,ww}^T N_{r,ww}\, dw - m_r V^2 \int_0^{l_e} N_{r,w}^T N_{r,w}\, dw - c_r V \int_0^{l_e} N_r^T N_{r,w}\, d + c_r V \int_0^{l_e} N_r^T N_{s,w}\, dw + k_r \int_0^{l_e} N_r^T N_r\, dw - k_r \int_0^{l_e} N_r^T N_s\, dw \quad (3.43)$$

Where partial derivative concerning w is indicated by dw. The second and third-layer matrix of slab track can be generated using the same method as described above. This includes element mass, dampening, and stiffness matrices.

$$\mathcal{M}_s = m_s \int_0^{l_e} N_s^T N_s\, dw \quad (3.44)$$

$$C_s = -2m_s V \int_0^{l_e} N_s^T N_{s,w}\, dw + c_s \int_0^{l_e} N_s^T N_s\, dw - c_s \int_0^{l_e} N_s^T N_h\, dw - c_r \int_0^{l_e} N_s^T N_r\, dw + c_r \int_0^{l_e} N_s^T N_s\, dw \quad (3.45)$$

$$K_s = \in_s I_s \int_0^{l_e} N_{s,ww}^T N_{s,ww}\, dw - m_s V^2 \int_0^{l_e} N_{s,w}^T N_{s,w}\, dw - c_s V \int_0^{l_e} N_s^T N_{s,w}\, dw + c_s V \int_0^{l_e} N_s^T N_{h,w}\, dw + c_r V \int_0^{l_e} N_s^T N_{r,w}\, dw - c_r V \int_0^{l_e} N_s^T N_{s,w}\, dw + k_s \int_0^{l_e} N_s^T N_s\, dw - k_s \int_0^{l_e} N_s^T N_h\, dw - k_r \int_0^{l_e} N_s^T N_r\, dw + k_r \int_0^{l_e} N_s^T N_s\, dw \quad (3.46)$$

For concrete supporting HB layer

$$\mathcal{M}_h = m_h \int_0^{l_e} N_h^T N_h\, dw \quad (3.47)$$

$$C_h = -2m_h V \int_0^{l_e} N_h^T N_{h,w}\, dw + c_h \int_0^{l_e} N_h^T N_h\, dw - c_s \int_0^{l_e} N_h^T N_s\, dw + c_s \int_0^{l_e} N_h^T N_h\, dw \tag{3.48}$$

$$K_s = \in_h \mathrm{I}_h \int_0^{l_e} N_{h,ww}^T N_{h,ww}\, dw - m_h V^2 \int_0^{l_e} N_{h,w}^T N_{h,w}\, dw - c_h V \int_0^{l_e} N_h^T N_{h,w}\, dw + c_s V \int_0^{l_e} N_h^T N_{s,w}\, dw - c_s V \int_0^{l_e} N_h^T N_{h,w}\, dw + k_h \int_0^{l_e} N_h^T N_h\, dw - k_s \int_0^{l_e} N_h^T N_s\, dw + k_s \int_0^{l_e} N_h^T N_h\, dw \tag{3.49}$$

In MEM, slab track element's mass, damping, and stiffness matrices are as follows:

$$\mathcal{M}_t^e = \mathcal{M}_r^e + \mathcal{M}_s^e + \mathcal{M}_h^e$$
$$C_t^e = C_r^e + C_s^e + C_h^e \tag{3.50}$$
$$K_t^e = K_r^e + K_s^e + K_h^e$$

Based on the finite element assembly principle, the element-level mass matrix, damping matrix, and stiffness matrix from Equation (3.50) are integrated to construct the global mass matrix, damping matrix, and stiffness matrix of the slab track element within the MEM.

$$\mathcal{M}_t = \sum_e \mathcal{M}_t^e \; ; \; C_t = \sum_e C_t^e \; ; \; K_t = \sum_e K_t^e \tag{3.51}$$

The finite element equation of slab track structure in MEM can be determined by applying the Lagrange equation:

$$M_t \ddot{u} + C_t \dot{u} + K_t u = F_t \tag{3.52}$$

F_t is slab track structure's global nodal load vector.

3.5.5. The finite element equation of the vehicle-track coupling system

When there is a vehicle-track coupling system, the moving element method (MEM) includes both the track element and the vehicle element in the finite element equation. Here, K_t^e , $M_t^{e,}$ and C_t^e represent the stiffness, mass, and damping matrices of the track element, respectively. During numerical computation, the global stiffness, mass, and damping matrices of the track structure, along with the global load vector, only need to be assembled once. In each iteration of the calculation, these global matrices are combined with the load vectors of both the vehicle-track coupling system and the vehicle element, integrating them into the equivalent global stiffness, mass, and damping matrices for the system. Apply standard finite element assembly rules to the track structure and acquire the track structure's worldwide load vector. The following is a finite element equation that was arrived at as a consequence of the vehicle-track coupling system:

$$M\ddot{u} + C\dot{u} + Ku = F \tag{3.53}$$

Where $\ddot{u}, \dot{u}$, and u denote global acceleration, velocity, and displacement vectors of vehicle-slab track coupling system, respectively; M, C, and K denote global mass, damping, and stiffness matrices, respectively.

$$\begin{aligned} M &= \sum_e \mathcal{M}_t^e + \mathcal{M}_v^e \\ C &= \sum_e C_t^e + C_v^e \\ K &= \sum_e K_t^e + K_v^e \\ F &= \sum_e F_t^e + F_v^e \end{aligned} \tag{3.54}$$

The Newmark integration method, a mathematical method frequently employed in the study of engineering issues, was applied to solve the above Equation. The Newmark integration method is employed to solve the governing dynamic equation of the coupled vehicle–track system because of its robustness and unconditional stability for second-order systems. Equation (3.53), which governs the dynamic response of the coupled

vehicle–track system, is a second-order differential equation in time and cannot be solved analytically for most practical cases involving time-varying loads and complex boundary conditions. Therefore, a numerical time integration method is required. In this study, the Newmark integration scheme is employed due to its accuracy, numerical stability, and widespread applicability in structural dynamics problems.

where u, u̇ and ü denote the global nodal displacement, velocity, and acceleration vectors, respectively, and M, C, and K represent the global mass, damping, and stiffness matrices. The Newmark integration method is adopted due to its proven stability and accuracy for time-domain simulations of second-order systems. The Newmark method discretizes time domain and enables the computation of the displacement (u), velocity ($\dot{u}$), and acceleration (ü) at each time step. If the solution vectors $u^t, \dot{u}^t$ and $\ddot{u}^t$ at time step t, are known, the solution at the vector next time step t+Δt is obtained by solving the following system of equations:

$$(K + a_1 M + a_2 C)\, u^{t+\Delta t} = F^{t+\Delta t} + M(a_1 u^t + a_3 \dot{u}^t + a_4 \ddot{u}^t) + C(a_2 u^t + a_5 \dot{u}^t + a_6 \ddot{u}^t) \quad (3.55)$$

Where, $F^{t+\Delta t}$ is the external load vector at time t+Δt, $u_t, \dot{u}_t$ and $\ddot{u}_t$ are the known displacement, velocity, and acceleration vectors at time, and a_1 through a_6 coefficients are derived from the Newmark scheme.

Once $u^{t+\Delta t}$ is obtained by solving Equation (3.55), the velocity and acceleration vectors at the same time step are updated using the following expressions:

$$\dot{u}^{t+\Delta t} = a_2(u^{t+\Delta t} - u^t) - a_5 \dot{u}^t - a_6 \ddot{u}^t \quad (3.56)$$

$$\ddot{u}^{t+\Delta t} = a_1(u^{t+\Delta t} - u^t) - a^3 \dot{u}^t - a_4 \ddot{u}^t \quad (3.57)$$

The constants used in the above equations are defined as

$$a_1 = \frac{1}{\beta\, \Delta t^2}, a_2 = \frac{\gamma}{\beta \Delta t}, a_3 = \frac{1}{\beta \Delta t}, a_4 = \frac{0.5}{\beta} - 1, a_5 = \frac{\gamma}{\beta} - 1, a_6 = \Delta t\left(\frac{0.5\gamma}{\beta} - 1\right)$$

In the above formulation, Δt is the selected time step size, β and γ are algorithmic parameters of the Newmark method that control numerical damping and stability. In this

study, the algorithmic parameters of the Newmark method are chosen as $\gamma = 0.5$ and $\beta = 0.25$, corresponding to the average acceleration scheme. This choice ensures unconditional stability and second-order accuracy and avoids artificial numerical damping, which is particularly important for capturing accurate dynamic responses in high-speed vehicle–track interaction problems. Equations (3.55)– (3.57) are iteratively used at each time step to compute the displacement, velocity, and acceleration histories of the coupled vehicle–track system under dynamic excitation. The flowchart outlines step-by-step deterministic procedure adopted in the present study to evaluate dynamic behavior of a high-speed train running over a track system, as shown in Figure 3.20.

Table 0.5 Parameters for high-speed train E-5 Series

Parameters	Values	Units
Mass of coach's body	42000	kg
Mass of train bogie	3000	kg
Mass of train wheel	1200	kg
Pitch inertia of coach body	5.38×10^5	$kg.m^2$
Pitch inertia of train bogie	6800	$kg.m^2$
Stiffness of primary suspension system	2.08	MN/m
Stiffness of secondary suspension system	0.8	MN/m
Damping of primary suspension system	120	kN.s/m
Damping of secondary suspension system	150	kN.s/m
Wheelbase length	2.4	m
Distance between Centre of rear train bogie and the Centre of front train bogie	17.375	m
Stiffness of wheel-rail interaction	1.346×10^3	MN/m
Axle load	140	kN

The developed model incorporates realistic design inputs and accounts for essential physical interactions, including nonlinear wheel–rail contact based on Hertzian theory and frictional behavior of the rail pad. Tables 3.2 and 3.5 include parameters for the high-speed bullet train and the Shinkansen slab track structure. The integrated train–track system is analyses over main track span of 150 meters, with an additional 50 meters

extended on both entry and exit ends to minimize boundary-induced disturbances during dynamic response. For the numerical analysis, the entire system is discretized into 300 elements and a single multi-body vehicle model. The dynamic governing equations were solved in the time domain using an implicit integration scheme to account for nonlinearities in wheel–rail interaction and rail pad stiffness.

The investigation considers critical influencing factors such as material characteristics of track structure, varying train speeds, and geometric imperfections arising from track irregularities. Key dynamic responses such as vertical displacements of track components, wheel–rail contact forces, and interlayer stress distributions are extracted and analyzed.

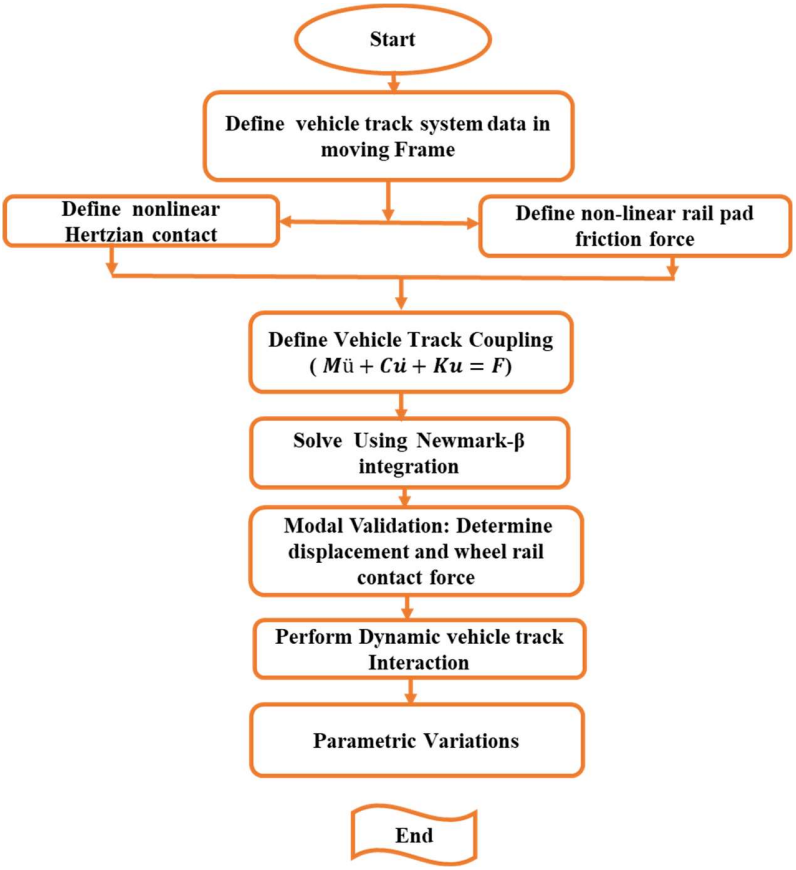

Figure 0.20 Flow chart of methodology for dynamic vehicle track interaction

3.6 Methodology for Objective 4 – Fatigue Study of Cement Asphalt Mortar (CAM)

"Fatigue Life Assessment and Modulus Degradation of Cement Asphalt Mortar for High-Speed Rail Applications"

The fatigue performance of the cement asphalt mortar (CAM) layer was evaluated through a laboratory-based experimental program, since this interlayer plays a critical role in transferring wheel loads from the slab to the foundation in high-speed railway tracks. The methodology adopted was designed to establish the static flexural strength of CAM and to assess its fatigue response under repeated flexural loading, thereby generating stress–life (S–N) curves and quantifying the strain and stiffness degradation behavior.

The CAM specimens were prepared using Ordinary Portland Cement (OPC, 53 grade), a slow-setting cationic asphalt emulsion, and graded fine aggregates, along with carefully selected admixtures to regulate shrinkage, workability, and air entrainment. The physical and chemical properties of cement are summarized in Table 3.6, demonstrating conformity with the relevant standards IS 12269: 2013(BIS, 2013). This selection ensures a balanced combination of workability and strength for the intended application. The technical properties of emulsified asphalt are evaluated following relevant test standards (Standard, 2018). A summary of their key properties is presented in Table 3.7.

Prismatic beams of dimensions 100 × 100 × 500 mm were cast in steel moulds, compacted by vibration, and cured for 28 days under controlled conditions of temperature and humidity to ensure proper hydration and asphalt film formation. A total of 24 specimens were prepared for study: 12 specimens have been designated for static flexural strength testing, while the remaining 12 were used for flexural fatigue testing.

Table 0.6 Physical and chemical properties of cement

Property	Test value
Fineness, m^2/kg, Min	240
Loss on ignition, % /mass, Max	3.0
Chloride content, % /, Max	0.8
Ratio of percentage of lime to percentages of silica, alumina, and iron oxide, when calculated by the formula: $\frac{(CaO - 0.7\,SO_3)}{(2.8\,SiO_2 + 1.2\,Al_2O_3 + 0.65\,Fe_2O_3)}$	0.95
Ratio of percentage of alumina to that of iron oxide, Min	0.7
Magnesia (MgO), % / mass, Max	4.5
Total Sulphur content calculated at SO_3, percent by mass, Max	3.0

Table 0.7 Technical properties of emulsified asphalt

Density (g/cm^3)	1.0
Storage Stability (24hr, 25 C)	0.6
Residue on 600 µm sieve (%)	0.04
Solid content (%)	65
Ductility (27 C/cm)	>50
Penetration (25 C/ 100g/5 sec)	80

The experimental program commenced with static flexural strength testing, conducted using a four-point bending configuration on a servo-hydraulic universal testing machine, as shown in Figure 3.21. The clear span was maintained at 400 mm with a pure bending zone of span/3. The average flexural strength obtained from these tests served as the reference strength for designing the subsequent fatigue tests. Fatigue testing was performed on identical CAM beams using the same four-point bending setup, but with cyclic loading applied in a sinusoidal waveform at a frequency of 2 Hz to replicate train-induced loading conditions. The Complete methodology of CAM fatigue study is discussed in Figure 3.22.

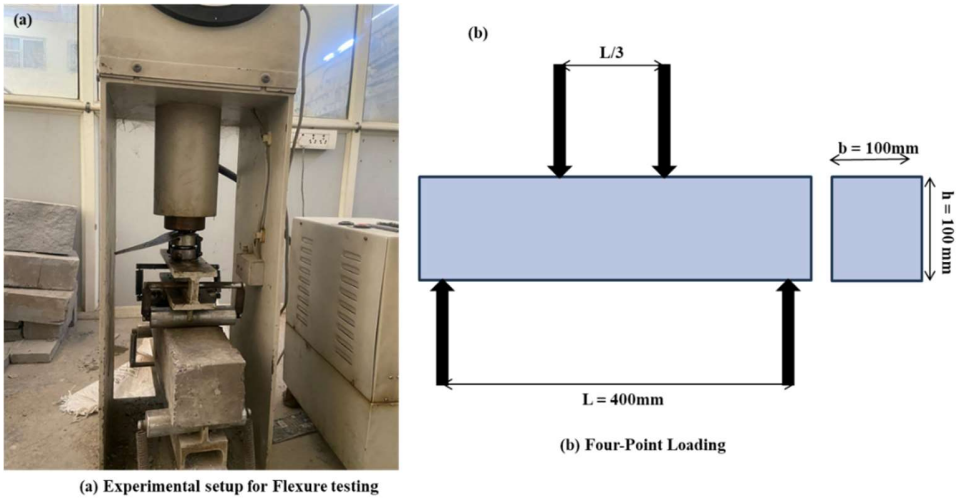

Figure 0.21 Experimental setup for the static four-point flexural strength test of CAM

The stress levels were selected as fixed percentages of the static flexural strength, specifically 0.65, 0.70, 0.75, and 0.80, with a minimum-to-maximum stress ratio of 0.1. For each stress level, the number of load cycles to failure (N_f) was recorded, and these results were plotted to develop the S–N relationship of CAM. In addition to fatigue life evaluation, strain gauges were mounted on the specimen surfaces to record strain histories throughout the fatigue tests. The fatigue strain evolution was analyzed in three characteristic stages: (i) a rapid strain increases during the initiation stage, (ii) a gradual and relatively stable strain growth during the propagation stage, and (iii) a final stage of accelerated strain rise leading to specimen failure. The fatigue modulus was also computed at different cycle ratios, allowing the assessment of stiffness degradation with increasing fatigue damage. The combination of S–N curves, strain evolution patterns, and modulus degradation characteristics provided a comprehensive understanding of CAM's fatigue behavior under repetitive flexural loading. These results formed the basis for predicting the fatigue performance of CAM in slab track applications.

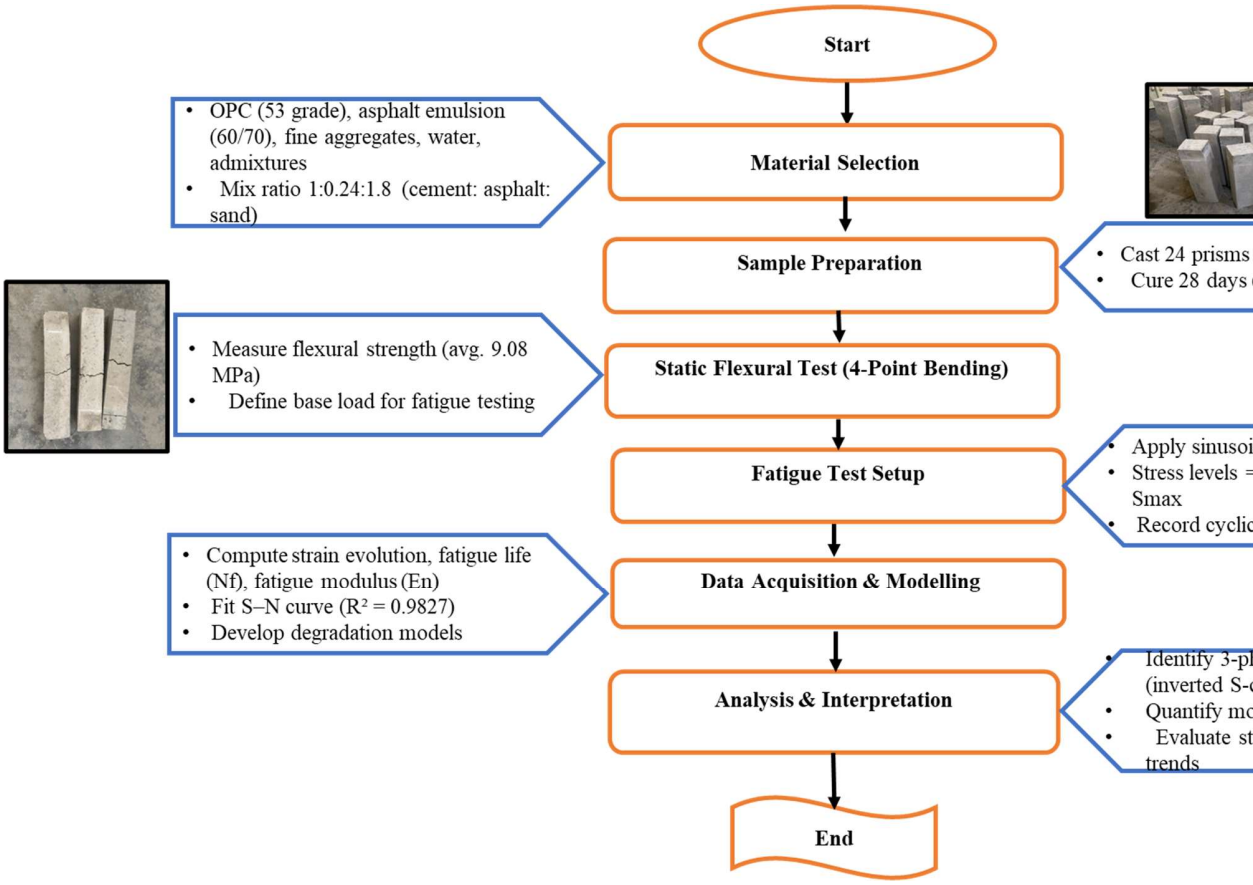

Figure 0.22 Flow chart of methodology for fatigue study of CAM

CHAPTER 4: STATIC RESPONSE RESULTS AND DISCUSSIONS

4.1 General

This chapter presents the outcomes of the static response analysis of slab and ballasted track systems, conducted using three-dimensional finite element modeling in ANSYS. The purpose of the analysis is to examine the comparative behavior of the two-track systems under standardized loading conditions and evaluate the influence of key track design parameters on the overall performance of the slab track systems. The UIC LM71 loading configuration, widely adopted in international practice for evaluating railway structures, has been applied to the developed models to simulate a loading condition representative of real train operations.

The static response is fundamental in understanding the immediate deformation and stress distribution of the track system under service loads. This analysis forms the basis for subsequent dynamic and fatigue evaluations, as it reveals structural stiffness, displacement control, and stress transfer mechanisms within track components. To ensure reliability, the modelling framework was validated against published studies and earlier finite element investigations.

The chapter is divided into two major sections. The first section presents a comparative analysis between conventional ballasted and modern slab track systems. The comparative discussion highlights the differences in vertical displacement, bending stresses, and stress redistribution patterns, thereby establishing the performance advantages and limitations of slab track systems in high-speed applications. The second section presents a comprehensive parametric study of slab track systems, in which the effects of variations in rail pad stiffness, CA mortar (CAM) stiffness, subgrade stiffness, slab thickness, CAM thickness, and hydraulic bonded layer (HBL) thickness are systematically evaluated. The results are interpreted in detail, followed by engineering implications for the design and optimization of slab track systems in India's high-speed railway corridors.

4.2 Comparative Analysis of Ballast and Slab Track

4.2.3 Comparative Results: Ballast vs. Slab Track

The comparative analysis between ballasted and slab track systems revealed significant differences in terms of displacement control, stress distribution, and overall structural stiffness.

Vertical Displacements: The mid-span displacement under LM71 loading was substantially lower in the slab track system compared to the ballasted track. As shown in Figure 4.1, the slab track exhibited a maximum deflection of approximately -1.08 mm, whereas the ballasted track displayed -1.5 mm. This represents a nearly 40–45% reduction in vertical displacement, demonstrating the superior stiffness of the slab track system.

Bending Stresses: The stress contours presented in Figure 4.2 illustrate the difference in stress distribution between the two track systems. On the ballasted track, stress concentrations were observed around the sleeper–ballast interface, leading to higher localized stresses. By contrast, the slab track provided a more uniform stress transfer through the concrete slab, reducing the maximum bending stress by nearly 30–35%.

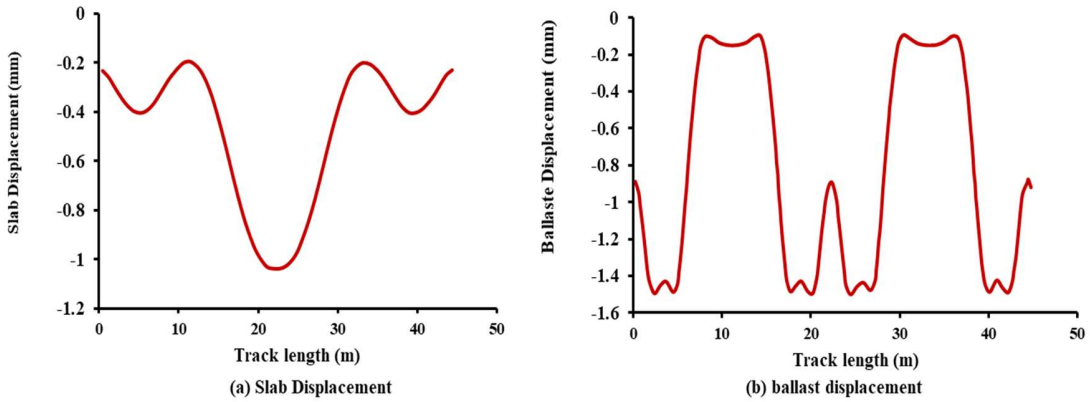

Figure 0.1 Vertical displacement of track under UIC LM71 load (a) Slab displacement (b) Ballast displacement

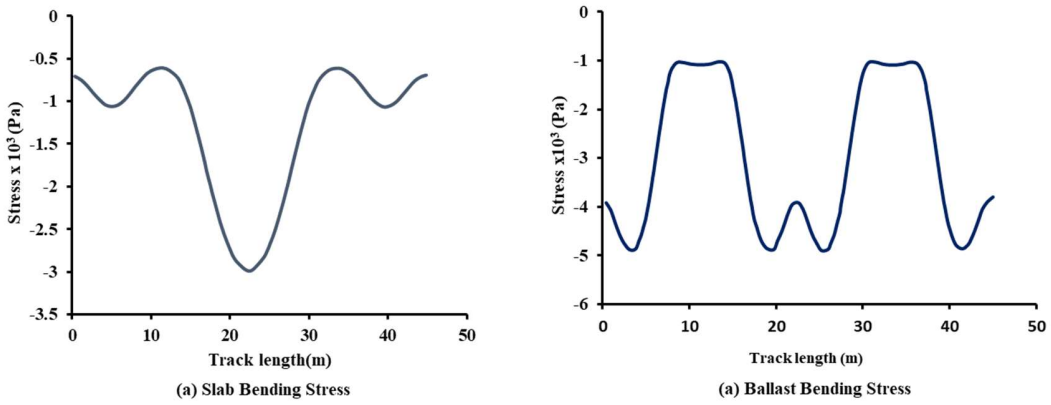

Figure 0.2 Bending stress distribution (a) Slab bending stress and (b) Ballast slab track

These results confirm that slab tracks are more effective in controlling deflections and distributing loads uniformly, making them more suitable for high-speed railway applications, such as the Mumbai–Ahmedabad High-Speed Rail (MAHSR). However, the increased rigidity of slab tracks also introduces challenges related to fatigue cracking of the slab and debonding at the CAM interface, issues that are not as severe in ballasted tracks due to their inherent flexibility.

4.3 Parametric Analysis of Slab Track

A parametric study was conducted to assess the impact of varying key design parameters on the static response of slab track systems. The parameters considered include rail pad stiffness, CAM stiffness, subgrade stiffness, slab thickness, CAM thickness, and HBL thickness. Each parameter was varied across a realistic design range, and the corresponding displacement, bending, and shear stresses were analyzed.

4.3.1 Effect of Rail Pad Stiffness

To explore the impact of rail fastening stiffness on Maximum bending stress, Maximum shear stress, and vertical deflection in rail, concrete slab, and concrete supporting HBL layer. The rail pad stiffness varies from 35 to 95 (MN/m^3). Rail pad stiffness for the standard track system has been considered to be 65 MN/m^3. Figures 4.3 illustrate the effects of rail pad stiffness variation on bending and shear stresses

across the track components. Compared to the standard stiffness, rail bending stress decreases by approximately 23% at 95 MN/m³ and increases by around 30% and 20% in the slab and HBL, respectively, demonstrating a redistribution of stress from the rail to other components. For shear stress, a similar pattern emerges. Shear stress in the rail reduces by about 16% at 95 MN/m³ relative to the standard value, while the slab and HBL experience increases of approximately 25% and 15%, respectively. This shift in stress highlights the role of increased stiffness in altering force transmission characteristics. Vertical deflection, on the other hand, decreases uniformly across all components as stiffness rises. Compared to the standard stiffness, rail vertical deflection decreases by around 33% at 95 MN/m³, while the slab and HBL experience reductions of approximately 20% and 17%, respectively. This reduction in deflection signifies enhanced stability and reduced deformation under vertical load.

55 The results show that as the stiffness of the rail pad increases, the vertical displacement of the rail decreases, indicating improved load transfer efficiency to the slab. However, this reduction in displacement comes at the cost of higher bending and shear stresses in the slab and HBL. Softer pads, while reducing stresses in the slab, lead to excessive rail deflections, which may compromise passenger comfort and track serviceability.

Thus, an optimal range of rail pad stiffness is necessary to strike a balance between displacement control and stress minimization. The results confirm that high-speed slab track design should avoid excessively stiff rail pads, as they increase the risk of premature slab cracking.

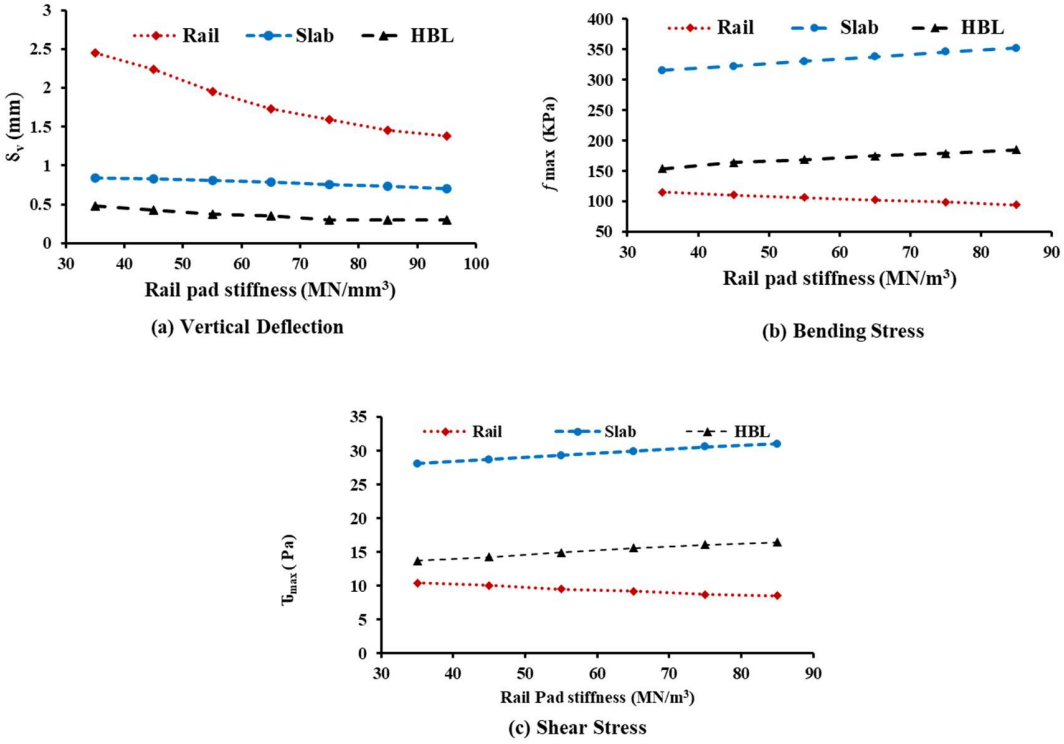

Figure 0.3 Impact of rail pad stiffness on both vertical deflection and stress (a) Vertical deflection (b) Bending stress (c) Shear stress

4.3.2 Effect of CAM Stiffness

The impact of varying stiffness of the CAM layer on the maximum stress, maximum shear stress, and vertical deflection of key track components rail, concrete slab, and the HBL was systematically analyzed. The CAM layer stiffness was varied from 300 MN/mm³ to 1800 MN/mm³, with the standard slab track stiffness set to 900 MN/mm³ for reference. Figures 4.4 illustrate the effects of CAM layer stiffness variation on bending and shear stresses across the track components. An increase in CAM stiffness from the standard track model resulted in negligible variation in the maximum stress of the rail, concrete slab, and HBL layer. This suggests that maximum bending stress in these components is relatively insensitive to moderate changes in CAM stiffness. The CAM stiffness significantly influenced the maximum shear stress of the track components: Concrete Slab: An increase of 9.88% in shear stress has been observed,

indicating that higher CAM stiffness amplifies shear stresses in the slab due to its role in redistributing load between the rail and underlying layers. Rail: A 4% decrease in shear stress has been noted, highlighting a reduction in shear load concentration within the rail, likely due to improved load transfer efficiency through the CAM layer. HBL Layer: A 4% increase in Maximum shear stress occurred, suggesting that higher CAM stiffness shifts additional shear forces into the substructure, potentially affecting the long-term durability of this layer. Changes in vertical deflection of the track components under varying CAM stiffness have also been assessed. Rail: A significant 11% reduction in vertical deflection has been predicted, implying improved rail stability and stiffness under increased CAM stiffness. Concrete Slab: The vertical deflection decreased by 16.67%, demonstrating that the concrete slab benefits from enhanced load distribution properties. HBL Layer: An 8.5% reduction in vertical deflection has been observed, reflecting the indirect effects of increased CAM stiffness on substructure displacement. These findings illustrate that while the stresses in the rail and slab remain largely unaffected, the vertical deflection and shear stress distribution across the track components are notably influenced by changes in CAM stiffness.

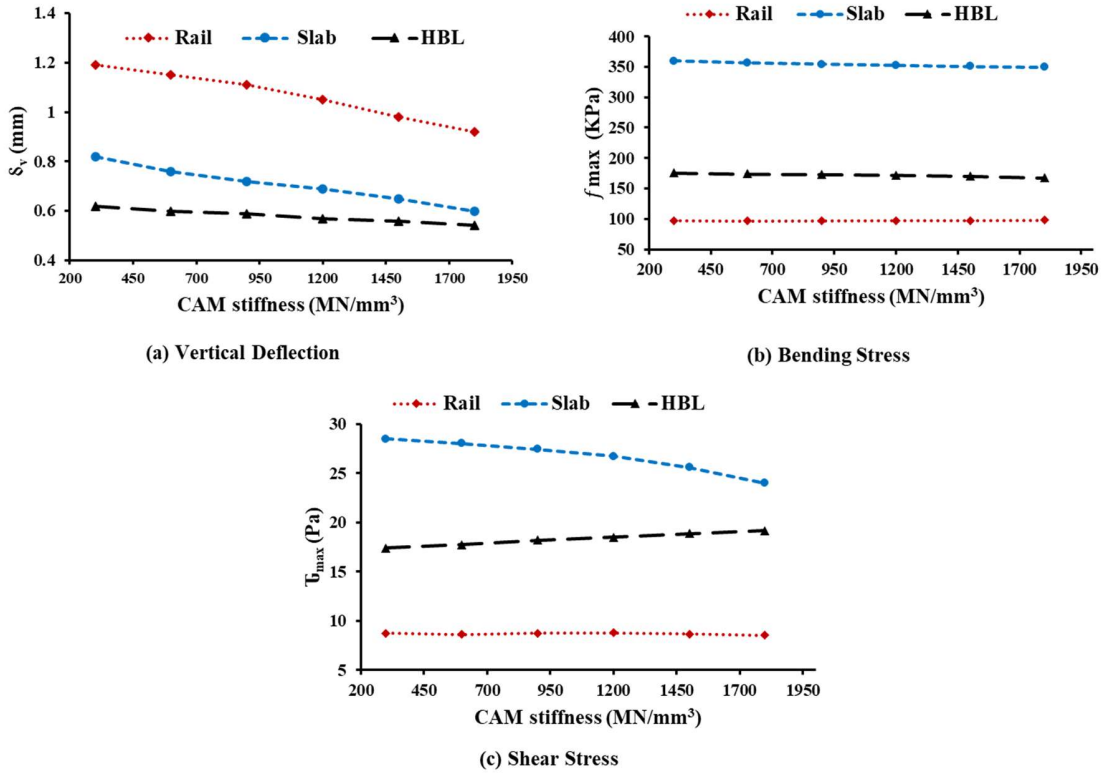

Figure 0.4 Effect of CAM stiffness on both vertical deflection and stress (a)vertical deflection (b)Bending stress (c) Shear stress

4.3.3 Effect of Subgrade Stiffness

To study the impact of subgrade stiffness on Maximum bending stress, Maximum shear stress, and vertical deflection in rail, concrete slab, and concrete supporting HBL layer. The subgrade stiffness varies from 30MN/mm^3 to 180MN/mm^3, and the stiffness for standard slab track has been considered as 65MN/ mm^3. Figures 4.5 illustrate the effects of subgrade stiffness variation on bending and shear stresses across the track components. Varying the subgrade stiffness from the standard track model, negligible variation in maximum bending HBL layer as compared to the standard track model, but an increase of 6.8 %. for concrete slab, and 2.4 % decrease for rail maximum bending stress. The maximum shear stress of rail and concrete slab has been increased to 13.72 % and 8.04 %, respectively. Whereas the shear stress of HBL layer has been

reduced by 6.4 %. Similarly, vertical deflection of track components has also been observed with varying subgrades. With the increase in subgrade stiffness, vertical deflection has decreased in all track components. The results show that increasing subgrade stiffness has notable effect on stress distribution and deformation across these components. subgrade stiffness plays a critical role in the performance of slab track systems. Higher stiffness improves track stability by reducing deflections but also intensifies stress and shear demands in some components, particularly the rail and slab. Optimizing subgrade stiffness is essential to balance stress distribution, minimize deformation, and ensure the durability and safety of high-speed railway systems.

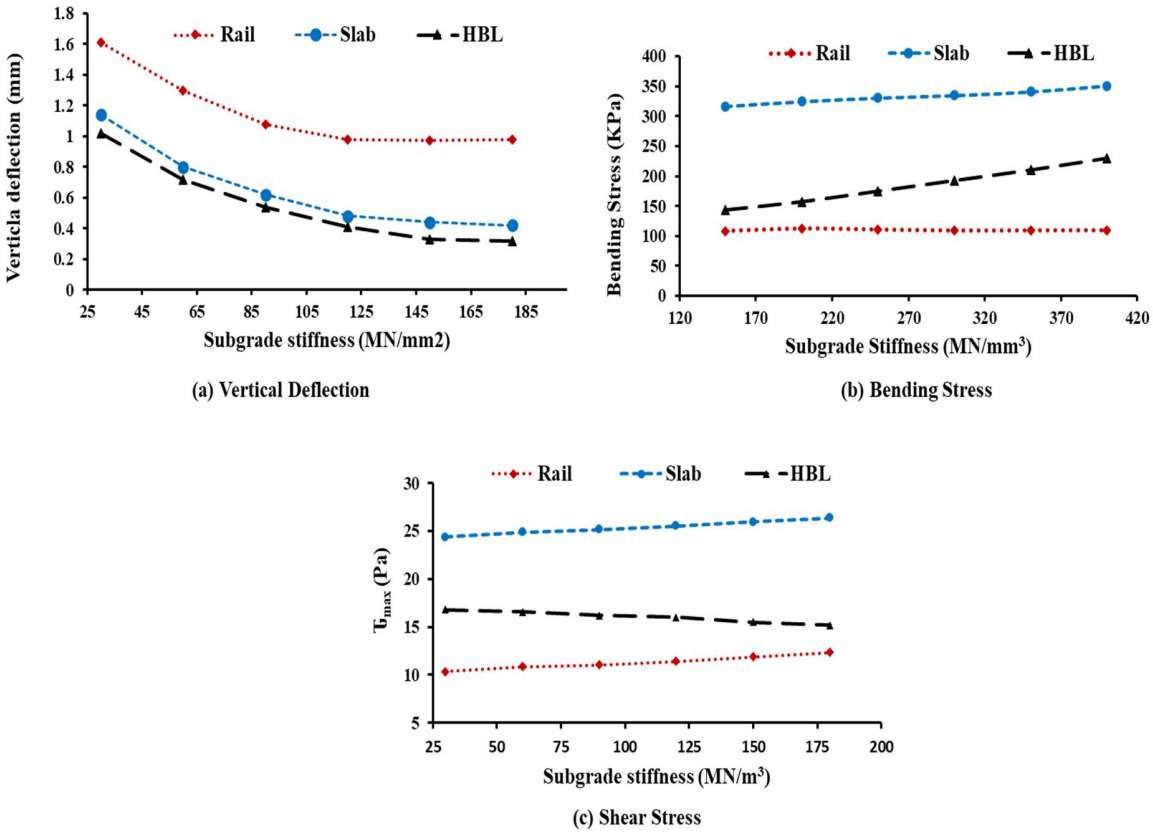

Figure 0.5 Influence of subgrade stiffness on both vertical deflection and stress (a)Vertical deflection (b)Bending stress (c) Shear stress

4.3.4 Effect of Slab Thickness

The influence of varying concrete slab thickness (120 mm to 300 mm, with 240 mm as standard) on maximum stress and maximum shear stress of key track components rail, concrete slab, and Hydraulically Bonded Layer (HBL) was systematically analyzed. The variation of slab thickness significantly affected both displacement and stress distribution. As shown in Figure 4.6, thicker slabs reduced bending and shear stresses in both slab and HBL layers, thereby enhancing overall durability. However, beyond a certain thickness, the improvements became marginal, suggesting diminishing returns on performance versus material cost.

Therefore, optimizing slab thickness is essential for balancing construction costs with long-term service performance.

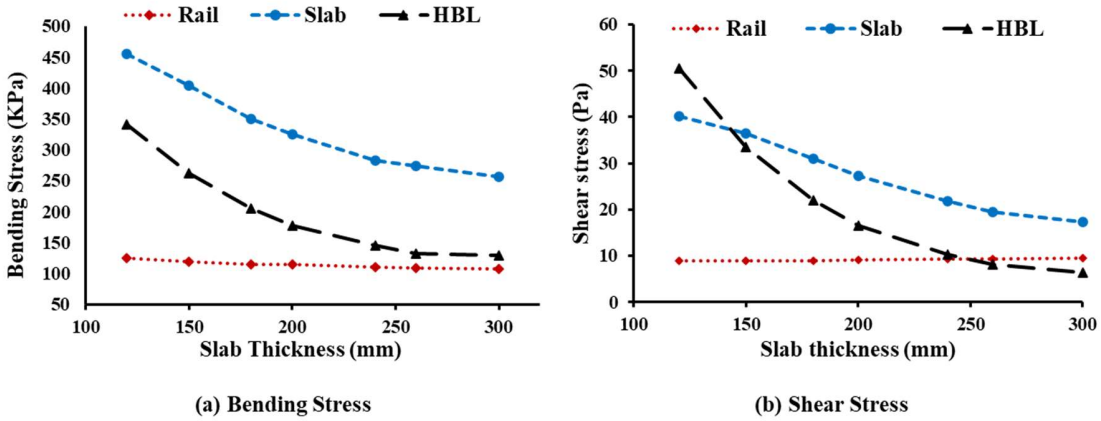

Figure 0.6 Effect of slab thickness (a) Bending stress (b) Shear stresses

4.3.5 Effect of CAM Thickness

The effect of varying CAM (Cement Asphalt Mortar) layer thickness (ranging from 30 mm to 180 mm, with 50 mm as the standard) on maximum stress and maximum shear stress of key track components rail, concrete slab, and HBL was analyzed. Results (Figure 4.7) showed that increasing thickness of CAM layer helped reduce stresses in HBL but simultaneously led to higher stresses in slab. This indicates redistribution of stresses rather than uniform reduction. Thus, excessively thick CAM layers may shift damage potential from HBL to slab, compromising long-term performance. In conclusion, variations in CAM layer thickness influence stress distribution across track components differently. While rail stresses remain unaffected, the concrete slab faces increased stress and shear demands, and the HBL layer benefits from reduced stresses, improving its durability. Optimizing CAM layer thickness is essential for balancing stress distribution and ensuring long-term performance and reliability of slab track systems, particularly in high-speed rail applications.

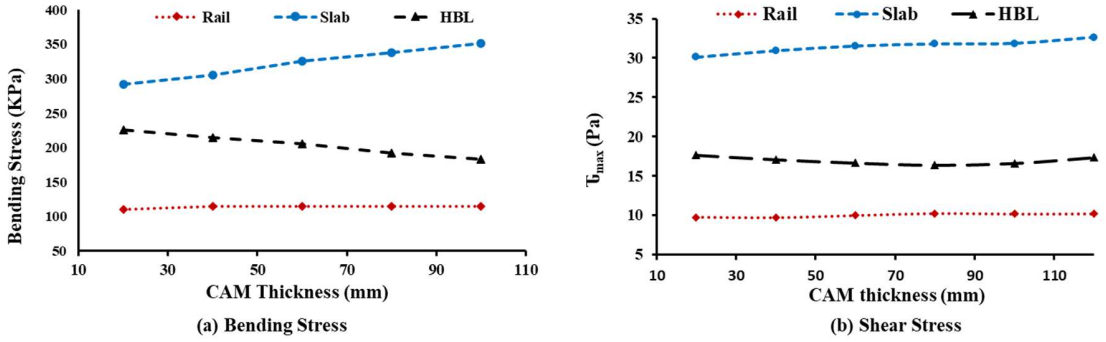

Figure 0.7 Effect of CAM thickness on stress redistribution between rail, slab and HBL (a) Bending stress (b) Shear Stress

4.3.6 Effect of HBL Thickness

The influence of varying thickness of concrete supporting HBL layer (ranging from 150 mm to 400 mm, with 200 mm as the standard) on stress and maximum shear stress of key track components rail, concrete slab, and HBL layer has been systematically analyzed. Figure 4.8 illustrates the influence of HBL thickness. Increasing thickness of HBL improved its ability to absorb stresses but resulted in higher stress transfer into slab. While a thicker HBL enhances stability of the substructure, it also imposes durability challenges for slab.

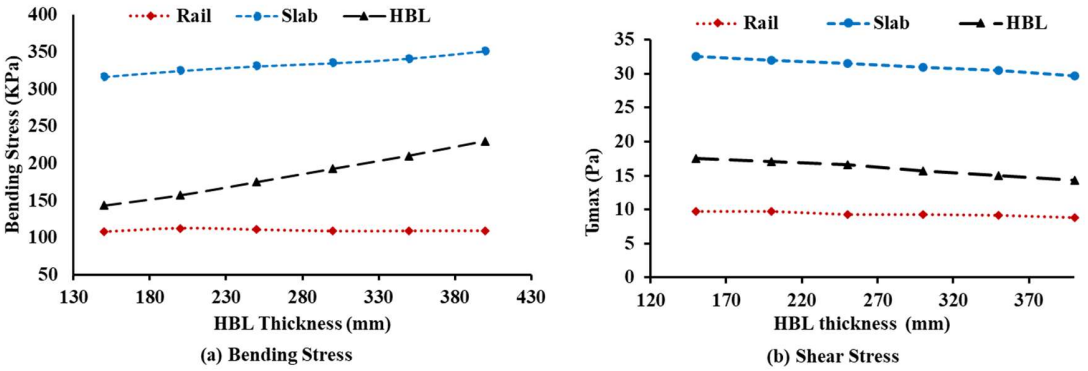

Figure 0.8 Effect of HBL thickness on stresses in Rail, slab and HBL (a) Bending stress (b)Shear Stress

In conclusion, varying the thickness of concrete supporting HBL layer affects bending and shear stresses of track components differently. While rail stresses remain

unaffected, concrete slab experiences increased shear stress potentially influencing its structural performance. Conversely, the HBL layer benefits from reduced stress and shear, which enhances its durability.

4.4 Discussion

The static response analysis has demonstrated the superior stiffness and reduced displacement of slab tracks compared to conventional ballasted tracks, making them highly suitable for high-speed rail applications. However, the increased stresses in the slab and CAM interface bring attention to the careful design of these structural components. The parametric study confirmed that variations in rail pad stiffness, CAM stiffness, subgrade stiffness, slab thickness, CAM thickness, and HBL thickness have significant effects on the load transfer and stress distribution within the slab track system. While increased stiffness and thickness generally improve displacement control, they also raise stress levels in critical components, creating a trade-off between serviceability and durability. These findings establish the groundwork for the subsequent chapters on dynamic vehicle–track interaction, vibration mitigation, and fatigue analysis, where the long-term behavior of slab track systems under high-speed train operations will be further investigated.

4.5 Chapter Summary

CHAPTER 5: VIBRATION RESPONSE RESULTS AND DISCUSSION

5.1 General

Vibration response plays a decisive role in the long-term durability and serviceability of slab track systems, particularly under high-speed train operations. Unlike static or quasi-static loading, vibrations generated from moving wheel–rail interactions propagate through the slab, cement asphalt (CA) mortar, and foundation layers, often resulting in resonance, increased stress concentrations, and discomfort to passengers. For high-speed corridors, where operating speeds exceed 300 km/h, mitigating the effects of vibration becomes essential to ensure structural integrity and service life.

In this study, the vibration performance of the precast slab tracking system was evaluated using numerical modelling approaches. The analysis incorporated both **modal analysis**, which identifies natural frequencies and mode shapes in the system, and **harmonic response analyses**, which evaluate slab and subgrade accelerations under train-induced dynamic loads. Furthermore, the effect of incorporating **slab mats** was studied as a vibration mitigation strategy. Slab mats, typically composed of elastic layers, are introduced between the concrete slab and supporting layers to reduce vibration transmission.

A series of **parametric studies** was conducted to investigate the influence of key factors, including slab mat stiffness, damping, thickness, foundation stiffness, axle load, and train speed. The outcomes are presented in terms of accelerations, displacements, and frequency-domain attenuation, with implications for the design and optimization of slab tracks in India's high-speed railway systems.

In order to generate vibration response result for slab track, ANSYS Workbench modal and harmonic response analyses were performed. In ANSYS Workbench, first performed a modal analysis and subsequently a harmonic response analysis. The simulations were run multiple times with varying slab mat stiffness, thickness and track foundation stiffness settings. To visualize the connection between the various parameters of the slab mat layer and the foundation stiffness and its vibration-damping effect, Excel graphs were generated. Examine the differences between the slab tracks that have a slab mat layer and those that don't, k_m = 25 MN/m^3 for this slab mat's stiffness. It is important to note that slab mat layer is primarily intended for high-speed passage of trains. The vibration response of layer between rail and concrete slab is selected as measure of vibration to analyze its dampening effects. As acceleration versus time, the vibration response curve must be determined. The simulations have been run multiple times with varying stiffness, slab mat thickness, and stiffness of foundation layer. Excel graphs depict results; characteristics of slab mat and amount of vibration they absorb are related to one another in ways that are described.

5.2 Modal Analysis

The modal analysis investigates dynamic characteristics of structures when subjected to vibrational stimulation. It uses structure's total mass and stiffness to determine natural frequencies at which it will achieve resonance. This comprehensive study facilitates identification of basic structural forms of vibration modes and their associated frequencies. A structure exhibits resonance when mode shape and frequency of an external stimulation are in alignment with the structure. Figure 5.1 depicts first four vibration modes, considering a slab rail superstructure and dirt subgrade. Apart from third mode, which signifies track structure settling, remaining three modes illustrate bending characteristics at various wavelengths. According to Figure 5.1, the modal analysis shows that the maximum deformation of slab occurs near the frequency (f_0) 24.65 Hz.

For effective vibration isolation, the system should operate when the excitation frequency exceeds $\sqrt{2}\, f_0$ which is approximately 34.8 Hz for the slab with the mat layer. This ensures that the system can function as intended. It is well recognized that high-speed train loads generate frequency components well above 34.8 Hz.

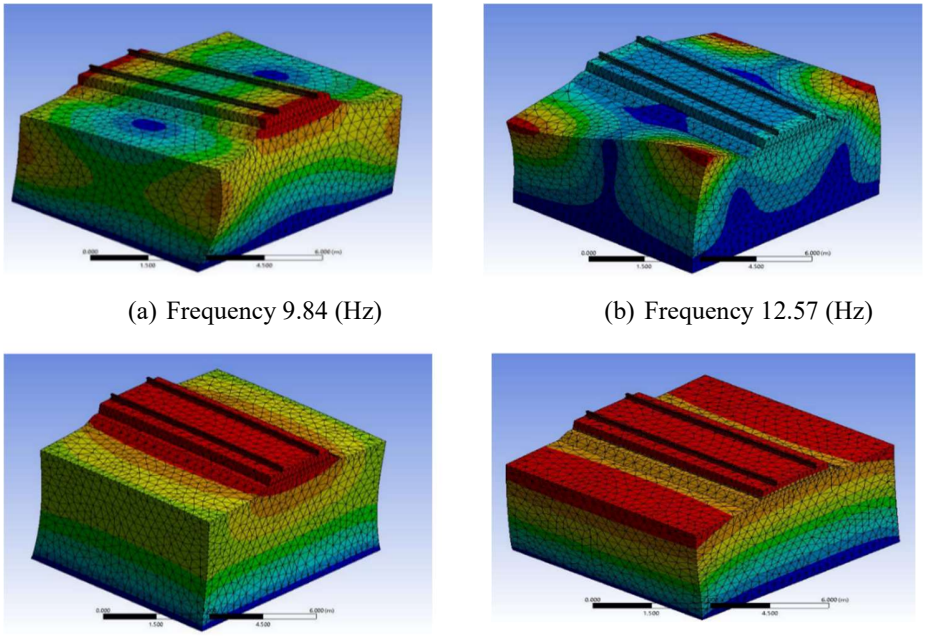

(a) Frequency 9.84 (Hz) (b) Frequency 12.57 (Hz)

(c) Frequency 18.35 (Hz) (d) Frequency 24.65 (Hz)

Figure 0.1 Modal analysis results (a) Frequency 9.84 Hz (b) Frequency 12.57 Hz (c) Frequency 18.35 Hz (d) Frequency 24.65 Hz

Therefore, ensuring that the slab track's natural frequencies remain adequately separated from these excitation frequencies is critical for avoiding resonance amplification. The modal analysis thus provided the basis for subsequent dynamic simulations.

5.3 Vibration Response

This study compared two types of slab tracks, one with an anti-vibration slab mat layer and one without, to evaluate their vibration-reducing effects at running speed of 280 km/h. The stiffness of slab mat layer used in the comparison is k_m = 25 MN/m^3. The primary function of this slab mat layer is to mitigate vibrations, particularly when trains are passing at high speeds. The acceleration of the concrete slab and subgrade layer serves as the key index to evaluate effectiveness of vibration reduction. The simulation results from mid-span section of the track shed light on the vibration-reducing effects in both the time and frequency domains. Figure 5.2 and Figure 5.3 illustrates the results.

5.3.1 Time-Domain analysis Results

Figure 5.2 shows the slab acceleration over time. When the slab mat layer is used, the results show a significant reduction in slab acceleration. Specifically, the acceleration decreased from 2.8 m/s² to 0.7 m/s², representing a reduction of approximately 75 %. This substantial decrease underscores the effectiveness of the slab mat layer in dampening vibrations.

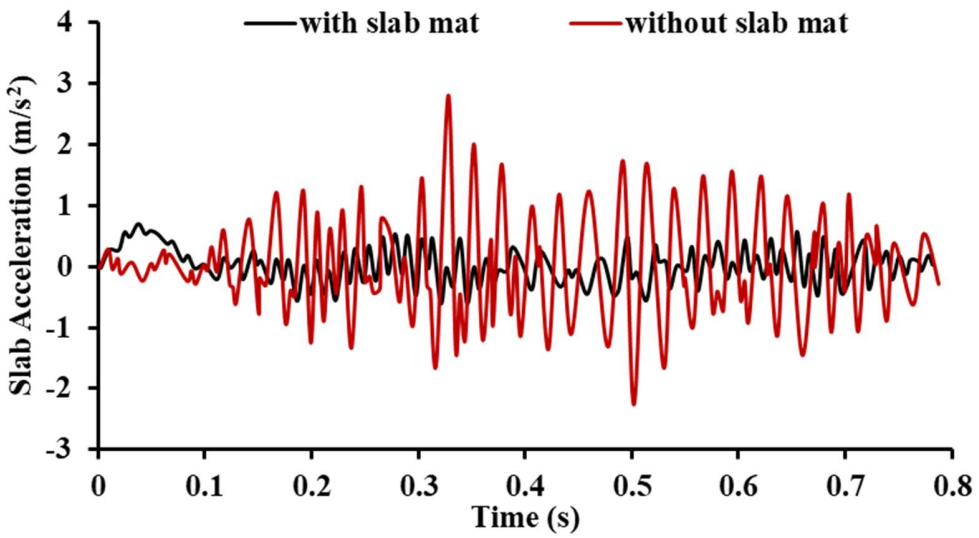

Figure 0.2 Vibration response of concrete slab layer of slab track

Research has shown that the slab mat layer can reduce vibrations transmitted from the slab track to the subgrade by more than 75% on high-speed slab tracks. While low-frequency vibrations are important for addressing environmental concerns, high-frequency vibrations are the dominant form that affects track structures in high-speed railways. However, in regions or situations where strict control over low-frequency vibrations is necessary, the limitations of the slab mat layer in mitigating such vibrations must be carefully considered. Relying solely on the slab mat layer is insufficient in these cases, necessitating the implementation of additional vibration reduction measures along the vibration transmission path, from the subgrade to nearby station buildings. The research demonstrates that the slab mat layer performs exceptionally well in high-speed railway applications, particularly for managing high-frequency vibrations.

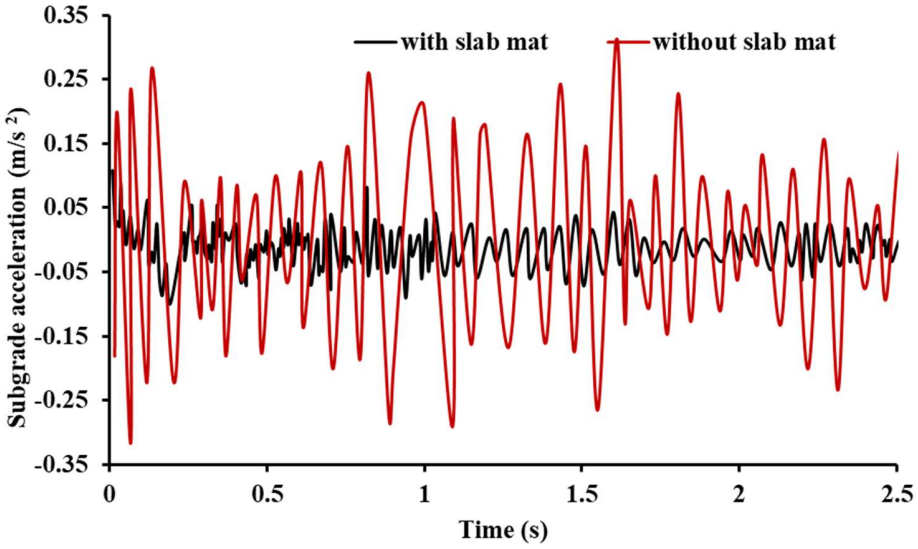

Figure 0.3 Vibration response of subgrade layer of slab track

Figure 5.3 shows the subgrade acceleration over time. When the slab mat layer is used, the results show a significant reduction in slab acceleration. Specifically, the acceleration decreased from 0.31 m/s² to 0.13 m/s², representing a reduction of approximately 58 %. Integrating a slab mat layer into construction of high-speed railway track is crucial for dampening vibration response that may otherwise be felt throughout the surrounding environment. This layer proves to be a valuable measure in controlling and minimizing the vibrations, ensuring smoother and more comfortable operation of the high-speed railway system.

5.3.2 Frequency Domain Analysis

In frequency domain, Figure 5.4 shows subgrade acceleration. The analysis shows that the slab mat layer reduces subgrade acceleration level by up to 21 dB in high-frequency range. The intersection point of the curves in frequency domain corresponds to a frequency of 33.5 Hz, which aligns closely with the results obtained from modal analysis ($\sqrt{2}\, f_0 = 34.8$ Hz). This indicates that the slab mat layer is particularly effective at isolating vibrations at frequencies above 33.5 Hz. The excellent vibration

isolation properties of the slab mat layer, especially in higher frequency ranges, are responsible for the remarkable reduction in vibration. This feature makes the slab mat layer an essential component in high-speed rail systems, where reducing vibrations is critical for maintaining structural integrity and passenger comfort.

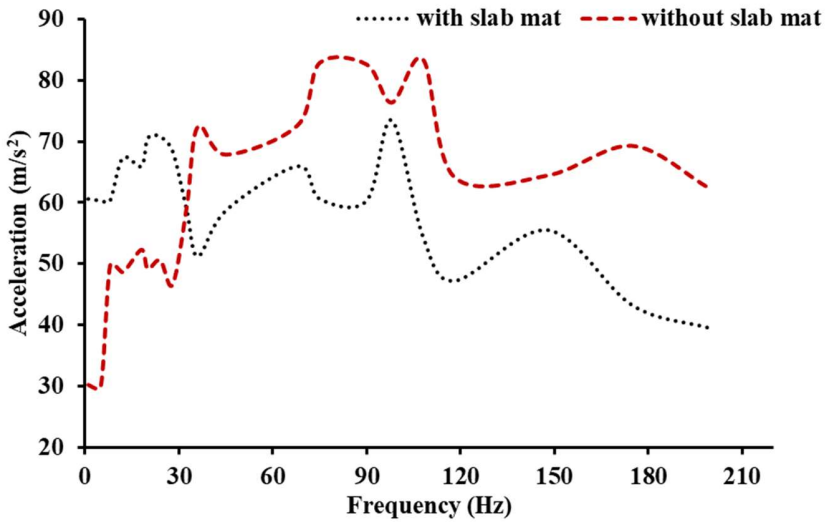

Figure 0.4 Vibration response of the subgrade layer of slab track in the frequency domain

5.4 Parametric investigation

Varying parameters that are such as the slab mat layer's stiffness and thickness and the stiffness of the subgrade/foundation, have been used in parametric studies to examine the track structure's vibration response. Figures 5.5 to 5.7 below demonstrate the vibration response in the rail and slab generated by altering these variables

5.4.1 Impact of slab mat stiffness variation on vibration in a precast slab track

In this study, slab mat layers made of elastic material with elastic moduli ranging from 15 MPa to 225 MPa are utilized to investigate their impact on reducing vibration response in high-speed precast slab track systems. The stiffness of a material is directly

related to its elastic modulus, given by $\kappa = AE/l$, implying that materials with higher elastic moduli exhibit greater stiffness properties. Figures 5.5 illustrate the effects of varying the slab mat stiffness on the displacement of rails, slab, and HBL, providing insights into the behavior of the system under different stiffness conditions. Increasing modulus of elasticity of slab mat layer reduces displacement of the rail, as determined by results of this study. The displacement of the slab is reduced by about 45%, and displacement of concrete supporting hydraulic bounded layer is reduced by about 65.5% when the elastic modulus is varied from 15 to 225 MPa (Figure 5.5).

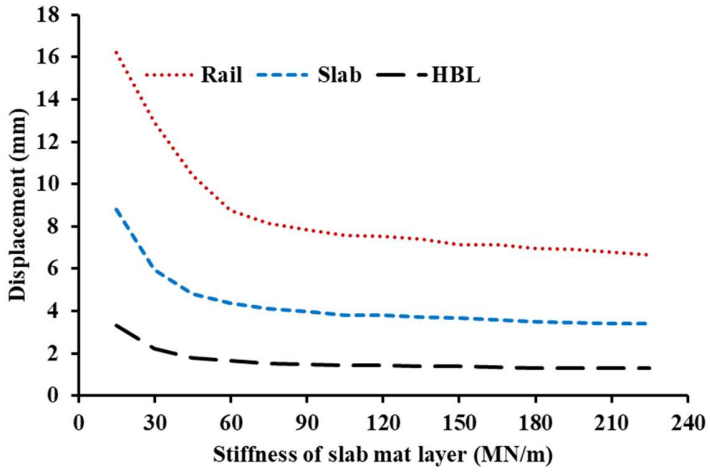

Figure 0.5 Effect of varying the slab mat stiffness on the displacement

The displacements of the rail and slab layer of track elements converge to a constant value for the modulus of elasticity that is higher than 135 MPa. In this case, the elastic modulus of the slab mat layer was increased, and results showed that vertical displacement of rail decreased. Figure 5.5 illustrates effects of changing this elastic modulus from 15–225 MPa on vertical acceleration of slab and vertical acceleration of concrete support layer, respectively. The above figure illustrates the effect of changing the elastic modulus from 15 to 225 MPa on the vertical acceleration of the slab and concrete support layer. As the elastic modulus of the interface increases beyond 120–140 MPa, the displacements of the track elements, particularly the rail

components, approach a constant value. In the slab layer, displacement convergence occurs at values above 90 MPa, while in the HBL, it surpasses 60 MPa.

5.4.2 Impact of slab mat damping variation on vibration in a precast slab track

The study primarily focuses on the rigidity of the slab mat layer as a critical factor in vibration mitigation, emphasizing how structural stiffness reduces the displacement of the rail and slab. However, it also highlights the equally significant role of damping in vibration isolation. Damping refers to the slab mat layer's ability to absorb and dissipate vibrational energy, particularly from dynamic loads generated by high-speed trains.

While rigidity controls movement and structural integrity, damping is essential for attenuating vibrations and minimizing their impact on the tracking system. The author examines five cases where the slab mat damping coefficients differ, but all other factors remain constant: 2×10^4 N·s/m, 4×10^4 N·s/m, 8×10^4 N·s/m, 1.6×10^5 N·s/m, and 3.2×10^5 N·s/m. The results, illustrated in *Figure 5.6 and Figure 5.7* reveal that increasing slab mat damping significantly reduces the vertical accelerations of the rail.

However, changes in the vertical acceleration of the track slab and the concrete support layer are relatively minor. Increasing slab mat damping significantly reduces the vertical displacement of the rail, concrete slab, and concrete support layer.

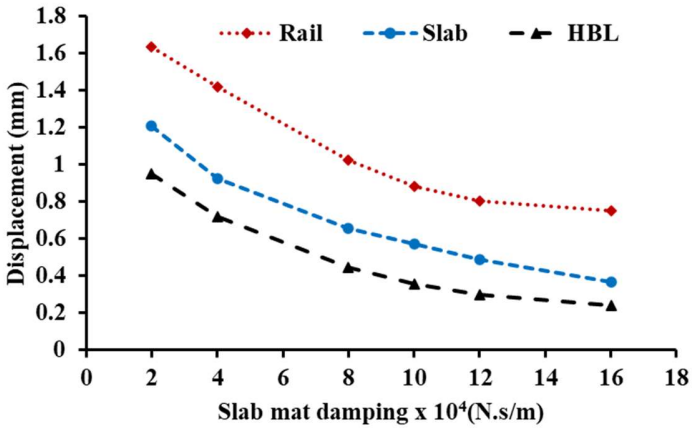

Figure 0.6 Effect of varying the slab mat damping on the vertical displacement

This analysis concludes that increased slab mat damping effectively reduces vibrations within the track structure. This contributes to extending the service life of the slab track and reducing the maintenance workload for the track system. The design can significantly enhance the overall performance and durability of the track structure, thereby improving the reliability and cost-effectiveness of high-speed rail systems.

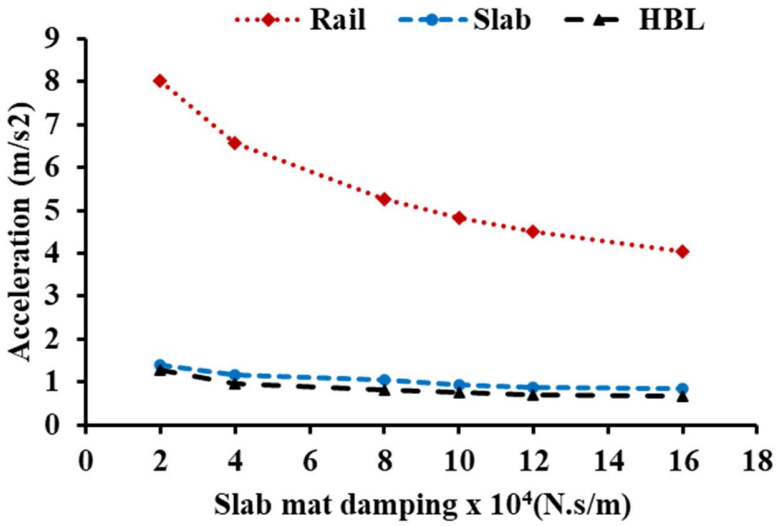

Figure 0.7 Effect of varying the slab mat damping on the vertical acceleration

5.4.3 The influence of slab mat thickness variation on precast slab track vibration

Starting with slab mat thickness of 35 mm, the study explores the impact of reducing vibration by analyzing effects of varying slab mat thickness from 25 mm to 45 mm. The slab mat's performance declines as slab track displacement increases; this is a result of the 10 mm decrease in thickness. In addition, the slab mat's efficiency was improved as a result of a 10 mm thickness increase when the slab track's displacement was reduced.

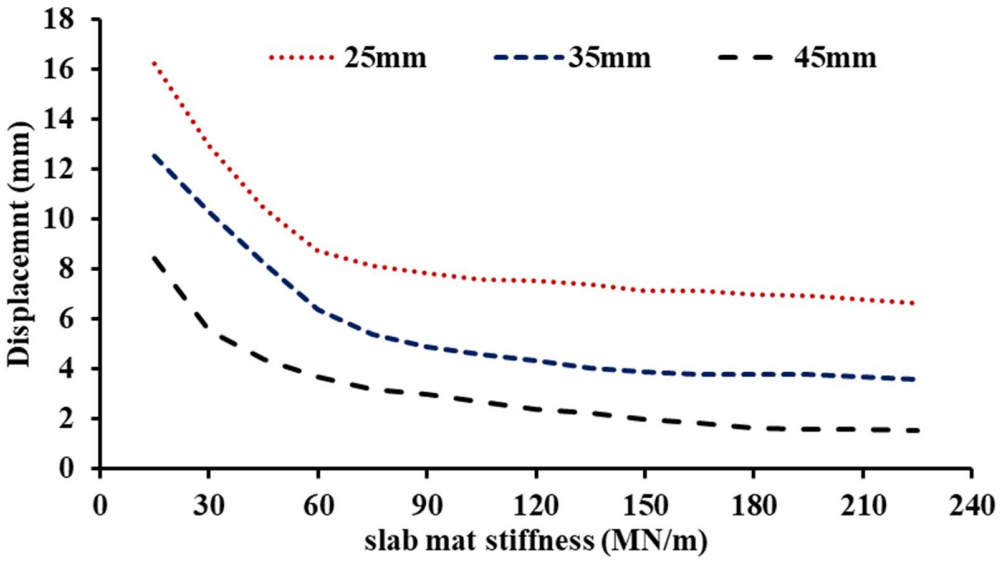

Figure 0.8 Effect of the slab mat thickness on rail displacement

Figure 5.8 shows that increasing the thickness of slab mat reduced vertical vibration propagated from railway track. Therefore, a thicker slab mat can absorb more force, diminish vibration, and minimize the influence of the continued repetition vibration that might damage the slab track's foundation.

5.4.4 Influence of Vehicle Speed on Precast Slab Track Vibration

The vibration responses of the track structure were analyzed at train speeds of 100, 120, 180, 220, 280, 320, and 350 km/h. The results highlight the effects of increasing

speeds on rail, slab, and subgrade displacements and accelerations, showing how dynamic responses intensify with higher velocities.

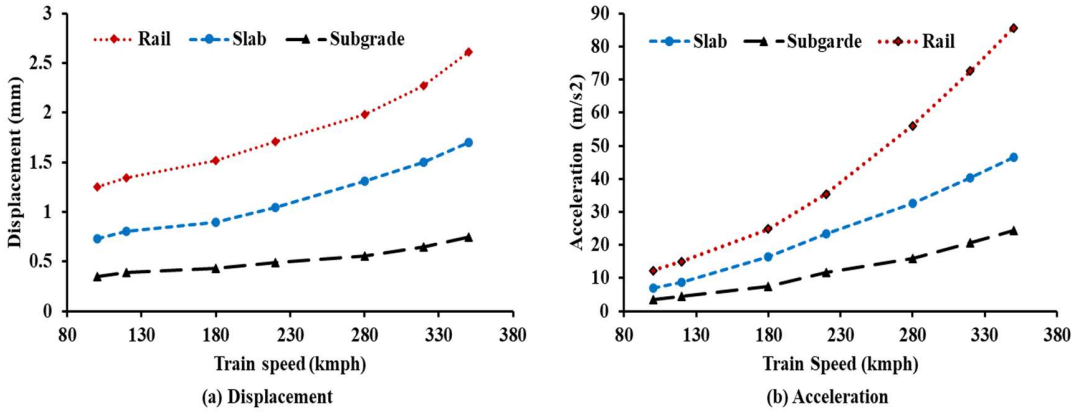

Figure 0.9 Effect of train speed on vibration response of track

When the train speed increases from 280 km/h to 350 km/h, the dynamic responses of the track components rail, slab, and subgrade show, as in *Figure 5.9*, varying levels of percentage increase in both displacements and accelerations. The rail experiences the most significant variation, with displacements increasing by approximately 15-20% and accelerations rising by around 20-25%. The slab shows a moderate response, with displacements increasing by about 10-15% and accelerations growing by 15-20%. In contrast, the subgrade exhibits the smallest variation, with displacements increasing by approximately 5-10% and accelerations rising by 10-15%. These results indicate that as train speeds approach higher limits, the rail is the most affected component, followed by the slab, while the subgrade remains relatively stable. This highlights the need for increased attention to the rail and slab performance when operating at very high speeds to ensure structural safety and durability.

The study analyzed the vibration responses of the track structure at an axle load of 25 t and across trains at speeds of 100, 120, 180, 220, 280, 320, and 350 km/h. To further extend this analysis, the impact of varying axle loads, particularly 30 t, was also considered. The computational results, as illustrated in the figure 5.10,

demonstrate the combined effects of increasing train speeds and axle loads on the dynamic behavior of track components, including rail displacements and accelerations, concrete slab displacements and accelerations, and subgrade displacements and accelerations. The study provides a comprehensive understanding of how faster speeds and heavier axle loads influence the vibration responses of the rail, slab, and subgrade, emphasizing the need to assess track performance under these conditions

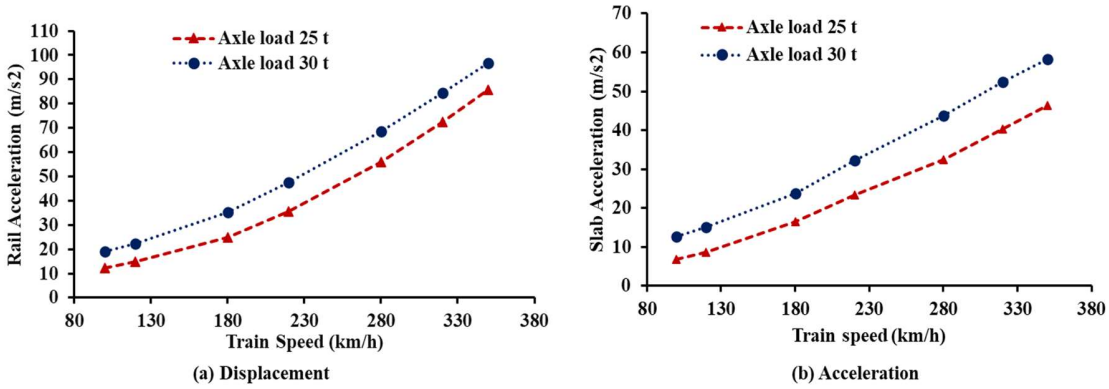

Figure 0.10 The effect of train speed on rail and concrete slab acceleration with varying axle load

The Figure 5.10 demonstrates the percentage variation in dynamic responses, specifically rail and slab accelerations, as train speed increases from 280 km/h to 350 km/h for axle loads of 25t and 30t. For rail acceleration, under the 25t axle load, the response increases from approximately 65 m/s² to 85 m/s², resulting in a 30.8% increase, while for the 30t axle load, it rises from 75 m/s² to 100 m/s², corresponding to a 33.3% increase. Similarly, for slab acceleration, under the 25t axle load, the response increases from 35 m/s² to 50 m/s², showing a notable 42.9% increase, whereas for the 30t axle load, it grows from 45 m/s² to 60 m/s², resulting in a 33.3% increase. These results highlight that the dynamic responses intensify significantly with

increasing speed, particularly for the slab under lighter axle loads, while the rail shows a relatively consistent rate of increase across both axle loads.

The combined effects of higher train speeds and axle load cause the observed increase in dynamic responses, specifically rail and slab accelerations, as train speed rises from 280 km/h to 350 km/h. At higher speeds, the frequency and magnitude of dynamic forces exerted on the track structure increase significantly due to greater wheel-rail interaction and inertia effects. These forces induce higher accelerations in both the rail and slab, as the track components must respond to the rapidly varying dynamic loads.

5.5 Discussion

The results demonstrate that slab mats are highly effective in mitigating vibration response, reducing slab accelerations by up to **75%** and subgrade accelerations by **58%**. The frequency-domain analysis confirmed vibration attenuation above **33 Hz**, ensuring resonance safety at high operating speeds.

Parametric studies further highlighted that **slab mat stiffness and damping** are the most influential factors. Optimum stiffness in the range of **25–60 MN/m³**, with adequate damping, produced the best results. Slab mat thickness and foundation stiffness also influenced performance, although their effects were secondary to those of stiffness and damping.

Finally, train speed and axle load were found to be critical in amplifying responses. At **350 km/h** and 30 t axle load, accelerations were nearly double compared to baseline conditions. This underlines the need for vibration mitigation strategies in the context of Indian high-speed corridors.

5.6 Chapter Summary

This chapter presented the vibration response results of precast slab track systems under high-speed railway loading. The key findings are:

1. Modal analysis identified critical natural frequencies ranging from 9.84 Hz to **24.65 Hz**, which remained safely separated from the excitation frequencies generated at high speeds (>33 Hz).
2. Slab mats effectively reduced vibration amplitudes, with slab acceleration decreasing by **75%** and subgrade acceleration by **58%**.
3. Frequency-domain analysis confirmed an attenuation of **21 dB** above 33.5 Hz, underscoring the efficiency of slab mats in filtering high-frequency vibrations.
4. Parametric studies revealed that slab mat stiffness and damping are the most influential parameters, followed by thickness and foundation stiffness.
5. Train speed and axle load significantly amplified vibration responses, highlighting the need for slab mats in the Indian HSR design.

Overall, the findings emphasize the value of slab mats as a vital vibration mitigation measure for precast slab track systems, thereby ensuring structural durability, passenger comfort, and long-term serviceability.

CHAPTER 6: DYNAMIC VEHICLE-TRACK INTERACTION RESULTS AND DISCUSSION

6.1 General

Dynamic vehicle–track interaction is a decisive factor in determining the safety, stability, and service life of slab track systems, especially for high-speed railways. Unlike static loading, where forces are applied in a steady and predictable manner, dynamic loading introduces time-dependent variations caused by the interaction of moving wheelsets with the track. These variations are not limited to vertical loads; they also include lateral and longitudinal force components influenced by irregularities, rail pad stiffness, subgrade resilience, and vehicle suspension properties.

In high-speed corridors such as the Mumbai–Ahmedabad High-Speed Rail (MAHSR), where trains are designed to operate at **320 km/h**, even small irregularities in the track surface or imperfections in wheel–rail contact can lead to amplified dynamic forces. These amplified forces contribute to greater rail and slab displacements, increased stresses in the slab and CA mortar layers, and potential degradation of passenger comfort. The ability to predict and control these dynamic responses is therefore crucial for ensuring both safety and long-term durability of slab track systems.

To capture this phenomenon, a **Moving Element Method (MEM)**-based numerical framework was employed, which allows efficient modelling of vehicle–track interactions under varying speeds and irregularities. The MEM-based model, validated against published FEM studies, integrates a **26-DOF vehicle system** with a layered slab track model, considering nonlinear wheel–rail contact based on Hertzian theory and nonlinear frictional behavior of the rail pads. This combination provides a realistic representation of the complex dynamics in high-speed railway systems.

This chapter presents the detailed results of the dynamic simulations, including model validation, the effects of track irregularities, the influence of train speed, and the role of track parameters such as rail pad stiffness, CAM stiffness, and subgrade stiffness.

Each result is explained using time-history plots, displacement profiles, and force spectra, followed by engineering interpretations relevant to high-speed track design.

6.2 Model Validation

Before conducting detailed parametric studies, the MEM-based framework was validated against finite element results from Lei Xi and Wange J [33]. The validation compared rail displacement histories and wheel–rail contact force responses under a standard set of conditions.

103

Figure 6.1 shows the time history of rail displacement as predicted by the MEM model compared with FEM benchmarks. Both curves follow a nearly identical oscillation pattern, with peak displacements differing by less than 16%. This close agreement demonstrates that MEM successfully replicates rail vibration amplitudes and damping trends while maintaining significantly reduced computational cost compared to FEM.

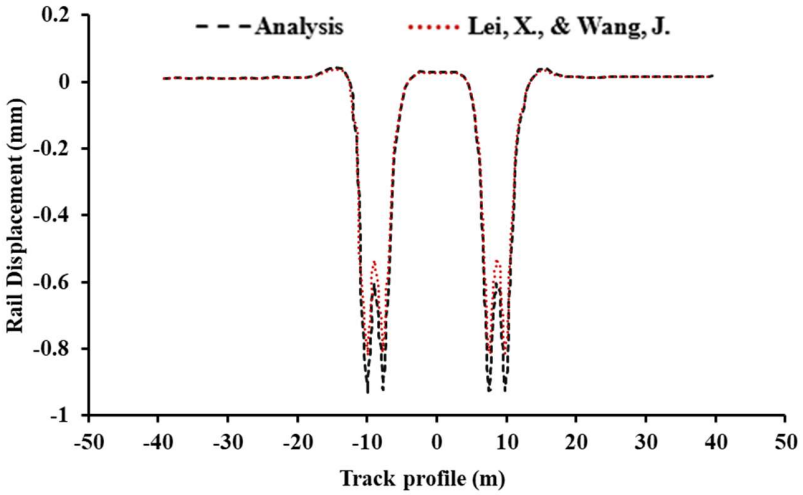

Figure 0.1 Rail displacement profile

Figure 6.2 presents the history of the vertical wheel–rail contact force. The MEM curve aligns well with published FEM data, capturing both the peak force amplitudes and the oscillatory fluctuations arising from track irregularities. The relative error

remained within 13–15%, which is acceptable for dynamic simulations of this complexity.

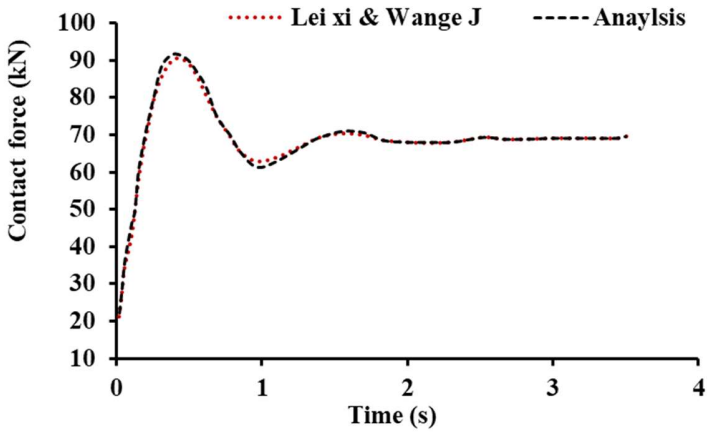

Figure 0.2 Wheel-rail contact force profile

This validation confirms that the MEM approach is robust and reliable, enabling its confident application to large-scale parametric simulations. The efficiency of MEM also makes it feasible to simulate long track segments and higher speeds, which would be computationally prohibitive with pure FEM.

6.3 Effect of Track Irregularities on Dynamic Response

The degree of track irregularity is known to impact the coupled train-track system's reaction substantially. Several potential causes of track irregularity include wear, clearances, settlement, and technologies used in track creation. The wavelengths vary from few centimeters to around three meters, and rail wear and weld faults are the most frequent causes of track irregularities (Ang & Dai, 2013). The creation of abnormalities in track at longer wavelengths is frequently associated with the foundation and structure of track [9]. Track irregularity is often described using stochastic processes and deterministic functions (Koh et al., 2003; Lei & Noda, 2002). In this study, influence of track irregularities on dynamic performance of the high-speed train–track system is examined using deterministic modelling approach. This method allows for controlled and systematic analysis of individual irregularity parameters specifically

105

amplitude and wavelength by isolating their effects on the system's dynamic behavior. By incorporating sinusoidal irregularity profiles into the rail geometry, variations in critical response quantities such as vertical displacements and wheel–rail contact forces across the layered track structure are thoroughly evaluated. For simulation, constant speed of v = 160 km/h is chosen for train. Here, track irregularity in vertical profile is represented by a sinusoidal function, which can be expressed as

$$\eta_x = \eta_0 sin(2\pi\kappa/\omega) \quad (37)$$

ω and η_0 stand for rail irregularity's wavelength and amplitude, respectively.

The track irregularity function can be expressed as x = Vt, where x is a function of time. In this context, four amplitudes (0.2 mm, 0.4 mm, 0.6 mm, and 0 mm representing smooth track) and two distinct track irregularity wavelengths (1.0 m and 1.5 m) are considered while the vehicle is in motion at 160 km/h speed.

The track irregularity period is calculated as 0.001s. Figures show dynamic responses for rail, slab, and HBL displacements at the contact point where track irregularities occur. Modeling the irregularity as a sinusoidal function reveals that all dynamic behavior of vehicle and slab track integrated system conforms to a sinusoidal pattern.

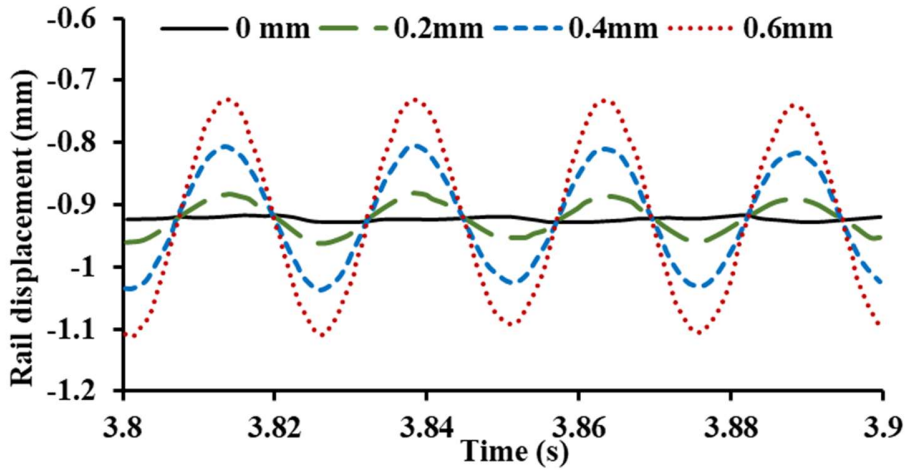

Figure 0.3 Rail displacement at contact point of first wheel when v = 160 km/h, η_x=0 mm, 0.2mm, 0.4mm, 0.6 mm at $\boldsymbol{\omega}$ =1.0 m

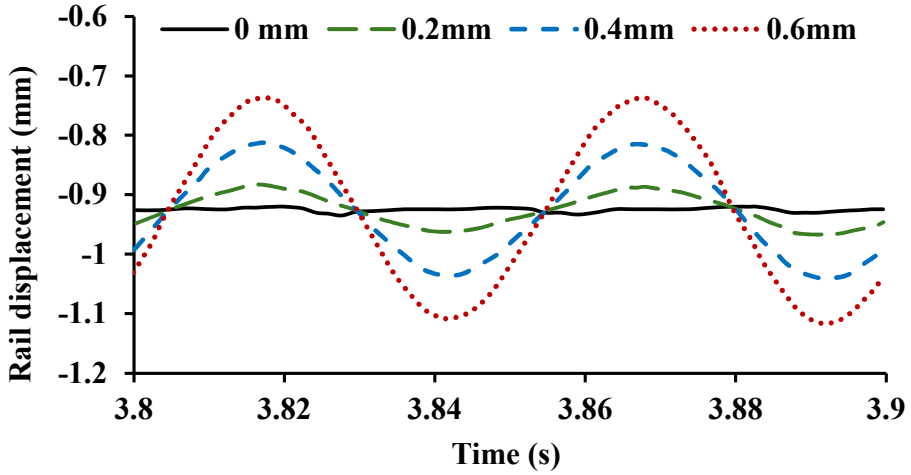

Figure 0.4 Rail displacement at contact point of first wheel when v = 160 km/h, η_x=0 mm, 0.2mm, 0.4mm, 0.6 mm at ω =1.5

Figure 6.4 shows the **rail displacement history** for different irregularity amplitudes. For the baseline case (smooth rail), the displacement remained stable with small oscillations. When a 0.2 mm irregularity was introduced, the displacement increased slightly but remained within control limits. At 0.6 mm, however, the rail displacement amplitude nearly doubled, reaching values that could compromise track serviceability.

.

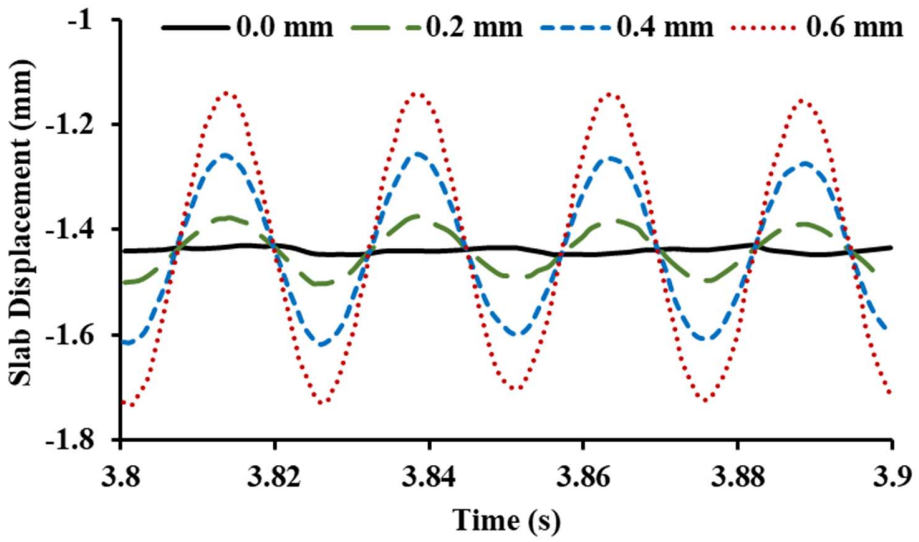

Figure 0.5 Slab displacement at contact point of first wheel when v = 160 km/h, η_x= 0 mm, 0.2mm, 0.4mm, 0.6 mm at ω =1.0m

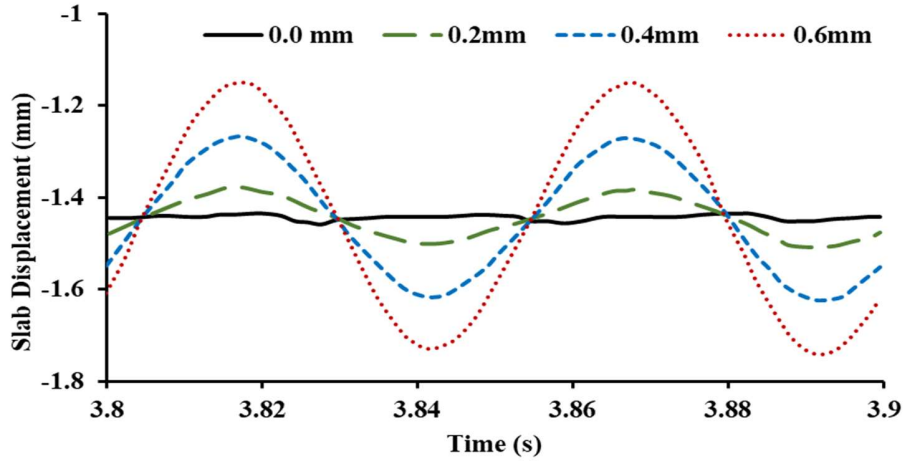

Figure 0.6 Slab displacement at contact point of first wheel when v = 160 km/h, η_x= 0 mm, 0.2mm, 0.4mm, 0.6 mm at ω =1.5 m

Figure 6.5 and 6.6 illustrates the slab displacement responses under the same irregularities. Similar to the rail, slab displacements grew proportionally with irregularity amplitude, showing that the slab, despite its stiffness, transmits vibratory

energy from the rail almost directly. This highlights the vulnerability of the CA mortar interface under rough track conditions.

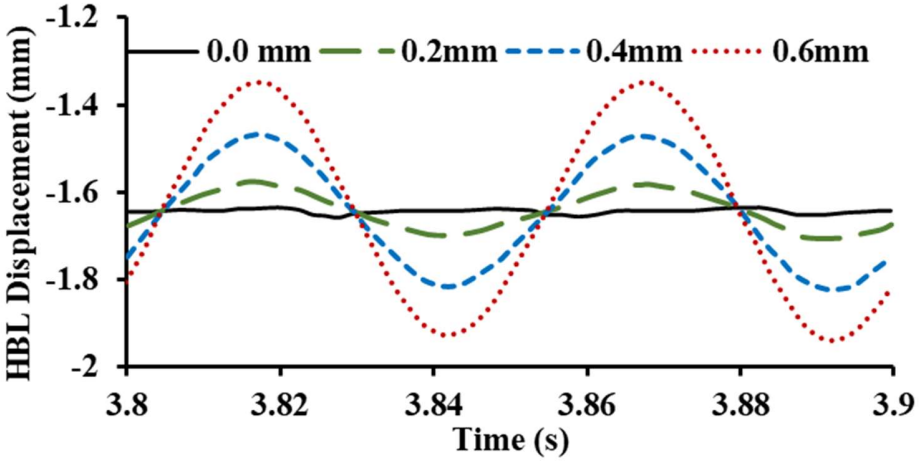

Figure 0.7 HBL displacement at contact point of first wheel when v = 160 km/h, η_x = 0 mm, 0.2mm, 0.4mm, 0.6 mm at $\boldsymbol{\omega}$ =1.0 m

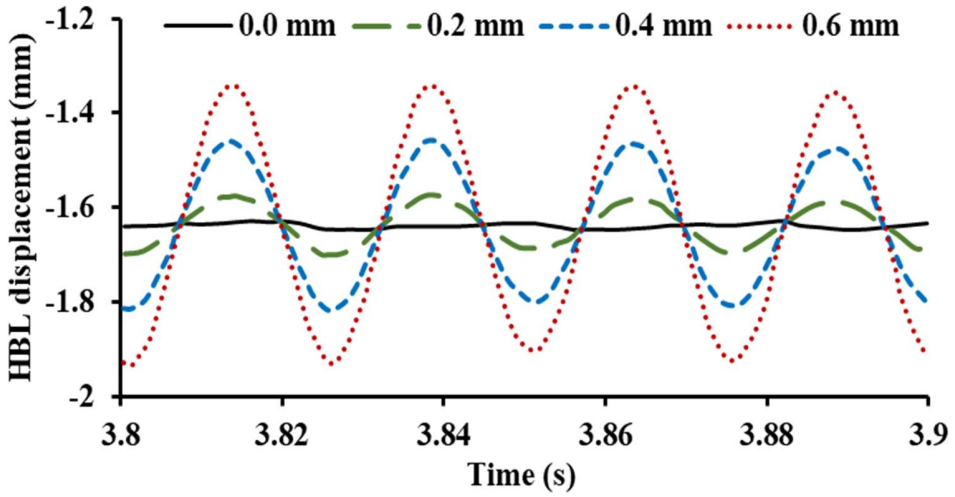

Figure 0.8 HBL displacement at contact point of first wheel when v = 160 km/h, η_x= 0 mm, 0.2mm, 0.4mm, 0.6 mm at $\boldsymbol{\omega}$ =1.5 m

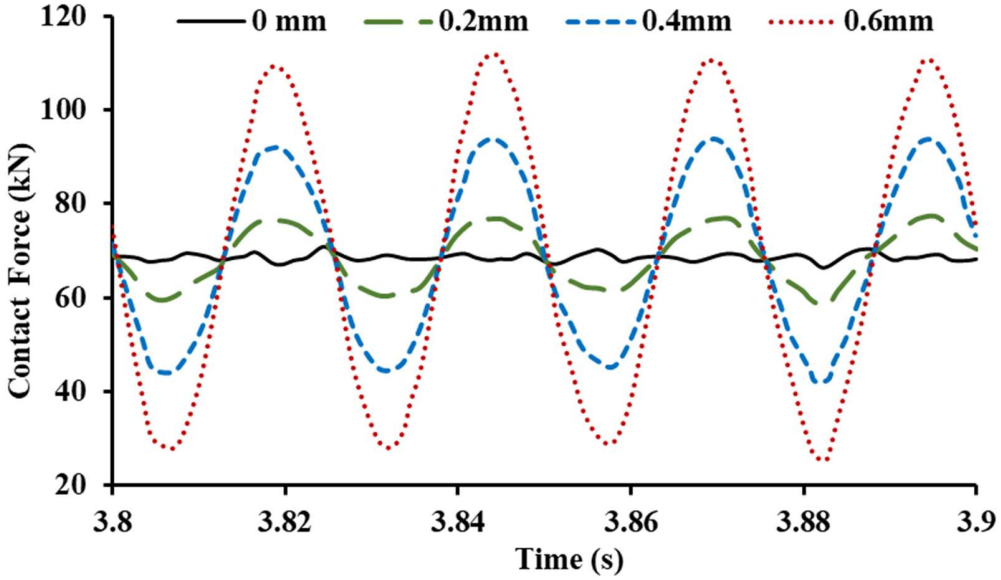

Figure 0.9 Wheel rail contact force at contact point of first wheel when v = 160 km/h, η_x=0 mm, 0.2mm, 0.4mm, 0.6 m at $\boldsymbol{\omega}$ =1.0 m

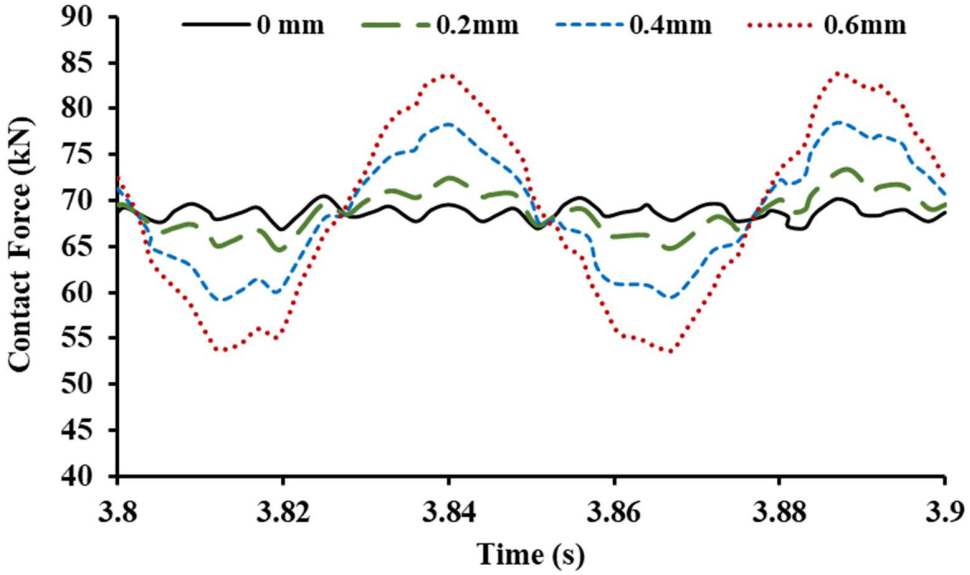

Figure 0.10 Wheel rail contact force at contact point of first wheel when v = 160 km/h, η_x=0 mm, 0.2mm, 0.4mm, 0.6 mm at $\boldsymbol{\omega}$ =1.5 m

Figures 6.9 and 6.10 present the histories of the wheel–rail contact forces. As irregularity amplitude increased, the contact force rose in magnitude and exhibited sharper peaks, signifying impact-like behavior. For shorter wavelengths (1.0 m), forces fluctuated more rapidly, demonstrating the stronger dynamic excitation effect of short-wavelength irregularities. These Figures illustrate a detailed chronological account of dynamic correlation between wheel and rail, providing insights into variations and patterns of contact force over time. The amplitude of track irregularity is primary cause of enhancement of wheel-rail contact force. A comparison of Figure 6.9 and 6.10 reveal noticeable periodic fluctuation in wheel-rail contact force, magnitude of which rises as the irregularity wavelength decreases. The irregular wavelength also has substantial impact on wheel-rail contact force. It is observed that increasing severity of rail irregularities, through reduced wavelengths and elevated amplitudes, leads to a suppression of the periodic variation in wheel–rail contact force. This phenomenon can be attributed to the significantly more extensive "roughness excitation."

These findings emphasize that irregularities as small as 0.2–0.4 mm well within practical tolerance limits can cause a greater than 40% increase in wheel–rail forces. For MAHSR, this indicates that rigorous track quality standards and maintenance cycles will be essential to prevent dynamic amplification.

6.4 Influence of Train Speed on Dynamic Performance

An investigation of coupled system's response to variations in vehicle speed involves a detailed analysis of wheel-rail contact force, displacement, and acceleration of both rail and slab track. This investigation considers five specific speeds: 180 kmph, 220 kmph, 260 kmph, 300 kmph, and 340 kmph.

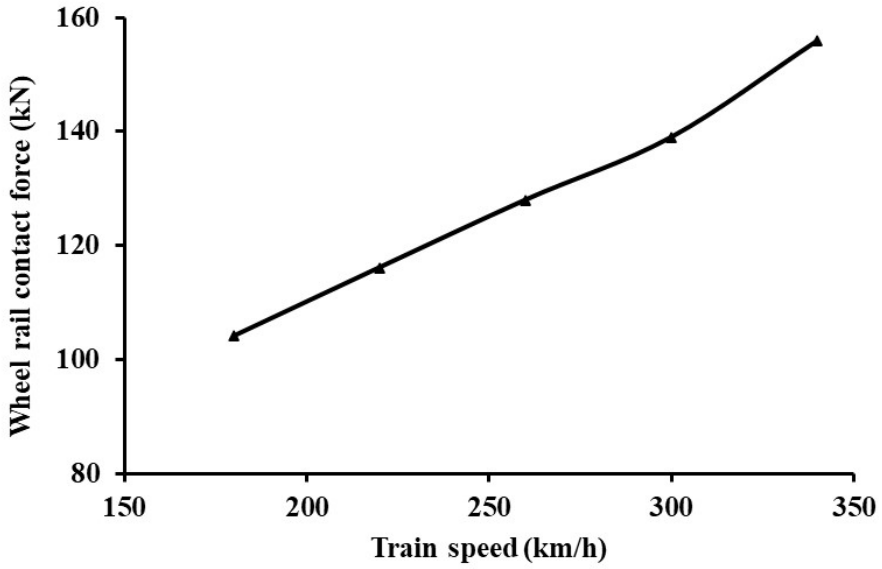

Figure 0.11 Wheel rail interaction force at varying train speed

Figure 6.11 illustrates the evolution of wheel–rail contact forces as speeds increase. At 180 km/h, forces remained stable with moderate oscillations. By 340 km/h, peak forces had increased by nearly 35%, and oscillation frequencies had risen substantially, reflecting the excitation of higher vibration modes.

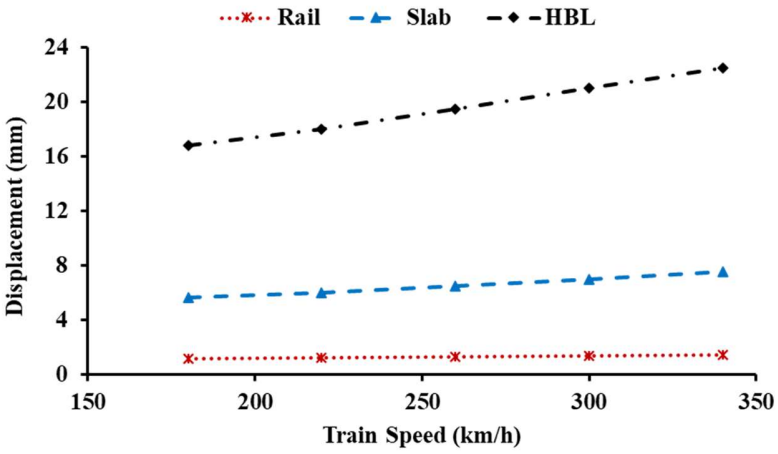

Figure 0.12 Displacement of track components

Figure 6.12 illustrates the **rail displacement profiles** at different speeds. Displacement increased by **28%** between 200 km/h and 340 km/h, showing clear speed sensitivity.

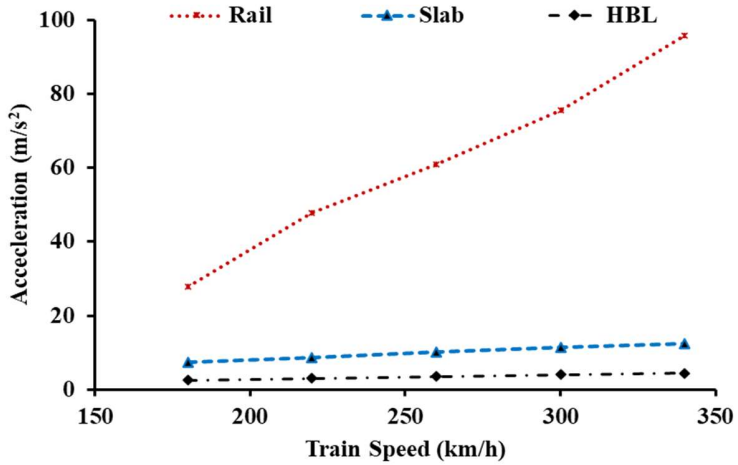

Figure 0.13 Acceleration of track components at varying train speed

Figure 6.13 presents the slab acceleration history. The slab accelerations increased by 42% at 340 km/h compared to 200 km/h. This higher dynamic amplification raises concerns about the long-term fatigue of the CA mortar layer and potential comfort issues for passengers.

These results indicate that while the precast slab track performs adequately up to 260–280 km/h, responses rise sharply beyond 300 km/h. Special measures such as slab mats or optimized CAM stiffness become critical for safe operation at the design speed of 320 km/h.

6.5 Influence of Track Parameters on Dynamic Response

The impact of altering parameters on the track's dynamic reaction is examined to develop an in-depth understanding of high-speed slab track's dynamic behavior for high-speed trains. The results of estimating various stiffness's for subgrade, rail pad, and CA mortar based on track's dynamic reaction are displayed in Figure 6.14 -6.16. The computation's outputs in that sequence are rail, concrete slab, and HBL displacements and accelerations.

6.5.1 Rail Pad Stiffness

Rail pad stiffness was varied between 50 MN/m and 150 MN/m. Figure 6.14 shows that as stiffness increased, rail displacement decreased by 31%, while slab displacement reduced by 19%. However, accelerations at the slab increased by nearly 14%, as stiffer pads transferred more force directly to the slab rather than absorbing energy. This trade-off highlights the dual role of rail pads: while they stabilize displacement, they may exacerbate vibration transmission if they are excessively stiff.

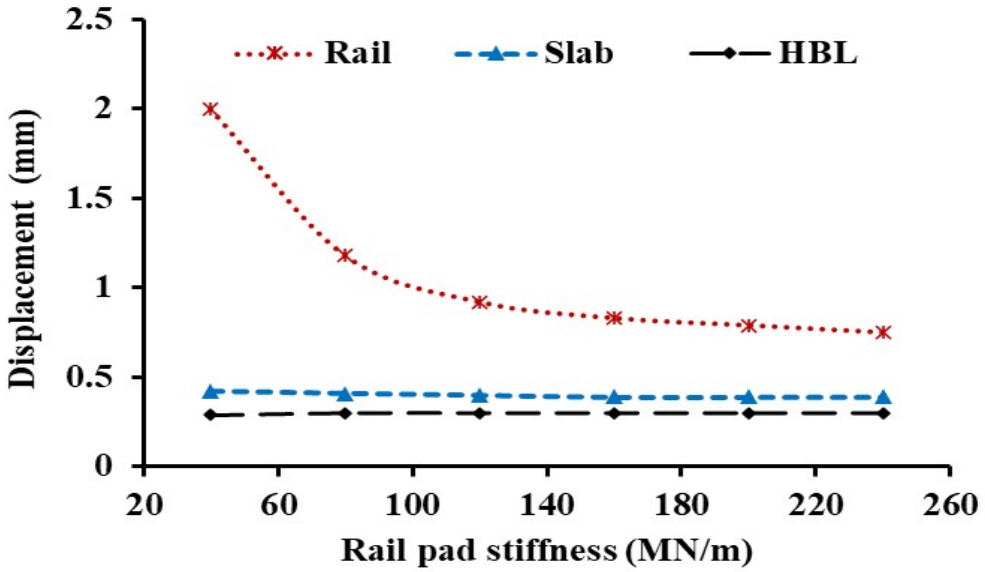

Figure 0.14 Influence of rail pad stiffness on displacement of track components

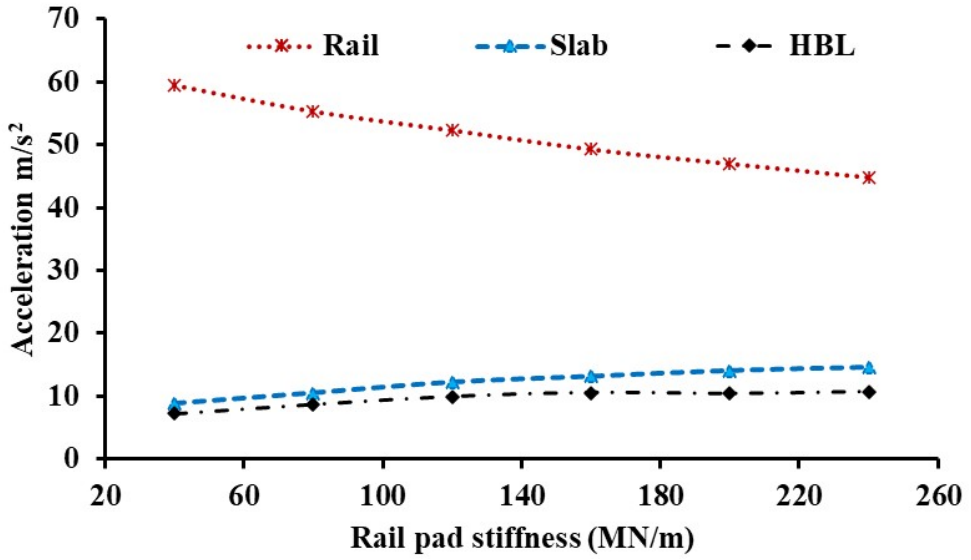

Figure 0.15 Influence of rail pad stiffness on acceleration of track components

6.5.2 CAM Layer Stiffness

CAM stiffness was doubled to assess its effect.

Figure 6.11 illustrates that slab displacement has been reduced by 37% and HBL displacement by 32%, indicating that stiffer CAM improves stability.

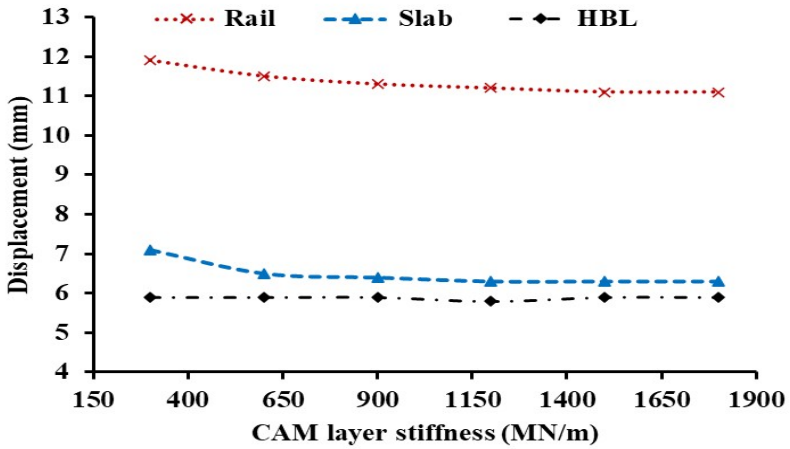

Figure 0.16 Influence of CAM stiffness on displacement of track components

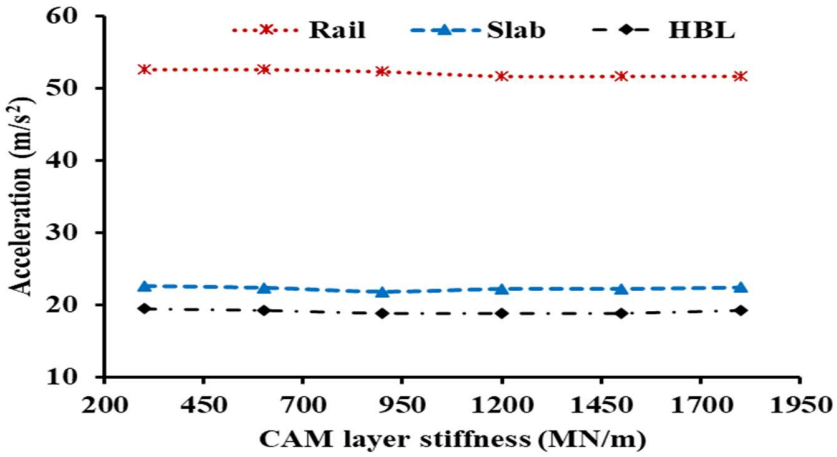

Figure 0.17 Influence of CAM layer stiffness on acceleration of track components

Accelerations, however, changed minimally (<5%), meaning CAM stiffness provides displacement benefits without worsening vibration transmission. This result identifies CAM stiffness as a favorable design parameter for improving slab durability.

6.5.3 Subgrade Stiffness

Among many elements that influence the track's dynamic performance, subgrade stiffness stands out. A significant decrease in the dynamic responsiveness of track construction may result from an increase in subgrade stiffness, as Figure 6.18 and 6.19 shows. Subgrade stiffness was increased by 60%.

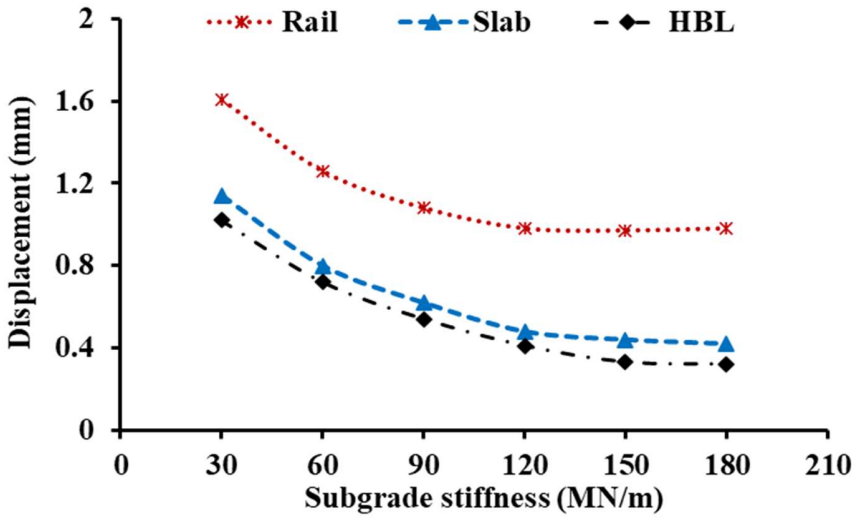

Figure 0.18 Influence of rail pad stiffness on displacement of track components

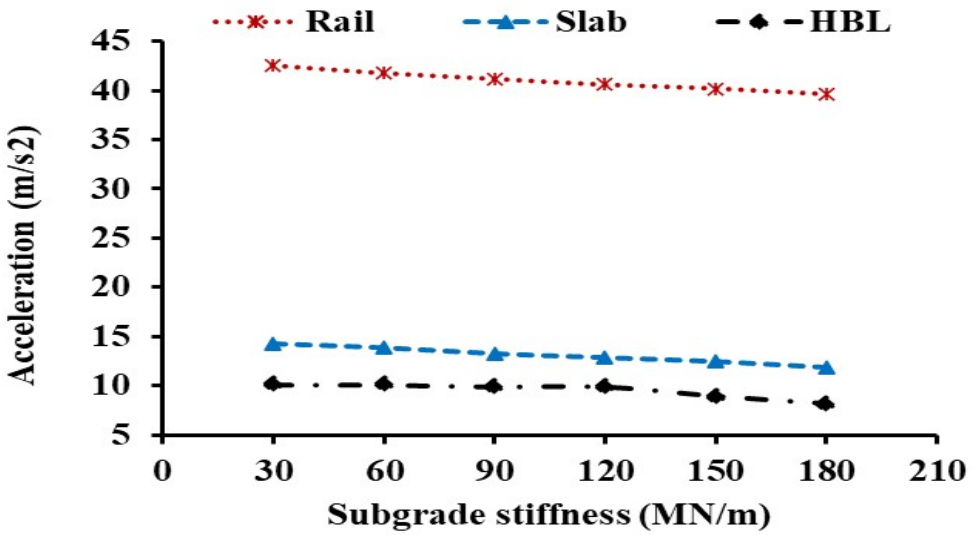

Figure 0.19 Influence of Subgrade stiffness on acceleration of track components

Figure 6.17 shows that rail displacement decreased by **22%**, slab displacement by **18%**, and HBL displacement by **15%**. Accelerations, however, showed little improvement beyond 10%. This indicates diminishing returns from excessive subgrade improvements, suggesting that moderate stiffness is sufficient.

To optimize the slab track structure, design parameters from parametric analysis must meet specific criteria for reducing dynamic responses effectively: Rail pad stiffness ranges from 90 to 150 MN/m, subgrade stiffness from 65 MN/m to 700 MN/m for both damping and stiffness of CA mortar.

6.6 Discussion

The results confirm that three factors strongly govern dynamic vehicle–track interaction: **speed, irregularities, and stiffness properties**.

1. **Speed** amplifies dynamic responses disproportionately; as trains approach 340 km/h, both displacements and accelerations rise sharply.
2. **Irregularities** as small as 0.2–0.4 mm can increase wheel–rail forces by 40% or more, indicating the importance of stringent maintenance.
3. **Rail pad stiffness** presents a trade-off: stiffer pads improve displacement but worsen accelerations.
4. **CAM stiffness** offers significant benefits in displacement control without compromising vibration response.
5. **Subgrade stiffness** improves displacements modestly but has limited impact on accelerations beyond a certain threshold.

6.7 Chapter Summary

This chapter presented the results of dynamic vehicle–track interaction analysis for a precast slab track system. The key outcomes are as follows:

1. The MEM-based model was validated against FEM results, with errors of less than **16%**.
2. Track irregularities significantly amplified displacements and contact forces, with shorter wavelengths causing stronger excitations.

3. Increasing train speed from 200 to 340 km/h raised wheel–rail forces by **35%**, rail displacement by **28%**, and slab acceleration by **42%**.
4. Rail pad stiffness reduced displacements but increased accelerations, while CAM stiffness provided strong displacement reduction benefits.
5. Subgrade stiffness offered limited additional improvements beyond moderate values.

Overall, the study highlights that **speed and irregularities are the primary drivers of dynamic amplification, and optimizing rail pad and CAM stiffness is crucial** for the safe operation of high-speed slab tracks in India.

CHAPTER 7: FATIGUE ANALYSIS RESULTS AND DISCUSSION

7.1 General

Fatigue performance is one of the most critical aspects in the long-term serviceability of precast slab track systems for high-speed railway applications. Unlike static loading, where stresses are applied only once or a few times, fatigue involves the repeated application of stresses and strains over millions of cycles during the entire service life of the track. This repeated loading leads to progressive damage, microcrack initiation, crack propagation, and eventually failure of the track layers, even when the applied stress is significantly below the static strength. In the context of the Mumbai–Ahmedabad High-Speed Rail (MAHSR), where design train speeds reach **320 km/h** and axle loads are typically **140 kN**, each slab and mortar layer is subjected to a high frequency of load cycles. The fatigue performance of the **cement asphalt mortar (CAM) layer** is therefore decisive in determining the track's overall durability and maintenance needs.

The present study employed a systematic framework for evaluating fatigue. First, static flexural strength tests were performed to establish baseline mechanical properties. Second, fatigue life experiments were conducted under different stress levels, and the data were used to construct an **S–N curve** (stress level versus number of cycles to failure). Third, fatigue strain evolution was monitored to capture the transition from an elastic to a damaged state. Finally, modulus degradation trends were assessed to quantify the reduction in stiffness associated with repeated loading. Together, these results provide an integrated understanding of how the CAM and slab materials degrade under service-like cyclic loading conditions.

7.2 Static Flexural Strength of CAM

Before conducting the fatigue analysis, the static flexural strength of CAM specimens was measured to establish a reference point for the fatigue stress levels. Table 7.1

presents the results. The average flexural strength was found to be **9.08 MPa**, with a relatively low coefficient of variation (COV) of **4.63%**, indicating consistency and reliability in the measured data.

Table 0.1 Static flexural test result of CAM

Specimen Number	Flexure Load (N)	Flexure Stress (MPa)	Specimen Number	Flexure Load (N)	Flexure Stress (MPa)
1	22248	8.8992	7	22602	9.0408
2	23946	9.5784	8	24090	9.636
3	24480	9.792	9	20124	8.0496
4	24528	9.8112	10	23730	9.492
5	20856	8.3424	11	21564	8.6256
6	21924	8.7696	12	22236	8.8944

This baseline strength serves as the denominator for defining fatigue stress levels, expressed as percentages of the maximum static strength (i.e., Smax). For example, fatigue tests were conducted at stress levels of 0.80 Smax, 0.75 Smax, 0.70 Smax, and 0.65 Smax, corresponding to applied stresses of approximately 7.26 MPa, 6.81 MPa, 6.36 MPa, and 5.90 MPa, respectively. The reliability of the baseline static strength ensures that these fatigue stress levels accurately represent real track conditions. The high flexural strength of CAM compared to conventional cement mortars demonstrates its superior crack-arresting ability, owing to the asphalt film coating on aggregates, which improves toughness and energy absorption. This property makes CAM highly suitable for the interface layer in slab track systems, where it must absorb vibrations and distribute wheel loads.

7.3 Fatigue Life Analysis

The fatigue life of CAM was evaluated using four different stress levels, and the results are summarized in Table 7.2. At the highest stress level (0.80 Smax,7.26 MPa), failure occurred after only **69 cycles**, indicating that near-ultimate stresses lead to rapid crack initiation and catastrophic fracture. As stress levels decreased, fatigue life increased exponentially: at 0.75 Smax (6.81 MPa), specimens survived around **412 cycles**; at 0.70 Smax (6.36 MPa), fatigue life extended to **1,543 cycles**; and at the lowest tested

level of 0.65 Smax (5.90 MPa), specimens survived as many as **38,110 cycles** before failure.

Table 0.2 Fatigue life evaluation of CAM specimens subjected to different stress amplitudes

Specimen Group No.	**Stress level**			
	0.80	**0.75**	**0.70**	**0.65**
G1	54	326	1472	32221
G2	72	408	1527	38711
G3	82	501	1629	43398
Mean value	69	412	1543	38110

These data were used to establish the **S–N relationship** (stress level vs logarithm of number of cycles), as plotted in *Figure 7.1*. A regression analysis yielded the following equation:

$$S = 0.9019 - 0.167 \times log\, N \quad ; R^2 = 0.9827 \tag{7.1}$$

The coefficient of determination, $R^2 = 0.9827$, indicates an excellent fit. The negative slope reflects the expected inverse relationship: higher stress levels correspond to shorter fatigue lives.

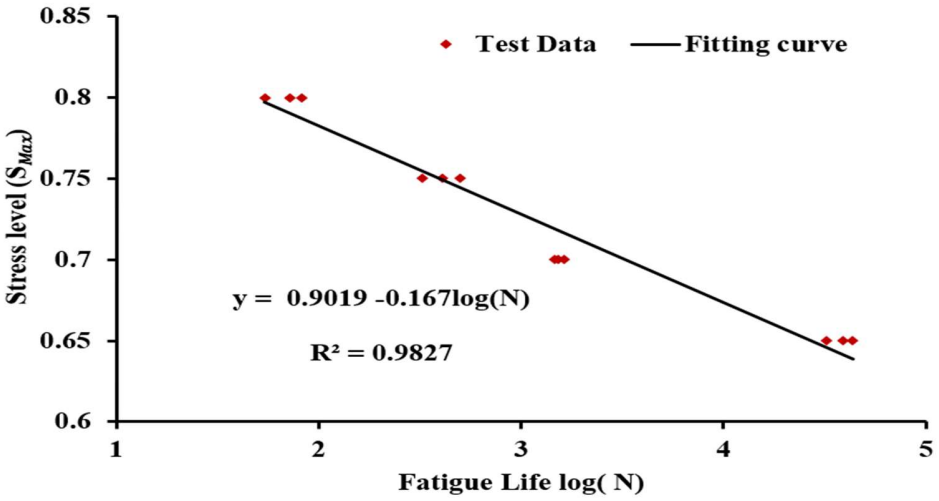

Figure 0.1Fatigue life curve for the CAM

Figure 7.1 clearly shows the steep drop in fatigue life at higher stress levels, illustrating the transition from low-cycle to high-cycle fatigue regimes. The trend also indicates a "knee point" around 0.70 Smax, below which fatigue life increases more rapidly. This knee point suggests a practical design threshold for CAM in slab tracks: operating below 70% of static flexural strength may provide a sufficiently long fatigue life for service conditions.

In real high-speed railway operations, the repeated load imposed by passing axles will typically correspond to stress levels of 0.65–0.70 Smax. The results here show that at these levels, CAM layers can withstand tens of thousands of cycles before failure, confirming their durability in the field. This validates the design principle of using CAM as a buffer between the stiff concrete slab and the resilient subgrade.

7.4 Fatigue Strain Evolution

Fatigue strain is divided into two categories: the first one is the maximum fatigue strain that occurs when the fatigue loading is at its highest and the second one is the residual fatigue strain which appears when there is the least amount of fatigue stress. The research studies done on the fatigue behavior of concrete have revealed a clear pattern

of three-phase evolution in the appearance of fatigue strain, which usually matches an inverted-S-shaped curve. The three phases are those of fast failure, slow development, and quick growth. Of the three phases, the second phase took the largest part of the fatigue process, during which strain showed nearly linear increase (C. Chen et al., 2021) (X. Chen et al., 2019; Q. Li et al., 2016). The degradation of the material under fatigue loading can be very precisely visible in the development curves of fatigue strain. Through both qualitative and quantitative analysis of the curves one can determine the material properties and predict the fatigue life. To better understand the internal damage mechanisms, the evolution of fatigue strain was recorded over multiple loading cycles. Liu et al. (F. Liu & Zhou, 2017b)introduced fatigue strain evolution model, which has been applied to characterize both maximum and residual strain development, as expressed in Eqs. (7.2) and (7.3).

$$\varepsilon_{max}^{n} = \varepsilon_{max}^{o} + \alpha \left(\frac{n/N}{\beta - n/N} \right)^{1/p} \tag{7.2}$$

$$\varepsilon_{res}^{n} = \varepsilon_{res}^{o} + \alpha \left(\frac{n/N}{\beta - n/N} \right)^{1/p} \tag{7.3}$$

In this case, the maximum and residual strains recorded during n^{th} fatigue cycle are indicated by ε_{max}^{n} and ε_{res}^{o}respectively, whereas initial maximum and residual fatigue strains are represented ε_{max}^{o} and ε_{res}^{o}. In the equation, α, β, and p are fitting parameters. The researchers selected second set of specimens used in fatigue testing to fit strain evolution curves, as discussed in Equations (7.2) and (7.3).

Table 0.3 Fitting variables for maximum strain formation curves

Stress level	α	β	p	ε_{max}^{o}	R^2
0.8	84.3	1.05	2.1	85.2	0.997
0.75	70.3	1.03	2.2	77	0.995
0.7	58.5	1.01	2.3	69	0.998
0.65	48.6	0.99	2.4	61	0.996

Table 0.4 Fitting variables for residual strain formation curves

Stress level	α	β	p	ε_{res}^{o}	R^2
0.65	36.8	1.01	5	0	0.982
0.7	43.9	1.02	4.5	0	0.983
0.75	50.1	1.04	4	0	0.984
0.8	55.3	1.05	3.5	0	0.984

Tables 7.3 and 7.4 present a summary of fitting parameters for strain formation curves. The variables α and β exhibited an increase corresponding to elevated stress levels. The goodness of fit at all levels of stress exceeded 0.99 and 0.98 for maximum strain and residual strain, respectively, demonstrating the reliability of the fitting model.

Figures 7.2 present the maximum strain evolution curves for stress levels of 0.65 S_{max}. All curves displayed the typical **three-phase inverted-S shape**:

1. **Initial Phase (Rapid Increase):** During the first 10–20% of cycles, maximum strain increased sharply. This phase corresponds to the initiation of microcracks at weak points in the CAM matrix, particularly at the asphalt–aggregate interfaces.

2. **Steady-State Phase (Gradual Increase):** Strain increased slowly and almost linearly with cycles, representing stable crack propagation and energy dissipation by the asphalt films.

3. **Failure Phase (Accelerated Increase):** The strain rose rapidly again just before failure, indicating the coalescence of microcracks into macrocracks and eventual rupture.

Figures 7.3 present the maximum strain evolution curves for stress levels of 0.70 S_{max}. Residual strain evolution followed a similar pattern, but with smaller absolute magnitudes, as shown in Figure 7.3. Residual strains reflect permanent deformation and plasticity within the CAM microstructure, which accumulate gradually over cycles.

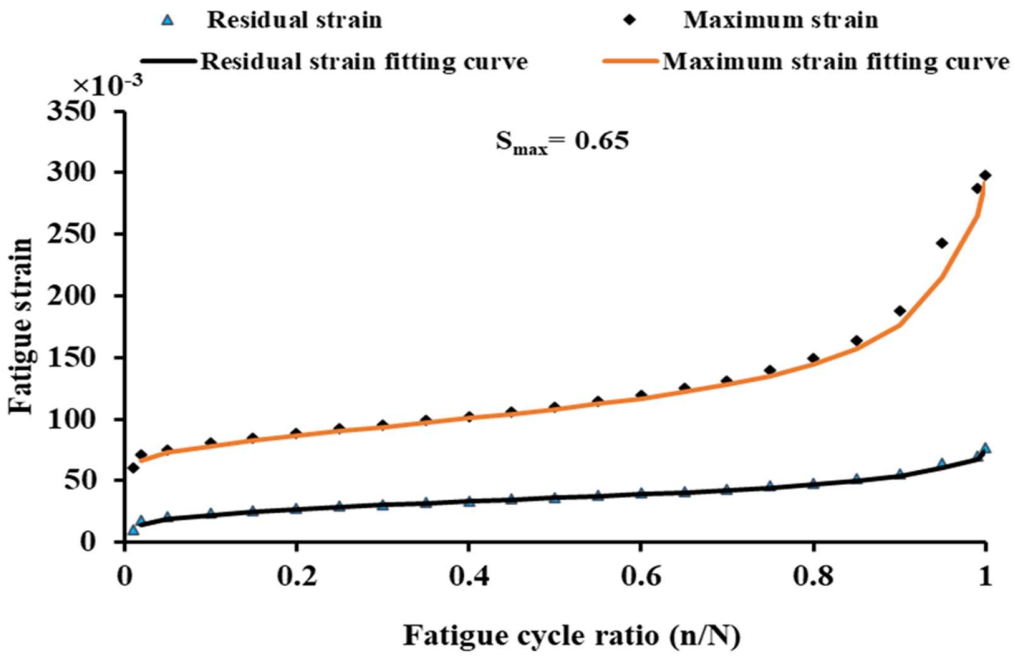

Figure 0.2 Fatigue strain in CAM under applied stress (0.65)

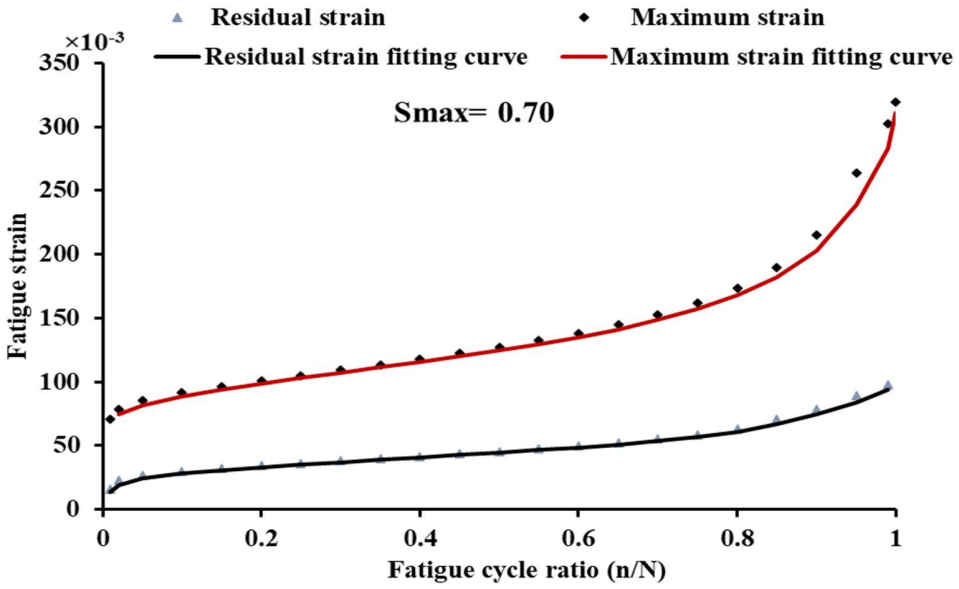

Figure 0.3 Fatigue strain in CAM under applied stress (0.70)

The three-phase evolution pattern confirms that CAM can dissipate cyclic energy effectively in the steady-state phase, delaying failure. However, once the transition to accelerated strain occurs, remaining fatigue life is very short. Monitoring strain evolution in real-time tracks (e.g., through embedded sensors) could therefore provide an early warning system for CAM failure.

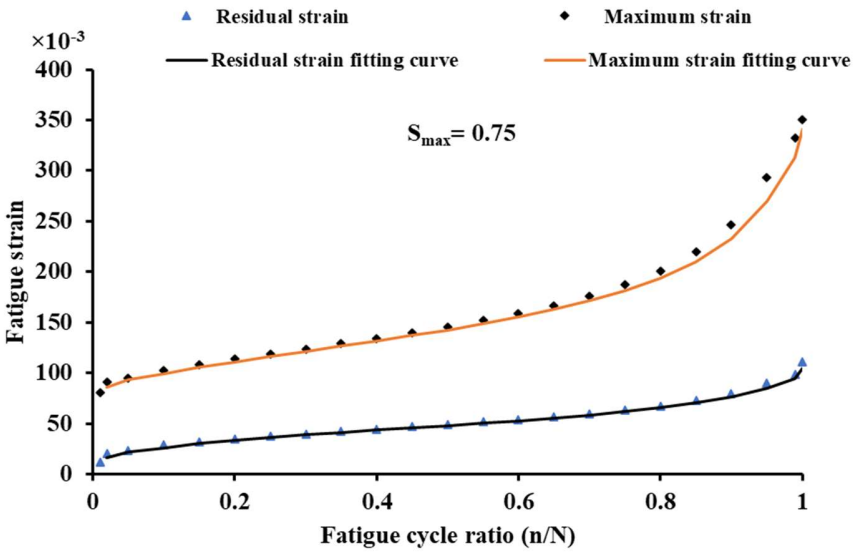

Figure 0.4 Fatigue strain in CAM under applied stress (0.75)

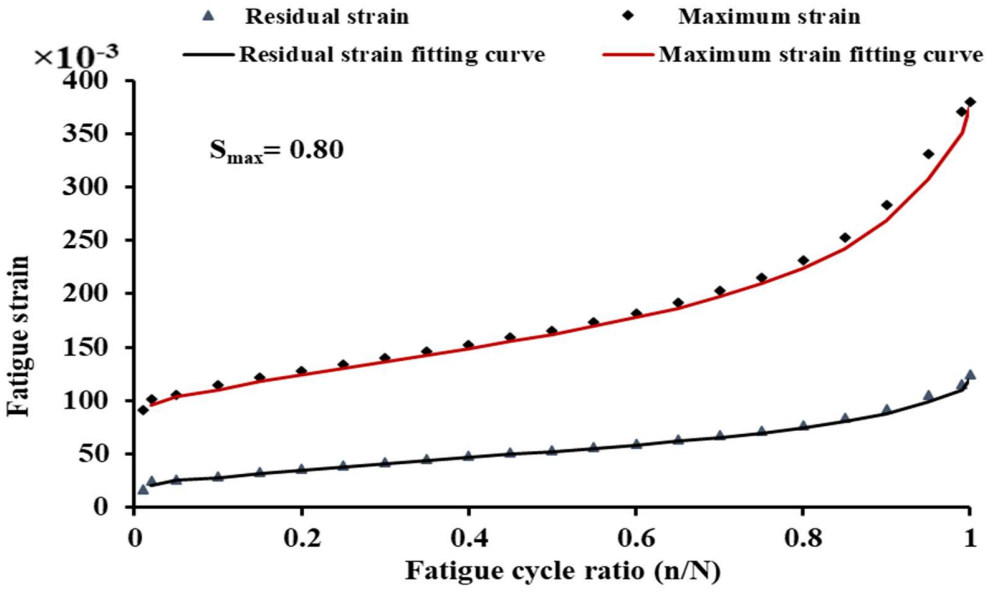

Figure 0.5 Fatigue strain in CAM under applied stress (0.80)

The evolution rate of residual strain, $d\varepsilon_{res}^{n}/d(n/N)$, can be determined using Equation (7.3) and the data presented in Table 7.4, as illustrated in Figure 7.6. The rate of strain evolution demonstrated a notable decrease from its high initial value in the

first stage, followed by a phase of relative stability in the second stage, and culminating in a swift increase during the third stage.

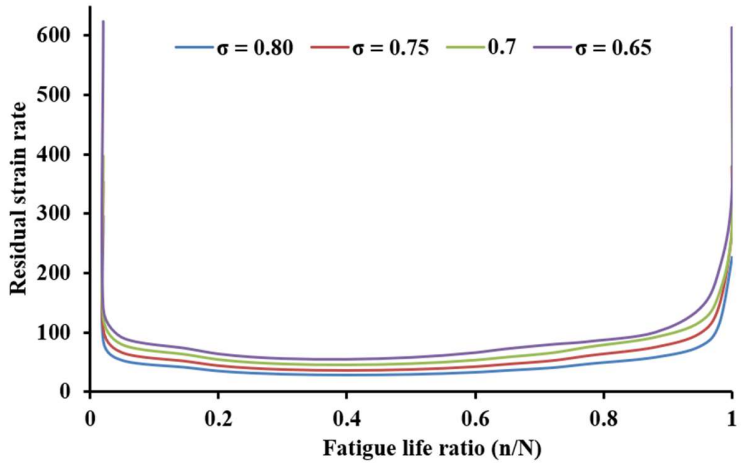

Figure 0.6 Variation of residual strain rate with number of fatigue cycles for CAM specimens

The evolution of the strain rate exhibited relatively consistent behavior across the entire stress range investigated (0.1–0.85 N). Prior investigations into the flexural fatigue characteristics of concrete (W. Li et al., 2011; W. Wang et al., 2006) have demonstrated that fatigue life is typically partitioned into three distinct regimes: an initial rapid response phase (10% of total life), a dominant quasi-stable propagation phase (75–80%), and a final acceleration-to-failure phase (10–15%). The three different CAM stages used in this study accounted for approximately 10%, 75%, and 15% of the fatigue life, as shown in Figure 7.6.

7.5 Fatigue Modulus Degradation

Previous experimental studies(C. Chen et al., 2021) (Lv et al., 2019) (Jin et al., 2024; Shu et al., 2024)established that concrete's fatigue modulus deteriorates under cyclic loading. The fatigue modulus for the Experimental study on fatigue properties of normal and rubberized self-compacting concrete under bending load cycle is determined using Equation (7.4):

$$E_n = \frac{\Delta\sigma}{\Delta\varepsilon_n} = \frac{\sigma_{max} - \sigma_{min}}{\varepsilon^n_{max} - \varepsilon^n_{min}} \tag{7.4}$$

The strain variation $\Delta\varepsilon_n$ and the fatigue modulus E_n was found to be inversely related because $\Delta\sigma$ remained stable when a constant amplitude loading was applied. As a result, E_n was obtained from the strain evolution curve, and its value decreased progressively with an increase in load cycles, which is attributed to a continuous rise in $\Delta\varepsilon_n$ During fatigue loading. Figure 7.7 illustrates the evolution of the fatigue modulus for CAM specimens, indicating a steady decline in modulus over time, characterized by a three-stage progression. Fatigue modulus values have been calculated at normalized cycle points of 0, 0.1, 0.85, and 1 for each specimen to quantify the degradation.

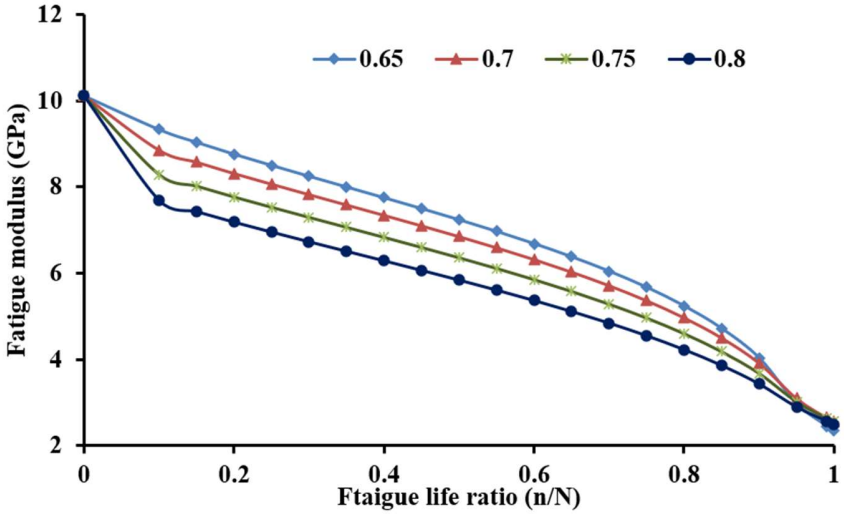

Figure 0.7 The fatigue modulus of CAM specimens is presented at various stress levels

Table 0.5 Degradation of fatigue modulus under cyclic loading

Stress Level	Fatigue Modulus Degradation			Total Degradation
	Stage 1	Stage 2	Stage 3	
0.65	0.512	2.6224	3.3661	6.5005
0.7	0.598	2.3578	2.9438	5.8996
0.75	0.856	2.631	1.8271	5.3141
0.8	1.079	3.8349	1.291	6.2049

Table 7.5 summarizes the elastic modulus reductions for each phase, indicating a total degradation of 5.3 to 6.5 GPa. The modulus loss during the initial stage was less significant compared to later stages.

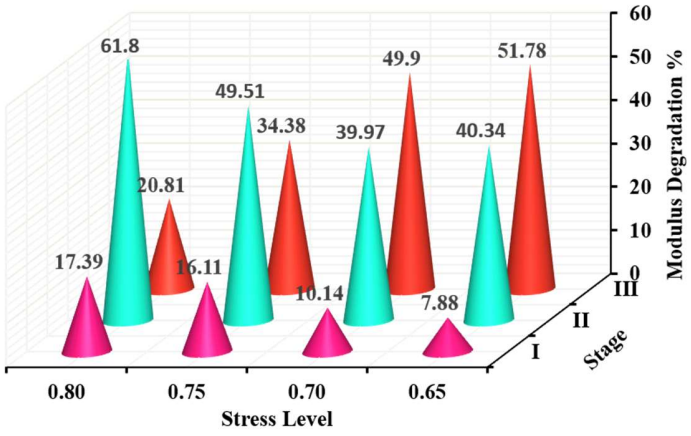

Figure 0.8 Modulus degradation of CAM specimens during flexural fatigue

Figure 7.8 depicts the distribution of fatigue modulus reduction at various stress levels and phases. The fatigue modulus has been determined at fatigue life ratios of 0, 0.1, 0.85, and 1 across different maximum stress levels (Smax), facilitating the calculation of the modulus degradation ratio at each respective fatigue stage, as illustrated in Figure 11. At S_{max} = 0.65, the degradation ratio was 7.8% in Stage I, increased to 40.34% in Stage II, and peaked at 51.78% in Stage III. Under S_{max} = 0.80, the highest

reduction occurred in the initial stage at 17.39%, followed by 61.8% in the second stage, with the lowest degradation recorded in Stage III at 20.81%. The degradation trend of the fatigue modulus across the Smax range of 0.60 to 0.80 shifted from an increasing pattern in Stage I to a decreasing pattern in Stage III.

As Smax increased, the degradation ratio in Stage I rose from 7.8% to 17.39%, whereas in Stage III, a contrasting trend was noted, with a decrease from 51.78% to 20.81%. The initial stage of the three-phase evolution of the CAM fatigue modulus was short and characterized by minor damage, resulting in negligible modulus loss.

These results suggest that operating CAM at ≤0.70 Smax maintains stiffness for longer durations, while higher stress levels accelerate the loss of stiffness. For Indian HSR, careful design is crucial to minimize stress transfer to the CAM, ensuring a long service life.

7.6 Discussion

The combined results of fatigue life, strain evolution, and modulus degradation highlight the following key points:

- CAM exhibits superior fatigue resistance compared to conventional cement mortar due to its asphalt films, which delay crack propagation.
- Fatigue life increases exponentially as stress decreases, confirming the critical importance of limiting applied stresses to ≤0.70 Smax.
- Strain evolution and modulus degradation curves both follow three-stage patterns, confirming consistency in the damage mechanism.

7.7 Chapter Summary

This chapter presented a comprehensive fatigue evaluation of CAM for high-speed railway slab track systems. The main findings are:

1. **The static flexural strength** of CAM was 9 MPa, establishing a strong baseline.

2. **S–N curve analysis** confirmed the logarithmic stress–life relation, with excellent $R^2 = 0.9827$.
3. **Fatigue life** increased from 69 cycles at 0.80 Smax to 38,110 cycles at 0.65 Smax.
4. **Strain evolution** exhibited a three-phase inverted-S pattern, consistent with crack initiation, propagation, and failure.
5. **Modulus degradation** also followed a three-phase trend, with stiffness loss accelerated at higher stress levels.
6. **Engineering design implication:** Limiting applied stresses to ≤0.70 Smax ensures a longer service life for CAM, making it suitable for MAHSR and other HSR corridors.

CHAPTER 8: CONCLUSION, FUTURE SCOPE AND SOCIAL IMPACT

8.1 General

The present research has been carried out with the objective of developing a comprehensive evaluation framework for slab track systems in high-speed rail applications in India. While conventional ballasted tracks have served Indian Railways for decades, their inherent limitations under high-speed conditions such as ballast degradation, uneven settlement, and high maintenance demand make them unsuitable for the next generation of railway infrastructure. In contrast, slab track systems offer higher stability, longer service life, and reduced maintenance; however, their adoption requires a careful scientific assessment of both structural and functional performance.

In this context, the study systematically examined the behavior of slab tracks under static, dynamic, vibration, and fatigue conditions, with each stage forming an integral part of a connected framework. The static response, analyses using finite element modelling, established the baseline performance of the slab and ballasted track systems under quasi-static UIC LM71 loading, revealing vital details about deflection and stress patterns as per codal provisions. Building upon this foundation, the dynamic response was explored through a coupled vehicle–track interaction model, which revealed how increased train speeds and resonance effects amplify displacements, stresses, and wheel–rail forces, thereby extending the understanding of performance from static equilibrium to real-time operational conditions. Recognizing the importance of passenger comfort and structural longevity, the study further incorporated a vibration mitigation analysis, where slab mats were introduced as elastic layers and their parametric variations in stiffness, damping, and thickness were investigated to assess their role in reducing vibration propagation and enhancing durability. Finally, attention was directed to the fatigue behavior of cement–asphalt mortar (CAM), the most fatigue-sensitive layer of slab tracks, through both numerical modelling and experimental validation. A three-stage fatigue strain evolution was

identified in the most fatigue-sensitive layer of slab tracks through both numerical modelling and experimental validation, where a three-stage fatigue strain evolution was identified, and stress–life relationships were derived to predict service life.

By weaving together these four strands, the research ensured that each objective addressed its specific domain and provided inputs to the subsequent analyses. The static study informed the dynamic modelling; the outcomes of dynamic response guided the vibration analysis; and the combined static, dynamic, and vibration results provided the boundary conditions for fatigue life assessment. This interdependency allowed the study to capture both the short-term structural adequacy and the long-term durability of slab tracks in a unified manner. The collective insights drawn from these interconnected objectives serve as the foundation for the specific conclusions presented in Sections 5.2 to 5.5, while also shaping the recommendations (Section 5.7) and identifying directions for future research (Section 5.6). Thus, this general section not only summarizes the broad scope of the work but also establishes a logical continuity with the detailed conclusions that follow.

8.2 Conclusions for Static Response

This research comprehensively evaluated the structural performance of slab and ballasted track systems under static loading conditions using finite element modelling (FEM). The comparative study confirmed the superiority of slab track systems in terms of stability, durability, and load distribution when subjected to standard UIC LM71 loading.

The FEM simulations revealed that the slab track exhibited nearly 45% lower maximum deflection compared to the ballasted track system. Furthermore, the slab track also experienced significantly lower bending stresses, primarily due to its enhanced bending stiffness and optimized design configuration. These characteristics highlight the fundamental advantage of slab track systems in maintaining structural integrity under high-speed railway operations.

A detailed parametric analysis of component properties yielded the following insights:

a) Increasing rail pad stiffness from 35 MN/m to 95 MN/m reduced rail deflections by approximately 20%. This improvement lowered the bending and shear stresses in the rail itself. However, stresses in the concrete slab and hydraulic bonded layer (HBL) increased, illustrating the necessity of maintaining an optimal stiffness range that avoids overloading secondary components.
b) Enhancing CAM stiffness from 300 MN/mm³ to 1800 MN/mm³ resulted in a 16.7% reduction in slab deflection and an 11% improvement in rail stability. Conversely, the shear stress within the slab increased by 9.88%, underscoring the trade-off between deflection reduction and stress redistribution.
c) Improving subgrade stiffness enhanced overall track stability by reducing deflections. However, it also led to a 6.8% increase in slab bending stress and an 8.04% rise in shear stress, demonstrating that subgrade stiffness plays a governing role in stress distribution and must be optimized carefully.
d) Increasing slab thickness from 120 mm to 300 mm significantly decreased bending and shear stresses in both the slab and HBL layers, thereby improving structural efficiency and service life. Importantly, rail stresses remained unchanged.
e) A thicker HBL layer effectively reduced shear stress within itself, improving its durability. However, this caused an increase in bending stress in the concrete slab, again highlighting the importance of balancing thickness for optimal load transfer and stress distribution.

Overall, the static analysis demonstrated the inherent advantages of slab track systems in effectively distributing loads and maintaining long-term structural integrity. The study further demonstrated that the careful optimization of component stiffness, thickness, and material properties is crucial for achieving a balanced performance.

By employing real-world parameters from the Mumbai–Ahmedabad High-Speed Rail (MAHSR) project, the research ensures high practical relevance and applicability. The findings suggest that optimized slab track designs can deliver safer, more durable, and cost-effective infrastructure for future high-speed railway networks in India and beyond. Moreover, the conclusions provide insights into addressing long-standing challenges such as deformation control, stress concentration, and long-term maintenance in high-speed rail systems.

8.3 Conclusions for Vibration Response

The purpose of this research is to examine how a slab mat layer made of elastic material affects the response to vibrations of a high-speed train's precast slab track system. The dynamic behavior of a three-dimensional prefabricated slab track is analyzed by numerical simulation using ANSYS software. The simulation includes changes in slab mat layer stiffness, thickness, and slab track foundation stiffness. The results indicate that the presence of the elastic material slab mat layer leads to a reduction in the vibration response of the slab track. Furthermore, the study investigates the effects of altering the material and geometry properties of the slab mat layer, including its stiffness, the subgrade layer stiffness, and the thickness of the slab mat layer. There are some results can be observed from this study:

The effects of changing the elastic modulus from 15 MPa to 225 MPa on the vertical acceleration of the rail and the concrete slab layer, respectively.

The thickness of the slab mat reduced the vertical vibration propagated from the railway track. Therefore, a thicker slab mat can absorb more force, diminish the vibration, and minimize the influence of the continued repetition vibration that might damage the slab track's foundation.

The impact of the foundation layer's modulus of elasticity ranges from 35 MP to 245 MPa. The elastic properties of the foundation substantially impact the

displacement response of the slab; the elastic characteristics of the foundation minimize the displacement of the concrete slab layer.

Increasing slab mat damping significantly reduces the vertical displacement of the rail, concrete slab, and concrete support layer. This analysis concludes that increased slab mat damping effectively reduces vibrations within the track structure. This contributes to extending the service life of the slab track and reducing the maintenance workload for the track system

The slab mat layer has a disproportionately large impact on the displacement of the subgrade. A slab mat layer with a lower stiffness is preferable to one with a higher stiffness. The lowest does not always mean the most desirable. Increased rail and slab displacements caused by a slab mat layer with insufficient stiffness can reduce the track's smoothness and shorten its lifespan. In conclusion, increasing train speeds and axle loads significantly amplifies rail and slab accelerations, with slab responses being more sensitive to lighter loads. The findings highlight the need to assess track performance to ensure safety under high-speed and heavy-load conditions.

The most suitable stiffness for a slab mat layer is between 25 and 60MN/m^3. All results and inferences drawn from this research are valid only within the context of the specific model employed here. Incorporating a slab mat layer into the design of the high-speed railway track structure is essential to mitigate the propagation of vibration response from the track structure to the adjacent area. This addition serves as an effective measure for controlling and minimizing vibrations, ensuring smoother and more comfortable operation of the high-speed railway system while reducing disturbances to nearby surroundings. The parametric study conducted in the present work provides valuable insights that can be utilized to evaluate the economic feasibility of implementing thicker and stronger slab mats in current rail infrastructure.

Overall, the study concludes that incorporating slab mats into slab track systems is crucial for reducing vibration propagation, enhancing ride comfort, and prolonging track life. The findings emphasize the importance of selecting the optimal stiffness, damping, and thickness of slab mats to balance vibration control with structural efficiency.

8.4 Conclusions for Dynamic Vehicle–Track Interaction

A comprehensive and high-fidelity numerical framework was developed to evaluate vertical dynamic responses of high-speed railway slab track systems under realistic operating conditions. The methodology adopted the Moving Element Method (MEM), which resolves governing equations in a moving coordinate system. This approach proved superior to conventional FEM, as it avoided repetitive remeshing during train passage and significantly enhanced computational efficiency for long track domains.

The slab track was idealized as a three-layer Euler–Bernoulli beam system, with rails supported on discrete pads overlying a concrete slab layer, a cement–asphalt mortar (CAM) layer, and hydraulically bonded bearing layers. Coupled with a 26-DOF vehicle model, the simulation captured complex nonlinear interactions, including Hertzian wheel–rail contact and nonlinear frictional pad forces.

The following conclusions were drawn:

a) The MEM-based model demonstrated strong agreement with FEM benchmarks, with acceptable errors (13–16%) for vertical rail displacements and wheel–rail contact forces. This validated its robustness and accuracy.
b) Increasing train speed and track irregularities substantially amplified dynamic responses, underscoring the need for stringent surface maintenance and operational speed control.
c) Optimizing CAM stiffness reduced displacements across the slab track structure by up to 37%, significantly enhancing stability while maintaining manageable acceleration levels.

d) Overly stiff rail pads reduced displacements but increased accelerations in deeper layers, suggesting the need for balance. Subgrade improvements moderately reduced vibrations but exhibited diminishing returns beyond certain stiffness thresholds.

e) The MEM approach was demonstrated to be computationally superior, providing faster simulations without compromising accuracy. This makes it particularly suitable for real-time dynamic analysis of high-speed rail systems.

In conclusion, the MEM-based framework provided a powerful predictive tool for the performance-based design and optimization of slab track systems. By realistically incorporating nonlinearities and coupling effects, the study advanced understanding of vehicle–track interactions and provided practical pathways for improving safety, stability, and comfort in high-speed railway operations.

8.5 Conclusions for Fatigue Study of CAM

The flexural fatigue performance of cement–asphalt mortar (CAM), a critical component in slab track systems, was rigorously investigated using four-point bending fatigue tests at stress levels of 0.65, 0.70, 0.75, and 0.80 of ultimate flexural strength. The experimental results revealed a clear three-stage fatigue strain evolution, consisting of an initial rapid growth phase, a stable plateau phase, and an accelerated failure phase.

The study produced the following key findings:

a) Static bending tests showed an average CAM flexural strength of ~9.08 MPa, with a failure load of ~22,694 N.

b) Fatigue life decreased sharply with increasing stress levels. Average lives were 38,110 cycles (0.65 Smax), 1,543 cycles (0.70 Smax), 412 cycles (0.75 Smax), and just 69 cycles (0.80 Smax). The relationship between maximum stress and fatigue life followed a logarithmic law:

$$S = 0.9019 - 0.167 \times log\, N \quad ; R^2 = 0.9827$$

c) Fatigue strain curves followed an inverted S-shaped trajectory. At lower stress levels, the three-phase behaviour was more pronounced, with longer stable phases and a delayed onset of rapid failure.
d) The fatigue modulus continuously decreased with cycling. Total degradation ranged from 5.3 to 6.5 GPa. The stable second phase contributed most to the loss, while the third phase exhibited a rapid decline in modulus due to the accumulation of microcracks.

In conclusion, CAM was confirmed as the fatigue-critical layer of slab track systems. Its performance directly dictates the service life of the track, reinforcing the need for material optimization and preventive maintenance strategies. The experimental insights not only advance fundamental understanding of CAM fatigue mechanisms but also provide practical guidelines for engineering applications in high-speed railway projects.

8.6 Future Scope of the Study

Although the present work has contributed significantly to understanding slab track behaviour under static, dynamic, vibration, and fatigue loading conditions, the scope of further research remains wide and multifaceted. The conclusions derived from this study provide a strong foundation; however, several aspects demand deeper exploration before the findings can be fully generalized for large-scale application in Indian high-speed railway projects such as the Mumbai–Ahmedabad High-Speed Rail (MAHSR) corridor.

Field validation of numerical models is one of the most pressing future requirements. While the present FEM- and MEM-based simulations have been calibrated against codal provisions and literature benchmarks, their accuracy can only be fully established through real-time monitoring of high-speed rail tracks. Once operational data from the MAHSR corridor becomes available, measurements of rail deflections, slab accelerations, vibration levels, and cumulative fatigue degradation should be systematically compared with model predictions. Such calibration would enhance the

robustness of the developed framework and provide confidence in its applicability to other Indian corridors.

Another area that requires attention is the incorporation of **advanced constitutive models for track materials**. In this study, the slab concrete, cement–asphalt mortar (CAM), and subgrade were treated as linear elastic for computational feasibility. In reality, however, these materials exhibit nonlinear, viscoelastic, and time-dependent behaviours under repeated training loads. Developing models that account for creep, shrinkage, plasticity, and progressive stiffness degradation would provide more realistic life-cycle predictions. Similarly, **fatigue models with damage accumulation laws** that reflect real-world deterioration should be explored, moving beyond the constant amplitude tests performed in this work.

The present work primarily focused on **vertical responses of slab tracks**, yet high-speed trains also induce significant lateral and torsional forces, especially under conditions such as braking, acceleration, and hunting instability. Future studies should therefore extend to **three-dimensional coupled dynamics of vehicle–track–soil systems**, allowing for the assessment of lateral displacements, rail-seat forces, and potential instability phenomena. Such 3D frameworks would also enable the evaluation of derailment safety and riding comfort under more realistic scenarios.

The fatigue study of CAM can be advanced further by incorporating **variable amplitude loading conditions**, since operational trains impose non-uniform load spectra rather than constant amplitude cycles. Laboratory fatigue testing under variable loading, combined with stochastic modeling of load histories, would produce more reliable service-life predictions. Moreover, scaling laboratory results to field-sized slab sections through **accelerated fatigue testing** would help bridge the gap between specimen behavior and full-scale performance.

Additionally, soil–structure interaction effects warrant detailed investigation. Indian high-speed routes traverse diverse subgrade conditions, ranging from soft clays to stiff sandy strata. The interaction between cyclic loading and subgrade heterogeneity can

influence settlement patterns, stiffness degradation, and overall track stability. Advanced coupled geotechnical-structural models, validated with field data, would help predict these effects more reliably and guide appropriate ground improvement measures.

Finally, the issue of **sustainability** cannot be overlooked. Future work should explore alternative materials for CAM, such as polymer-modified binders, fiber-reinforced mortars, and blends incorporating recycled aggregates. These alternatives may not only improve fatigue resistance but also align with India's commitment to sustainable infrastructure development. Investigating the carbon footprint, durability, and life-cycle cost implications of such materials would add further depth to the current research.

In summary, the present study represents a significant advancement in understanding slab track systems for high-speed applications in India. Yet, its true potential lies in serving as a platform upon which future work—spanning field validation, material modeling, three-dimensional vehicle–track dynamics, advanced fatigue testing, soil–structure interaction, AI-based predictive tools, and sustainable material innovations—can be systematically built. Pursuing these directions will not only refine the predictive capability of slab track design frameworks but also ensure that Indian high-speed rail systems remain safe, durable, cost-effective, and future-ready.

8.7 Recommendations

The outcomes of this research extend beyond academic contributions, carrying strong **practical implications for the design, construction, and maintenance of slab track systems in India's emerging high-speed railway sector**. By systematically examining the static, dynamic, vibration, and fatigue behavior of slab track structures, this study generates recommendations that can directly support both engineers and policymakers in developing safe, durable, and cost-effective track infrastructure.

From a **design perspective**, the findings underscore the importance of optimizing the stiffness of track components. The finite element simulations revealed that while

turnitin Page 180 of 200 - Integrity Submission Submission ID trn:oid:::27535:124127336

increasing rail pad and CAM stiffness reduces overall deflections, it can simultaneously elevate local stresses in the slab and hydraulically bonded layers. Thus, the study recommends adopting **balanced stiffness ranges** that minimize deflections without overstress critical components. Similarly, the parametric analyses highlighted the benefits of **increasing slab and HBL thicknesses**, which significantly improve load distribution and reduce stresses. However, excessive thickness may induce secondary stress concentration, and hence, **rational optimization rather than indiscriminate enhancement** must guide design practice.

The **dynamic analyses** demonstrated that resonance effects and high train speeds amplify rail and slab displacements, making it essential to incorporate **vehicle–track interaction models** in design codes rather than relying solely on static load cases. This shift would allow designers to account for coupled dynamics, nonlinear rail pad responses, and realistic wheel–rail contact conditions. Indian standards for high-speed track design should formally incorporate such provisions, aligning them with international practices.

The **vibration studies** provided strong evidence for the use of slab mats as an effective mitigation measure. With optimal stiffness in the range of 25–60 MN/m³ and higher damping capacity, slab mats can substantially reduce vibration transmissibility, thereby improving riding comfort and prolonging the life of CAM. Their incorporation should be made a standard recommendation in the design of high-speed slab tracks, particularly in urban and environmentally sensitive corridors where vibration impact is a concern.

Perhaps the most significant practical outcome arises from the **fatigue analysis of cement–asphalt mortar (CAM)**. The experimental and numerical results confirmed that CAM is the fatigue-critical component of slab track systems, and its long-term performance dictates the overall durability of the track. Recommendations from this study include maintaining operating stress levels below 0.70 Smax to extend fatigue life, refining CAM mix design through binder–aggregate optimization and fibre

reinforcement, and integrating S–N models into durability-based service-life prediction frameworks. These steps will directly improve the resilience and maintainability of slab tracks.

Beyond technical design recommendations, the study also offers **policy-level implications**. The adoption of slab track systems in India should be guided not only by initial construction costs but also by **life-cycle cost analyses** that account for reduced maintenance and longer service lives. Government agencies and project authorities, such as NHSRCL, are encouraged to incorporate the outcomes of this research in feasibility reports and tender specifications. The results also support the need for **continuous health monitoring systems**, which can track CAM degradation and slab deflections in real time, shifting maintenance strategies from reactive to predictive modes.

Finally, the broader implication of this work lies in its ability to serve as a **reference framework for future Indian high-speed corridors**. The methodologies and results developed here can be extended to similar projects, thereby providing consistency in design philosophy and reducing duplication of effort. By integrating vibration control, fatigue assessment, and dynamic analyses into standard practice, India can develop a **strong culture for designing slab tracks** that not only ensures safety and comfort but also aligns with global benchmarks of reliability and sustainability.

In essence, the recommendations derived from this study emphasize the **practical translatability of research into engineering practice**. They bridge the gap between advanced numerical modeling and real-world infrastructure needs, ensuring that the next generation of Indian high-speed railways is not only technically sound but also economically viable and socially responsible.

71

8.6 Future Scope of the Study

Although the present work addresses multiple aspects of slab-track behaviour, the following areas remain open for further research and development:

1. **Field Validation**: Future studies should incorporate in-situ monitoring from the MAHSR corridor once operational, including displacement, vibration, and strain measurements, to validate and calibrate the FEM–MEM models.
2. **Advanced Material Models:** More realistic viscoelastic, viscoplastic, and nonlinear fatigue models for CAM and subgrade materials should be developed to capture their behavior under temperature, moisture, and long-term degradation effects.
3. **Three-Dimensional Coupling:** While this research focused on vertical dynamics, lateral and torsional effects (yaw, hunting, and braking forces) should be integrated into a full 3D vehicle–track–soil interaction framework.
4. **Variable-Amplitude Fatigue:** Laboratory and field-based fatigue studies should extend beyond constant amplitude loading to **variable amplitude spectra**, simulating real high-speed train load histories more accurately.
5. **Soil–Structure Interaction:** The influence of layered soils, embankment heterogeneity, and potential settlement under cyclic high-speed loading requires detailed coupled analyses.
6. **Sustainability:** Investigation into alternative mortar formulations (e.g., fiber-reinforced CAM, polymer-modified composites, or recycled aggregates) can improve fatigue resistance and reduce environmental footprint.

REFERENCES

AASHTO. (1993). Standard Specifications for Highway Bridges. *American Association of State Highway and Transportation Officials, Washington, D.C., USA,*.

Aggestam, E., & Nielsen, J. C. O. (2020). Simulation of vertical dynamic vehicle–track interaction using a three-dimensional slab track model. *Engineering Structures*, *222*(June), 110972. https://doi.org/10.1016/j.engstruct.2020.110972

Aggestam, E., Nielsen, J. C. O., & Bolmsvik, R. (2018). Simulation of vertical dynamic vehicle–track interaction using a two-dimensional slab track model. *Vehicle System Dynamics*, *56*(11). https://doi.org/10.1080/00423114.2018.1426867

Ang, K. K., & Dai, J. (2013). Response analysis of high-speed rail system accounting for abrupt change of foundation stiffness. *Journal of Sound and Vibration*, *332*(12), 2954–2970. https://doi.org/10.1016/J.JSV.2013.01.005

ANSYS. (n.d.). *Ansys 2010 Meshing User Guide Europe*.

Atalan, M., Prendergast, L. J., Grizi, A., & Thom, N. (2022). A Review of Numerical Models for Slab-Asphalt Track Railways. In *Infrastructures* (Vol. 7, Issue 4). MDPI. https://doi.org/10.3390/infrastructures7040059

Axinte, T. (2014). Hertz Contact Problem between Wheel and Rail. *Advanced Materials Research*, *837*, 733–738. https://doi.org/10.4028/www.scientific.net/AMR.837.733

Bastin, R. (2006). Development of German non-ballasted track forms. *Proceedings of the Institution of Civil Engineers-Transport*, *159*(1), 25–39.

Berg, M. (1997). A model for rubber springs in the dynamic analysis of rail vehicles. *Proceedings of the Institution of Mechanical Engineers, Part F: Journal of Rail and Rapid Transit*, *211*(2), 95–108. https://doi.org/10.1243/0954409971530941

BIS. (2013). *IS 12269 (1987): 53 grade ordinary Portland cement*.

Blanco, B., Alonso, A., Kari, L., Gil-Negrete, N., & Giménez, J. G. (2019). Implementation of Timoshenko element local deflection for vertical track modelling. *Vehicle System Dynamics*, *57*(10), 1421–1444. https://doi.org/10.1080/00423114.2018.1513538

Cai, X., Zhang, Q., Wang, Q., Cui, X., & Dong, B. (2022). Effects of the subgrade differential arch on damage characteristics of CRTS III slab track and vehicle dynamic response. *Construction and Building Materials*, *327*, 126982. https://doi.org/10.1016/J.CONBUILDMAT.2022.126982

Cao, T. N. T., Reddy, J. N., Ang, K. K., Luong, V. H., Tran, M. T., & Dai, J. (2018). Dynamic analysis of three-dimensional high-speed train-track model using moving element method. *Advances in Structural Engineering*, *21*(6), 862–876.

CEBECI, A. (2020). A Review Study on Assessing the Sustainability of Design and Maintenance of Slab Track Systems for Turkey. *Uluslararası Muhendislik Arastirma ve Gelistirme Dergisi*, 325–336. https://doi.org/10.29137/umagd.635267

Charoenwong, C., Connolly, D. P., Colaço, A., Alves Costa, P., Woodward, P. K., Romero, A., & Galvín, P. (2023). Railway slab vs ballasted track: A comparison of track geometry degradation. *Construction and Building Materials*, *378*. https://doi.org/10.1016/j.conbuildmat.2023.131121

Chen, C., Chen, X., & Zhang, J. (2021). Experimental study on flexural fatigue behavior of self-compacting concrete with waste tire rubber. *Mechanics of Advanced Materials and Structures*, *28*(16), 1691–1702. https://doi.org/10.1080/15376494.2019.1701152

Chen, H. P., Li, W. Bin, Jiang, Y., & Xiao, L. F. (2024). Fatigue life prediction for CA mortar in CRTS II railway slab track subjected to combined thermal action and vehicle load by mesoscale numerical modelling. *Construction and Building Materials*, *437*. https://doi.org/10.1016/j.conbuildmat.2024.136987

Chen, M., Sun, Y., Zhu, S., & Zhai, W. (2021). Dynamic performance comparison of different types of ballastless tracks using vehicle-track-subgrade coupled dynamics model. *Engineering Structures*, *249*, 113390.

Chen, X., Liu, Z., Guo, S., Huang, Y., & Xu, W. (2019). Experimental study on fatigue properties of normal and rubberized self-compacting concrete under bending. *Construction and Building Materials*, *205*, 10–20. https://doi.org/10.1016/j.conbuildmat.2019.01.207

Chen, X., Wu, S., & Zhou, J. (2013). Experimental and modeling study of dynamic mechanical properties of cement paste, mortar and concrete. *Construction and Building Materials*, *47*, 419–430. https://doi.org/10.1016/j.conbuildmat.2013.05.063

Chen, Z., Zhai, W., & Yin, Q. (2018). Analysis of structural stresses of tracks and vehicle dynamic responses in train–track–bridge system with pier settlement. *Proceedings of the Institution of Mechanical Engineers, Part F: Journal of Rail and Rapid Transit*, *232*(2), 421–434.

Colajanni, P., Falsone, G., & Recupero, A. (2009). Simplified formulation of solution for beams on winkler foundation allowing discontinuities due to loads and constraints. *International Journal of Engineering Education*, *25*(1), 75–83.

Connolly, D. P., & Costa, P. A. (2020). Geodynamics of very high speed transport systems. *Soil Dynamics and Earthquake Engineering*, *130*(July 2019), 105982. https://doi.org/10.1016/j.soildyn.2019.105982

Connolly, D. P., Dong, K., Alves Costa, P., Soares, P., & Woodward, P. K. (2020). High speed railway ground dynamics: a multi-model analysis. *International Journal of Rail Transportation*, *8*(4), 324–346. https://doi.org/10.1080/23248378.2020.1712267

Cui, X., & Ling, X. (2021). Effects of differential subgrade settlement on damage distribution and mechanical properties of CRTS II slab track. *Construction and Building Materials*, *271*. https://doi.org/10.1016/j.conbuildmat.2020.121821

Dahlberg, T. (2003). Railway track dynamics-a survey. *Linköping University*.

Dahlberg, T. (2004). Railway track settlements-a literature review. *Report for the EU Project SUPERTRACK*, *463*.

Edwards, J. R., Lima, A. de O., Dersch, M. S., University of Illinois, U.-C., & Administration, F. T. (2020). *Resilient Concrete Crosstie and Fastening System Designs for Light, Heavy, and Commuter Rail Transit*. *February*, 124p.

En, B. S. (2003). 2. Eurocode 1: Actions on Structures–Part 2: Traffic Loads on Bridges. *British Standard Institution, UK: London*.

Esen, İ. (2011). DYNAMIC RESPONSE OF A BEAM DUE TO AN ACCELERATING MOVING MASS USING MOVING FINITE ELEMENT APPROXIMATION. In *Mathematical and Computational Applications* (Vol. 16, Issue 1).

Esveld, C. (2001). Modern railway track, 2nd editon. *Delft University of Technology*.

Esveld, C., & Markine, V. (2003). Slab track design for high-speed. *Delft University of Technology*.

Fang, C., Jaafar, S. A., Zhou, W., Yan, H., Chen, J., & Meng, X. (2023). Wheel-rail contact and friction models: A review of recent advances. *Proceedings of the Institution of Mechanical Engineers, Part F: Journal of Rail and Rapid Transit*, *237*(10), 1245–1259.

Ferreira, E., Sotoudeh, P., & Svecova, D. (2024). Fatigue life of plain concrete subjected to low frequency uniaxial stress reversal loading. *Construction and Building Materials*, *411*, 134247. https://doi.org/10.1016/j.conbuildmat.2023.134247

Freudenstein, S. (2010). RHEDA 2000®: Ballastless track systems for high-speed rail applications. *International Journal of Pavement Engineering*, *11*(4), 293–300. https://doi.org/10.1080/10298431003749774

Furkan Esen, A. (2022). *EXPERIMENTAL AND NUMERICAL ANALYSIS OF HIGH-SPEED RAILWAY INFRASTRUCTURE*.

Gautier, P. E. (2015). Slab track: Review of existing systems and optimization potentials including very high speed. *Construction and Building Materials*, *92*, 9–15. https://doi.org/10.1016/j.conbuildmat.2015.03.102

Giunta, M., & Praticò, F. G. (2017). Design and maintenance of high-speed rail tracks: A comparison between ballasted and ballast-less solutions based

on life cycle cost analysis. *Transport Infrastructure and Systems - Proceedings of the AIIT International Congress on Transport Infrastructure and Systems, TIS 2017*, 87–93. https://doi.org/10.1201/9781315281896-14

Güllü, A., Özden, B., Ölçer, B., Özcan, A. İ., Binbir, E., Durgun, Y., Saruhan, H., Şahin, F., Şenol, E., Khajehdehi, A., Noobakhtjoo, A., & Yüksel, E. (2021). Rapid and Easily Applicable Procedure for Full-Scale Laboratory Tests of Ballastless Slab Tracks. *Journal of Transportation Engineering, Part A: Systems*, *147*(9), 04021050. https://doi.org/10.1061/jtepbs.0000563

Guo, G., Hao, C., & Du, B. (2023). Static and dynamic response characteristics of a ballastless track structure of a high-speed railway bridge with interlayer debonding under temperature loads. *Engineering Failure Analysis*, *151*, 107377. https://doi.org/10.1016/J.ENGFAILANAL.2023.107377

Guo, Y., & Zhai, W. (2018). Long-term prediction of track geometry degradation in high-speed vehicle–ballastless track system due to differential subgrade settlement. *Soil Dynamics and Earthquake Engineering*, *113*, 1–11. https://doi.org/10.1016/j.soildyn.2018.05.024

Hoff, I., Mork, H., & Garba Saba, R. (n.d.). *PROCEEDINGS ELEVENTH INTERNATIONAL CONFERENCE ON THE BEARING CAPACITY OF ROADS, RAILWAYS AND AIRFIELDS*.

Jee, G. S., Nguyen, H. H., Jang, S. Y., Lee, H., & Chung, W. (2018). Key Characteristics of a Floating Slab Track Based on Longitudinal Interaction Analysis. *Mathematical Problems in Engineering*, *2018*. https://doi.org/10.1155/2018/3730649

Jiang, H. G., Bian, X. C., Xu, X., Chen, Y. M., & Jiang, J. Q. (2014). Full-scale model tests on dynamic performances of ballastless high-speed railways under moving train loads. *Yantu Gongcheng Xuebao/Chinese Journal of Geotechnical Engineering*. https://doi.org/10.11779/CJGE201402013

JICA, & MOR. (2015). *Joint Feasibility Study for Mumbai-Ahmedabad High Speed Railway Corridor FINAL REPORT 3.6.5 Design Parameters*. https://www.jica.go.jp/Resource/english/our_work/social_environmental/id/asia/south/india/c8h0vm00009v1ylc-att/c8h0vm0000bzv4e5.pdf

Jin, T., Yuan, J., Peng, X., Li, J., & Yang, R. (2024). A fatigue damage model of asphalt mixture considering tensile and compressive modulus decay. *Case Studies in Construction Materials*, *20*. https://doi.org/10.1016/j.cscm.2024.e03133

Junco, C., Rodríguez, A., Calderón, V., Muñoz-Rupérez, C., & Gutiérrez-González, S. (2018). Fatigue durability test of mortars incorporating polyurethane foam wastes. *Construction and Building Materials*, *190*, 373–381. https://doi.org/10.1016/j.conbuildmat.2018.09.161

Kaewunruen, S., & Remennikov, A. M. (2007). Field trials for dynamic characteristics of railway track and its components using impact excitation technique. *NDT and E International*, *40*(7), 510–519. https://doi.org/10.1016/j.ndteint.2007.03.004

Kaewunruen, S., & Remennikov, A. M. (2008). An alternative rail pad tester for measuring dynamic properties of rail pads under large preloads. *Experimental Mechanics*, *48*(1), 55–64. https://doi.org/10.1007/s11340-007-9059-3

Kalker, J. J. (2013). *Three-dimensional elastic bodies in rolling contact* (Vol. 2). Springer Science & Business Media.

Kerr, A. D. (2000). *On the determination of the rail support modulus k*. 4335–4351. https://doi.org/doi.org/10.1016/S0020-7683(99)00151-1

Koh, C. G., Ong, J. S. Y., Chua, D. K. H., & Feng, J. (2003). Moving element method for train-track dynamics. *International Journal for Numerical Methods in Engineering*, *56*(11), 1549–1567. https://doi.org/10.1002/nme.624

Kouroussis, G., Verlinden, O., & Conti, C. (2011). Free field vibrations caused by high-speed lines: Measurement and time domain simulation. *Soil Dynamics and Earthquake Engineering*, *31*(4), 692–707. https://doi.org/https://doi.org/10.1016/j.soildyn.2010.11.012

Le, T. H. M., Lee, S. H., & Park, D. W. (2020). Evaluation on full-scale testbed performance of cement asphalt mortar for ballasted track stabilization. *Construction and Building Materials*, *254*. https://doi.org/10.1016/j.conbuildmat.2020.119249

Lei, X., & Noda, N.-A. (2002). Analyses of dynamic response of vehicle and track coupling system with random irregularity of track vertical profile. *Journal of Sound and Vibration*, *258*(1), 147–165.

Lei, X., & Wang, J. (2014). Dynamic analysis of the train and slab track coupling system with finite elements in a moving frame of reference. *JVC/Journal of Vibration and Control*, *20*(9), 1301–1317. https://doi.org/10.1177/1077546313480540

Li, M. X. D., & Berggren, E. G. (2010). A study of the effect of global track stiffness and its variations on track performance: Simulation and measurement. *Proceedings of the Institution of Mechanical Engineers, Part F: Journal of Rail and Rapid Transit*, *224*(5), 375–382. https://doi.org/10.1243/09544097JRRT361

Li, Q., Huang, B., Xu, S., Zhou, B., & Yu, R. C. (2016). Compressive fatigue damage and failure mechanism of fiber reinforced cementitious material with high ductility. *Cement and Concrete Research*, *90*, 174–183. https://doi.org/10.1016/j.cemconres.2016.09.019

Li, W., Sun, W., & Jiang, J. (2011). Damage of concrete experiencing flexural fatigue load and closed freeze/thaw cycles simultaneously. *Construction and Building Materials*, *25*(5), 2604–2610. https://doi.org/10.1016/j.conbuildmat.2010.12.007

Li, Z. qiang, Li, Z., Huang, W. wei, Zhang, H. rui, & Zhang, H. (2022). Fatigue damage analysis of ballastless slab track in heavy-haul railway tunnels. *Underground Space (China)*, *7*(3), 440–452. https://doi.org/10.1016/j.undsp.2021.10.003

Lichtberger, B. (2011). *Track compendium*. PMC Media House.

Lin, Y.-H., & Trethewey, M. W. (1990). FINITE ELEMENT ANALYSIS OF ELASTIC BEAMS SUBJECTED TO MOVING DYNAMIC LOADS. In *Journal of Sound and Vibration* (Issue 2).

Ling, L., Jiang, P., Wang, K., & Zhai, W. (2020). Dynamic interaction between rail vehicles and vibration-attenuating slab tracks. *Construction and Building Materials*, *258*, 119545. https://doi.org/10.1016/j.conbuildmat.2020.119545

Liu, B., & Liang, D. (2017). Effect of mass ratio of asphalt to cement on the properties of cement modified asphalt emulsion mortar. *Construction and Building Materials*, *134*, 39–43. https://doi.org/10.1016/j.conbuildmat.2016.12.137

Liu, C., Thompson, D., Griffin, M. J., & Entezami, M. (2019). Effect of train speed and track geometry on the ride comfort in high-speed railways based on ISO 2631-1. *Proceedings of the Institution of Mechanical Engineers, Part F: Journal of Rail and Rapid Transit*, *234*(7), 765–778. https://doi.org/10.1177/0954409719868050

Liu, F., & Zhou, J. (2017a). Research on Fatigue Strain and Fatigue Modulus of Concrete. *Advances in Civil Engineering*, *2017*. https://doi.org/10.1155/2017/6272906

Liu, F., & Zhou, J. (2017b). Research on Fatigue Strain and Fatigue Modulus of Concrete. *Advances in Civil Engineering*, *2017*. https://doi.org/10.1155/2017/6272906

Liu, X., Yu, Z., Xiang, P., & Jin, C. (2019). Composite action of the track slab and the self-compacting concrete filling layer subjected to train-induced fatigue load: An experimental investigation. *Proceedings of the Institution of Mechanical Engineers, Part F: Journal of Rail and Rapid Transit*, *233*(5), 580–592. https://doi.org/10.1177/0954409718803821

Liu, X., Zhao, P., Yang, R., & Wang, P. (2010). Ballastless track design theory and methods [M]. *Publishing House of Southwest Jiaotong University*, 56–85.

Long, X., Shi, J., Wang, Y., & Liu, X. (2024). Dynamic Modeling and Application of a Vehicle-Track-Bridge System Subjected to Track Alignment for High-Speed Railways. *KSCE Journal of Civil Engineering*, *28*(12), 5582–5592. https://doi.org/10.1007/s12205-024-2732-6

Lv, S., Yuan, J., Liu, C., Wang, J., Li, J., & Zheng, J. (2019). Investigation of the fatigue modulus decay in cement stabilized base material by considering the difference between compressive and tensile modulus. *Construction and Building Materials*, *223*, 491–502. https://doi.org/10.1016/j.conbuildmat.2019.07.003

Madshus, C., & Kaynia, A. M. (2000). High-speed railway lines on soft ground: dynamic behaviour at critical train speed. *Journal of Sound and Vibration*, *231*(3), 689–701. https://doi.org/10.1006/jsvi.1999.2647

Maider, O., Alfredo, N., Rolf, D., & Zili, L. (2017). Sensitivity Analysis of Railpad Parameters on Vertical Railway Track Dynamics. *Journal of Engineering Mechanics*, *143*(5), 04017011. https://doi.org/10.1061/(ASCE)EM.1943-7889.0001207

Matias, J. (. (2019). "Zublin system: An affordable construction method." *Proceedings of the International Conference on Railway Engineering, Lisbon, Portugal*.

Matias, S. R., & Ferreira, P. A. (2020). Railway slab track systems: review and research potentials. *Structure and Infrastructure Engineering*, *16*(12), 1635–1653. https://doi.org/10.1080/15732479.2020.1719167

Meng, Y., Liu, D., Rong, H., & Yang, X. (2024). Review and prospect of four-point bending fatigue test of asphalt mixture. In *Journal of Road Engineering*. KeAi Publishing Communications Ltd. https://doi.org/10.1016/j.jreng.2023.05.004

Michas, G. (2012). Slab Track Systems for High-Speed Railways. *MSc Thesis*.

Moghadas Nejad, F., Habibi, M., Hosseini, P., & Jahanbakhsh, H. (2017). Investigating the mechanical and fatigue properties of sustainable cement emulsified asphalt mortar. *Journal of Cleaner Production*, *156*, 717–728. https://doi.org/10.1016/j.jclepro.2017.04.105

Newton, S. G, & Clark, R. A. (1979). An Investigation into the Dynamic Effects on the Track of Wheelflats on Railway Vehicles. *Journal of Mechanical Engineering Science*, *21*(4), 287–297. https://doi.org/10.1243/JMES_JOUR_1979_021_046_02

Nielsen, J. C. O., & Li, X. (2018). Railway track geometry degradation due to differential settlement of ballast/subgrade – Numerical prediction by an iterative procedure. *Journal of Sound and Vibration*, *412*, 441–456. https://doi.org/10.1016/j.jsv.2017.10.005

Oneschkow, N., & Timmermann, T. (2022). Influence of the composition of high-strength concrete and mortar on the compressive fatigue behaviour. *Materials and Structures/Materiaux et Constructions*, *55*(2). https://doi.org/10.1617/s11527-021-01868-7

Padhi, S., Sharma, S., & Patel, Y. (2022). Rail Pad Dynamic Properties: A Review. *Advances in Mechanical Engineering and Technology: Proceedings of 6th International Conference on Advanced Production and Industrial Engineering (ICAPIE)-2021*, 57–70.

Park, D. W., Choi, C., Phan, T. M., & Minh Le, T. H. (2024). Mobilizing railway track stability with nonionic cement asphalt mortar for floating sleeper mitigation – 2D/3D numerical investigation and full-scale testing verification. *Case Studies in Construction Materials*, *20*. https://doi.org/10.1016/j.cscm.2024.e03088

Patel, Y., Rastogi, V., & Borutzky, W. (2023). Simulation study on the influence of wheel irregularity on the vertical dynamics of wheel–rail interaction for high-speed railway track using bond graph. *Simulation*, *99*(6), 643–656. https://doi.org/10.1177/00375497221138943

Prabhakaran, P., Subbaiyan, A., Gopalakrishnan, D., Harsha, H. V., Ramkumar, S., Veluswamy, S., Murugesan, D. K., Seerangagounder, S., Arunachalam, S., Velusamy, P., & Bhaskaran, P. (2022). Maintenance Methodologies Embraced for Railroad Systems: A Review. In *Advances in Materials Science and Engineering* (Vol. 2022). Hindawi Limited. https://doi.org/10.1155/2022/7655245

Qin, L., Guo, C., Sun, W., Zhang, M., Chu, X., & Wang, F. (2022). Experimental study on interfacial damage characteristics of CRTS II slab track and CA mortar with AE and DIC techniques. *Engineering Failure Analysis*, *142*, 106777. https://doi.org/https://doi.org/10.1016/j.engfailanal.2022.106777

Qiu, K., Chen, H., Sun, W., Sun, L., Hong, J., & Zhao, G. (2014). Determination of Mechanical Properties of Cement Asphalt Mortar via UPV Method. *Journal of Materials in Civil Engineering*, *26*(6). https://doi.org/10.1061/(asce)mt.1943-5533.0000939

Real, T., Zamorano, C., Hernández, C., García, J. A., & Real, J. I. (2016). Static and dynamic behavior of transitions between different railway track typologies. *KSCE Journal of Civil Engineering*, *20*(4), 1356–1364. https://doi.org/10.1007/s12205-015-0635-2

Ren, J., Deng, S., Wei, K., Li, H., & Wang, J. (2019). Mechanical property deterioration of the prefabricated concrete slab in mixed passenger and freight railway tracks. *Construction and Building Materials*, *208*, 622–637. https://doi.org/10.1016/j.conbuildmat.2019.03.039

Ren, J., Deng, S., Zhang, K., Du, W., & Wu, Q. (2021). Design theories and maintenance technologies of slab tracks for high-speed railways in China: a review. In *Transportation Safety and Environment* (Vol. 3, Issue 4). Oxford University Press. https://doi.org/10.1093/tse/tdab024

Ren, J., Li, X., Yang, R., Wang, P., & Xie, P. (2016). Criteria for repairing damages of CA mortar for prefabricated framework-type slab track. *Construction and Building Materials*, *110*, 300–311. https://doi.org/10.1016/j.conbuildmat.2016.02.036

Restrepo-Barrientos, Pablo, Torres Garay, Jesús Arturo, Arbeláez-Toro, Juan José, Toro, Alejandro, & Santa, Juan Felipe. (2025). Evaluation of the effect of rail pad stiffness and wheel polygonization on the dynamic behavior of corrugated railway tracks. *Proceedings of the Institution of Mechanical Engineers, Part F: Journal of Rail and Rapid Transit*, *239*(10), 878–889. https://doi.org/10.1177/09544097251365527

Rungskunroch, P., Kaewunruen, S., & Shen, Z. J. (2019). An improvement on the end-of-life of high-speed rail rolling stocks considering cfrp composite material replacement. *Frontiers in Built Environment*, *5*. https://doi.org/10.3389/fbuil.2019.00089

Rutherford, T., Wang, Z., Shu, X., Huang, B., & Clarke, D. (2014). Laboratory investigation into mechanical properties of cement emulsified asphalt mortar. *Construction and Building Materials*, *65*, 76–83. https://doi.org/10.1016/j.conbuildmat.2014.04.113

Shamalta, M., & Metrikine, A. V. (2003). Analytical study of the dynamic response of an embedded railway track to a moving load. *Archive of Applied Mechanics*. https://doi.org/10.1007/s00419-002-0248-3

Sheng, X., Jones, C. J. C., & Thompson, D. J. (2004). A theoretical model for ground vibration from trains generated by vertical track irregularities. *Journal of Sound and Vibration*, *272*(3–5), 937–965. https://doi.org/10.1016/S0022-460X(03)00782-X

Sheng, X. W., Zheng, W. Q., Zhu, Z. H., Luo, T. J., & Zheng, Y. H. (2020). Properties of rubber under-ballast mat used as ballastless track isolation layer in high-speed railway. *Construction and Building Materials*, *240*, 117822. https://doi.org/10.1016/j.conbuildmat.2019.117822

Shu, L., Xu, D., Ni, F., Jiang, J., Wang, J., & Zhang, Z. (2024). Evaluating the aging and fatigue performance of in-situ asphalt mortar through multiple stress creep recovery and energy-based methods. *Construction and Building Materials*, *456*. https://doi.org/10.1016/j.conbuildmat.2024.139304

Singh Jitendra. (2023). *Basics of Track Structure and Components*. https://indianrailways.gov.in

Song, X., Qian, Y., Wang, K., & Liu, P. (2020). Effect of rail pad stiffness on vehicle–track dynamic interaction excited by rail corrugation in metro. *Transportation Research Record*, *2674*(6), 225–243.

Standard, I. (2018). *Bitumen Emulsion for Roads (Cationic Type)-Specification (Third Revision)*. www.standardsbis.in

Tarifa, M., Zhang, X., Ruiz, G., & Poveda, E. (2015). Full-scale fatigue tests of precast reinforced concrete slabs for railway tracks. *Engineering Structures*, *100*, 610–621.

Tayabji, S. D., & Bilow, D. (2001). Concrete slab track state of the practice. *Transportation Research Record*, *1742*(1), 87–96.

Tian, D. M., & Yin, J. (2016). Fatigue Behavior of Cement Asphalt Emulsion Mortar. *Applied Mechanics and Materials*, *847*, 25–30. https://doi.org/10.4028/www.scientific.net/amm.847.25

Timoshenko, S., Young, D. H., & Weaver, W. (1974). Vibration Problems in Engineering. John Willey and Sons. *Inc., New York*.

Tran, M. T., Ang, K. K., Luong, V. H., & Dai, J. (2016). High-speed trains subject to abrupt braking. *Vehicle System Dynamics*, *54*(12), 1715–1735. https://doi.org/10.1080/00423114.2016.1232837

Ul, M. R., & Uzzal, A. (2012). *ANALYSIS OF A THREE-DIMENSIONAL RAILWAY VEHICLE-TRACK SYSTEM AND DEVELOPMENT OF A SMART WHEELSET*.

United Nation Development Programme. (2024). *The 17 Goals | Sustainable Development* .

Vesali, F., Rezvani, M. A., & Shadfar, M. (2024). Attuned Dynamic Response of Double Track Multi-span Railway Bridges Under the Delayed Entry of a Second Train. *Journal of Vibration Engineering and Technologies*, *12*(1), 925–940. https://doi.org/10.1007/s42417-023-00884-x

Vossloh. (2019). *"Rail fastening systems for concrete sleepers*. Available: Https://Www.Vossloh.Com/En/Products-Solutions/Rail-Fastening-Systems/Rail-Fastening-Systems-for-Concrete-Sleepers/.

Vu, L., Jang, D. D., & Kang, Y. S. (2021). Assessment of structural dynamic response and vehicle-track interaction of precast slab track systems. *Applied Sciences (Switzerland)*, *11*(8). https://doi.org/10.3390/app11083558

Wang, L., Wang, P., Wei, K., Dollevoet, R., & Li, Z. (2022). Ground vibration induced by high speed trains on an embankment with pile-board foundation: Modelling and validation with in situ tests. *Transportation Geotechnics*, *34*. https://doi.org/10.1016/j.trgeo.2022.100734

Wang, M., Cai, C., Zhu, S., & Zhai, W. (2017). Experimental study on dynamic performance of typical nonballasted track systems using a full-scale test rig. *Proceedings of the Institution of Mechanical Engineers, Part F: Journal of Rail and Rapid Transit*, *231*(4), 470–481. https://doi.org/10.1177/0954409716634751

Wang, Q., Yan, P., Kong, X., & Yang, J. (2011). Compressive strength development and microstructure of cement-asphalt mortar. *Journal Wuhan*

University of Technology, Materials Science Edition, *26*(5), 998–1003. https://doi.org/10.1007/s11595-011-0351-9

Wang, W., Wu, S., & Dai, H. (2006). Fatigue behavior and life prediction of carbon fiber reinforced concrete under cyclic flexural loading. *Materials Science and Engineering: A*, *434*(1–2), 347–351. https://doi.org/10.1016/j.msea.2006.07.080

Wang, X., Wei, K., Ma, Q., Liu, Y., Guo, G., Pu, Q., & Xie, C. (2024). Research on fastener lateral nonlinear stiffness characteristics and its impact on wheel-rail stick-slip vibration. *Nonlinear Dynamics*, *112*(19), 16917–16939. https://doi.org/10.1007/s11071-024-09990-1

Wanming Zhai. (2020). Vehicle–Track Coupled Dynamics. Theory and Applications. In *Vehicle–Track Coupled Dynamics. Theory and Applications*. Springer Singapore. https://doi.org/doi.org/10.1007/978-981-32-9283-3

Xiao, H., Zhang, Y. R., Li, Q. H., Jin, F., & Nadakatti, M. M. (2019). Analysis of the initiation and propagation of fatigue cracks in the CRTS II slab track inter-layer using FE-SAFE and XFEM. *Proceedings of the Institution of Mechanical Engineers, Part F: Journal of Rail and Rapid Transit*, *233*(7), 678–690. https://doi.org/10.1177/0954409718805296

Xiao, X., Ling, L., & Jin, X. (2012). A study of the derailment mechanism of a high speed train due to an earthquake. *Vehicle System Dynamics*, *50*(3), 449–470. https://doi.org/10.1080/00423114.2011.597508

Xiao, Y., Luo, X., Liu, J., & Wang, K. (2020). Dynamic Response of Railway Bridges under Heavy-Haul Freight Trains. *Advances in Civil Engineering*, *2020*. https://doi.org/10.1155/2020/7486904

Xie, H., Yan, B., & Huang, J. (2020). Vertical Dynamic Analysis of Ballastless Tracks on Train-Track- Bridge System. *MATEC Web of Conferences*, *306*(20 20), 02003. https://doi.org/10.1051/matecconf/202030602003

Xie, Y. J., Fu, Q., Long, G. C., Zheng, K. R., & Song, H. (2014). Creep properties of cement and asphalt mortar. *Construction and Building Materials*, *70*, 9–16. https://doi.org/10.1016/j.conbuildmat.2014.07.103

Xu, L., Li, Z., Bai, W., Pan, L., & Yu, Z. (2021). Numerical simulation platform for slab track systems subjected to a moving vehicle. *Advances in Engineering Software*, *154*. https://doi.org/10.1016/j.advengsoft.2021.102984

Xu, L., & Zhai, W. (2019). A three-dimensional model for train-track-bridge dynamic interactions with hypothesis of wheel-rail rigid contact. *Mechanical Systems and Signal Processing*, *132*, 471–489. https://doi.org/10.1016/j.ymssp.2019.04.025

Xu, Q., & Wang, X. (2023). Experimental study on high-cycle flexural fatigue behavior of cement mortar for ballastless track of high-speed railway. *Construction and Building Materials*, *385*. https://doi.org/10.1016/j.conbuildmat.2023.131525

Xu, Q.-Y., & Zeng, Z.-P. (2009). Influence of longitudinal connection mode of ballastless slab track on vibration characteristic of train-ballastless slab track-subgrade system. In *ICCTP 2009: Critical Issues In Transportation Systems Planning, Development, and Management* (pp. 1–8).

Yan, W., & Fischer, F. D. (2000). Applicability of the Hertz contact theory to rail-wheel contact problems. *Archive of Applied Mechanics*, *70*(4), 255–268. https://doi.org/10.1007/s004199900035

Yang, J., Zhu, S., & Zhai, W. (2020). A novel dynamics model for railway ballastless track with medium-thick slabs. *Applied Mathematical Modelling*, *78*, 907–931. https://doi.org/10.1016/j.apm.2019.09.051

Yang, X., Gu, S., Zhou, S., Yang, J., Zhou, Y., & Lian, S. (2015). Effect of track irregularity on the dynamic response of a slab track under a high-speed train based on the composite track element method. *Applied Acoustics*, *99*, 72–84. https://doi.org/10.1016/j.apacoust.2015.05.009

Yang, Y., Yang, D., Gou, H., & Bao, Y. (2019). Research on static and dynamic behaviors of PC track beam for straddle monorail transit system. *Steel and Composite Structures*, *31*(5), 437–452. https://doi.org/10.12989/scs.2019.31.5.437

Yang, Y., Zhang, G., Wu, G., & Cao, D. (2022). Study on fatigue damage laws and life prediction of CRTS-II ballastless track slab. *Engineering Structures*, *252*. https://doi.org/10.1016/j.engstruct.2021.113659

Yousif Aziz, H. (2012). Experimental and Theoretical Static Analysis of High-Speed Railway Bridge Settlement for Deep Soft Soil. *The Open Construction and Building Technology Journal*, *6*(1), 17–31. https://doi.org/10.2174/1874836801206010017

Yu, R. C., Poveda, E., Lancha, J. C., Arredondo, E., & Ruiz, G. (2012). Numerical study on the fatigue behaviour of a concrete slab track. *Civil-Comp Proceedings*. https://doi.org/10.4203/ccp.98.15

Zeng, Z., He, X., Zhao, Y., Yu, Z., Chen, L., Xu, W., & Lou, P. (2015). Random vibration analysis of train-slab track-bridge coupling system under earthquakes. *Structural Engineering and Mechanics*, *54*(5), 1017–1044.

Zeng, Z. P., Liu, F. S., & Wang, W. D. (2022). Three-dimensional train–track–bridge coupled dynamics model based on the explicit finite element method. *Soil Dynamics and Earthquake Engineering*, *153*, 107066. https://doi.org/10.1016/J.SOILDYN.2021.107066

Zhai, W., He, Z., & Song, X. (2010). Prediction of high-speed train induced ground vibration based on train-track-ground system model. *Earthquake Engineering and Engineering Vibration*, *9*(4), 545.

Zhai, W., & Sun, X. (1994). A Detailed Model for Investigating Vertical Interaction between Railway Vehicle and Track. *Vehicle System Dynamics*, *23*(sup1), 603–615. https://doi.org/10.1080/00423119308969544

Zhai, W., Wang, K., & Cai, C. (2009). Vehicle System Dynamics Fundamentals of vehicle–track coupled dynamics Fundamentals of vehicle–track coupled dynamics. *Vehicle System Dynamics*, *47*(11), 1349–1376. http://www.tandfonline.com/action/journalInformation?journalCode=nvsd20

Zhang, Y., Wu, K., Jiang, J., Hu, Y., Liu, L., Cai, X., & Lu, Z. (2025). Static and fatigue performance of the interface between the epoxy resin and cement asphalt mortar for CRTS II slab track. *Case Studies in Construction Materials*, *22*, e04642. https://doi.org/https://doi.org/10.1016/j.cscm.2025.e04642

Zhao, H. Y., Indraratna, B., & Ngo, T. (2021). Numerical simulation of the effect of moving loads on saturated subgrade soil. *Computers and Geotechnics*, *131*, 103930. https://doi.org/10.1016/J.COMPGEO.2020.103930

Zhou, M., Zhong, S., Liu, Y., Liu, Z., Yang, B., Jiang, Z., Zhou, L., & Tang, L. (2025). Damage Evolution and Lifetime Prediction of Cement Asphalt Mortar Under High-Speed Train Frequency and Temperature Gradient Load. *Materials*, *18*(5), 1011. https://doi.org/10.3390/ma18051011

Zhou, S., Wang, B., & Shan, Y. (2020). Review of research on high-speed railway subgrade settlement in soft soil area. In *Railway Engineering Science* (Vol. 28, Issue 2, pp. 129–145). Springer. https://doi.org/10.1007/s40534-020-00214-x

Zhu, S., & Cai, C. (2014). Stress intensity factors evaluation for through-transverse crack in slab track system under vehicle dynamic load. *Engineering Failure Analysis*, *46*, 219–237. https://doi.org/10.1016/j.engfailanal.2014.09.004

Zoeteman, A., & Esveld, C. (1999). Evaluating track structures: life cycle cost analysis as a structured approach. *World Congress on Railway Research*. http://www.silvertipdesign.com/BR(Imperial)/[18] Paper WCRR99 Tokyo.pdf